Dissertation
submitted to the
Combined Faculty of Natural Sciences and Mathematics
of the Ruperto Carola University Heidelberg, Germany
for the degree of
Doctor of Natural Sciences

Presented by
M.Sc. Biomedical Engineering Elizaveta Chervyachkova
born in: Moscow, Russian Federation
Oral-examination: 26.10.2018

Light-controlled self-assembly and self-sorting of cell-like compartments

Referees: Prof. Dr. G. Elisabeth Pollerberg

Prof. Dr. Joachim P. Spatz

Acknowledgements

First of all, I would like to thank Prof. Dr. Joachim P. Spatz for giving me the opportunity to conduct my research in his interdisciplinary research group. Second, I would like to thank Prof. Dr. G. Elisabeth Pollerberg for kindly agreeing to become my supervisor at the Faculty of Biosciences and for her support during these years and feedback whenever needed. Next, I would like to thank Prof. Dr. Katharina Landfester for her kind support and for hosting me at the Max-Planck-Institute for Polymer Research for the last two-and-a-half years.

Furthermore, I would also like to thank Dr. Seraphine V. Wegner for her supervision, scientific discussions and for limitless ideas about my projects. I would then like to thank the whole Landfester, Spatz and Wegner research groups for all the fun we had together.

I would like to thank Solveig Bartelt not only for her scientific collaboration but also for all the fun and support along the way. Same goes to Julia Ricken for all the support and for being my connection to Heidelberg since I moved away and my unstoppable source of optimism. I would also like to thank my office mates Marc Müller and Samaneh Rasoulinejad for distracting me sometimes from work and for all the talks. Simge Yüz is also gratefully acknowledged for her kind support during the thesis writing phase. Additionally, I want to thank Stefan Schuhmacher for the IT support and for all the pictures he has drawn and posters he had printed for me throughout these years.

My special thanks go to my friends Varvara Sharova and Cynthia Frommelt for always supporting and encouraging me to go further and to succeed. Additionally, I am thankful to my friends back home, Tatiana Kudriashova, Natalia Kazakova, Eugene Ogloblin, Dmirty Lyskov and Elena Shapova for keeping in touch despite the long distance between us.

Above all I want to thank my boyfriend Maximilian Ziebell for all the great support he showed throughout good and bad times and for always being on my side but staying objective. I am thankful for his good mood, optimism and his love, he surrounded me with.

Further, I would like to thank Wolfgang Ziebell and Margrit Ziebell for becoming my family in Germany and for their support.

Last but not least I want to thank my parents Anna Shashmurina and Sergei Chervyachkov for making it possible for me to pursue my studies abroad first of all and for always standing behind me and my ideas. Thank you all very much!

Parts of this work were published in:

Chervyachkova, E. and Wegner, S. V.

Reversible Social Self-Sorting of Colloidal Cell-Mimics with Blue Light Switchable Proteins

ACS Synthetic Biology, 7, 1817-1824 (2018)

DOI: 10.1021/acssynbio.8b00250

Bartelt*, S. M., Chervyachkova*, E., Steinkühler, J., Ricken, J., Wieneke, R., Tampé, R., Dimova, R. and Wegner, S. V.

Dynamic blue light-switchable protein patterns on giant unilamellar vesicles

Chemical Communications, 54, 948-951 (2018)

DOI: 10.1039/c7cc08758f

Abstract

The organization of cells within tissues allows them to work together. Tight spatiotemporal control over cell-cell interactions is essential for individual cells to self-assemble and function as tissues. In addition, during many biological processes, such as embryogenesis and cancer development, cell-cell interactions undergo dynamic changes to alter their function. Analogously, in the context of bottom-up synthetic biology it is of interest to dynamically control the interactions between minimal synthetic cells and assemble them into precise multi-compartment prototissues with high spatiotemporal resolution.

The aim of the first part of this thesis was to reversibly self-assemble different types of micrometer-sized colloids, which were used as synthetic cell-mimics, with high spatiotemporal resolution using visible light. Light provides a dynamic, non-invasive, and biocompatible control with high spatiotemporal precision. In order to control the self-assembly of cell-mimics, I functionalized them with photoswitchable proteins that specifically interact with each other under blue or red light. For this purpose I used several combinations of photoswitchable proteins that are dimerizing under blue light: heterodimerizing iLID and Nano proteins, nMagHigh and pMagHigh proteins, and homodimerizing VVDHigh protein. For the red light switchable proteins I used both the heterodimerization of phytochrome B (PhyB) and phytochrome interaction partner (PIF6) proteins and the homodimerization of Cph1 protein. All of these light dependent protein interactions enabled controlling the self-assembly of cell-mimics with light. Additionally, blue light dependent protein interactions are reversible in the absence of light with red light dependent interactions reversing under far-red light illumination. Consequently, the self-assembly of cell-mimics mediated by these protein interactions was also reversible. Additionally, the high specificity and the independent response of these protein interactions to blue or red light offers the potential to self-assemble a specific population of cell-mimics in the presence of others on demand.

In multicellular organisms, cells do not just self-assemble but they also self-sort into precise arrangements in order to work together. As part of this thesis, I also mimicked the self-sorting behavior with synthetic compartments inspired by the observations in nature. Self-sorting is defined by the ability to distinguish between self and non-self, and happens in different modes depending on the interactions between the particles. One mode is social self-sorting, which leads to the separation of colloids into independent colloidal

families and requires heterophilic and orthogonal interactions. In this part of the thesis, I used heterodimerization of two blue light switchable protein pairs, iLID/Nano and nMagHigh/pMagHigh, for the social self-sorting between four different populations of colloids within one mixture. Each protein pair specifically and orthogonally brings together two different subpopulations of colloids providing tight and reversible control over their self-sorting into two distinct families using blue light. On the other hand, asocial sorting is another mode of self-sorting, which requires homophilic interactions to bring together compartments of the same type into isolated aggregates. This could potentially be achieved by combining homodimerization of VVDHigh and Cph1 proteins under blue and red light respectively. Eventually, all the versatile and orthogonal light-switchable proteins and different dimerization modes have the potential to be incorporated together in different combinations to achieve the desired self-sorting outcome in complex prototissues.

In the second part of the thesis, I addressed the spatiotemporally controlled formation of protein patterns on synthetic cell-mimics. Protein patterns and gradients on cell membranes are important during many biological processes to locally trigger events in multicellular structures with high spatiotemporal precision. To create and control protein patterns on synthetic membranes such as giant unilamellar vesicles (GUVs) with light, I used the blue light switchable heterodimerization of iLID and Nano proteins. For this purpose, the GUVs were functionalized with iLID. This allowed for the blue light mediated, reversible recruitment of a fluorescent protein (mOrange) fused to Nano using blue light with high spatiotemporal resolution. Further, this approach allowed scaling the size of protein patterns from the level of a single GUV to the level of a tissue-like GUV carpet. Hence, these photoswitchable proteins offer a versatile, reversible, dynamic, and non-invasive method to photopattern proteins with high spatiotemporal control that operates under mild conditions.

Overall, photoswitchable proteins are important building blocks in the bottom-up synthetic biology toolbox. Incorporating them onto minimal synthetic cells can be used to self-assemble and self-sort different types of cell-mimics and to generate protein patterns, thus mimicking complex processes that occur in nature. Most importantly, these protein interactions provide high spatiotemporal precision and specificity to control these biomimetic processes. Ultimately, this concept can be transferred to assemble prototissues using various types of cell-mimics that host different functionalities, which would allow for controlling, how different synthetic cells work together in a prototissue.

Zusammenfassung

Die Organisation von Zellen innerhalb eines Gewebes und ihre Interaktion sowie Kommunikation miteinander, erlaubt es ihnen zusammen zu arbeiten. Präzise zeitliche und räumliche Kontrolle über die Zell-Zell-Interaktionen ist essentiell für individuelle Zellen um sich im Verband anzuordnen und dadurch ihre jeweilige Funktion im Gewebe zu übernehmen. In vielen biologischen Prozessen, wie Embryogenese und in Krankheiten wie Krebs, unterliegen Zell-Zell-Interaktionen dynamischen Veränderungen welche zu einer veränderten Funktion führt. Analog dazu ist es in der synthetischen Biologie von großem Interesse, diese Interaktionen zu simulieren, indem sie zwischen minimalen synthetischen Zellen induziert und kontrolliert werden und diese dadurch in präzisen multi-kompartimentäre Protogewebe mit großer räumlicher und zeitlicher Auflösung angeordnet werden können.

Das Ziel des ersten Teils dieser Doktorarbeit war es unterschiedliche Typen von Mikrometer großen Kolloiden, hier als synthetischen Zellmimetika beschrieben, reversibel mit hoher räumlich-temporaler Auflösung durch sichtbares Licht anzuordnen. Licht bietet dynamische, nicht invasive und biokompatible Kontrolle mit der gewünschten zeitlichen und räumlichen Präzision. Um die Selbstorganisation über Zellmimetika kontrollieren zu können, wurden die Kolloide mit photoschaltbaren Proteinen funktionalisiert, welche spezifisch mit ihrem jeweiligen Interaktionspartner unter entweder blauem oder rotem Licht interagieren. Es wurden die Proteinheterodimere iLID und Nano, nMagHigh und pMagHigh sowie das homodimerisierende Protein VVDHigh benutzt, welche unter blauem Licht dimerisieren. Weiter wurden das rotlicht-schaltbare Dimerpaar Phytochrom B (PhyB) und Phytochrome-interaction-factor 6 (PIF6) als auch das Cph1 Protein als Homodimer eingesetzt. Durch Kombination der genannten lichtschaltbaren Proteininteraktionen konnte die Selbstorganisation von Zellmimetika mit sichtbarem Licht kontrolliert werden. Zusätzlich sind die Interaktionen der Proteine welche auf blaues Licht reagieren, im Dunkeln reversibel, während die rotlicht-schaltbare Proteine unter infrarotem Licht dissoziieren. Ich konnte zeigen, dass diese Reversibilität auch auf die Selbstorganisation der Zellmimetika übertragen werden kann. Darüber hinaus verspricht die hohe Spezifität zu dem jeweiligen Interaktionspartner, wie auch zu der jeweiligen Wellenlänge, dass durch diese Proteine Kolloide nach Bedarf zu spezifischen Populationen angeordnet werden können, selbst wenn das System durch die Anwesenheit von weiteren Proteinen komplexer wird.

In multizellulären Organismen müssen sich Zellen nicht nur zusammen finden, sondern auch deren Anordnung zueinander muss genauer Kontrolle unterliegen, um die gewünschte Funktion zu gewährleisten. Als Teil dieser Arbeit, wurde die Organisation von synthetischen Kompartimenten, imitiert. Bei der Selbstorganisation müssen die Kompartimente in der Lage sein zwischen „gleich“ und „nicht-gleich“ zu unterscheiden. In Abhängigkeit von der

Interaktion zwischen den Kolloiden wird zwischen zwei Modi unterschieden. Ein Modus ist die soziale Selbstorganisation, welche zur Isolierung von Kolloiden in abgegrenzten Familien führt und heterophile und orthogonale Interaktionen voraussetzt. In diesem Teil der Thesis wurde die orthogonale Interaktion von zwei Proteinpaaren, welche durch blaues Licht dimerisieren, iLid/Nano und nMagHigh/pMagHigh, genutzt, um vier unterschiedliche Populationen von Kolloiden zu organisieren. Beide Proteinpaare zeigen die Spezifität und Orthogonalität um zwei Partikelsubpopulationen zu organisieren und so hohe und reversible Kontrolle über die Organisation von Kolloiden in zwei unterschiedlichen Familien durch sichtbares Licht zu induzieren. Der zweite Modus ist asoziale Selbstorganisation, wobei durch homophile Interaktionen Kompartimente desselben Typs angeordnet werden. Das kann durch die Kombination der Proteine VVdhigh und Cph1 erreicht werden, welche auf blaues bzw. rotes Licht reagieren. Letztendlich haben alle lichtschaltbare Proteinpaare mit ihren unterschiedlichen Interaktionsmodi das Potential in unterschiedlichen Kombinationen eingesetzt zu werden, um die nötige Selbstorganisation zu komplexen Protogeweben zu ermöglichen.
Im Zweiten Teil der Arbeit wird die zeitliche und räumliche Formation von Proteinmustern auf synthetischen Zellmimetika untersucht. Proteinmuster und Proteingradienten auf Zellmembranen sind in vielen biologischen Prozessen von höchster Bedeutung um lokale Kontrolle über multizellulären Prozessen zu erreichen. Um Proteinmuster auf synthetischen Membranen z.B. von GUVs (Giant Unilamellar Vesicles), zu kreieren, wurden die Heterodimere iLID und Nano, welche auf blaues Licht reagieren, benutzt. Die GUV-Membran wurde mit iLID funktionalisiert. mOrange, ein fluoreszierendes Protein, welches mit Nano fusioniert wurde, konnte so mit hoher räumlicher und zeitlicher Auflösung durch blaues Licht an die Zellmembran reversibel rekrutiert werden. Die Rekrutierung kann durch den Einsatz von unterschiedlichen Lichtintensitäten gesteuert werde. Weiter kann dieser Ansatz von einzelnen GUVs auch auf einen Teppich von GUV hochskaliert werden. Dadurch bieten lichtschaltbare Proteine eine vielseitige, reversible, dynamische und nicht invasive Methode um unter physiologischen Bedingungen Proteinmuster zu erzeugen.
Lichtschaltbare Proteine sind ein wichtiger Baustein im Werkzeugkasten der „bottom-up“ synthetischen Biologie. Sie können dazu eingesetzt werden die Selbstorganisation unterschiedlicher Typen von Zellmimetika zu steuern und Proteinmuster auf Membranen zu erzeugen und damit komplexe Prozesse der Natur zu imitieren. Wesentlich ist, dass diese Proteininteraktionen die spezielle spatiotemporale Präzision und Spezifizität bieten, um diese biomimetischen Prozesse zu kontrollieren. Letztendlich kann dieses Konzept auch auf die Selbstorganisation von Geweben aus unterschiedlichen Typen von Zellmimetika, welche unterschiedliche Funktionen tragen, übertragen werden. Damit besteht die Möglichkeit die Zusammenarbeit von synthetischen Zellen in einem Zellverband zu steuern.

List of abbreviations

*As*LOV2	Light-oxygen-voltage 2 domain from the plant *Avena sativa*
APS	Ammonium persulfate
BSA	Bovine serum albumin
Cas9	CRISPR-associated protein 9
CID	Chemically induced dimerization
Cph1	Cyanobacterial phytochrome 1
CRISPR	Clustered regularly interspaced short palindromic repeats
Cy5	Cyanine 5
DGS-NTA	1,2-dioleoyl-sn-glycero-3-[(N-(5-amino-1-carboxypentyl)iminodiacetic acid) succinyl]
DiD	1,1'-Dioctadecyl-3,3,3',3'-Tetramethylindodicarbo-cyanine
DMSO	Dimethyl sulfoxide
DNA	Deoxyribonucleic acid
DOPC	1,2-Dioleoyl-sn-glycero-3-phosphocholine
DTT	DL-Dithiothreitol
E. coli	*Escherichia coli*
EDTA	Ethylenediaminetetraacetic acid
ELP	Elastin-like peptides
FAD	Flavine adenine dinucleoide
FITC	Fluorescein isothiocyanate
FMN	Flavin mononucleotide
FRAP	Fluorescence Recovery after Photobleaching
GEF	Guanine nucleotide exchange factor
GFP	Green fluorescent protein
GTP	Guanosine triphosphate
GUV	Giant Unilamellar Vesicle
HeNe	Helium–Neon
His6	Histidine tag

HPLC	High performance liquid chromatography
iLID	Improved light-inducible dimer
IMAC	Immobilized metal affinity chromatography
IPTG	Isopropyl-β-D-thiogalactopyranoside
LB medium	Luria-Bertani medium
LED	Light-emitting diode
LID	Light-inducible dimerization
LOV	Light-oxygen-voltage
LUV	Large Unilamellar Vesicle
MAPK	Mitogen-activated protein kinases
MBP	Maltose-binding protein
mFGFR1	Murine fibroblast growth factor receptor 1
nMag	Negative Magnet protein
NTA	Nitrilotriacetic acid
OD	Optical density
PAS	Per-ARNT-Sim domain
PCB	Phycocyanobilin
PFA	Paraformaldehyde
PIF6	Phytochrome interacting factor 6
Pfr	Far-red light absorbing phytochrome
Phy	Phytochrome
pMag	Positive Magnet protein
PMSF	Phenylmethylsulfonyl fluoride
PNIPAM	Poly(N-isopropylacrylamid)
POPC	Palmitoyl-2-oleoylphosphatidylcholine
POPG	1-palmitoyl-2-oleoyl-sn-glycero-3-phospho-(1'-rac-glycerol)
Pr	Red light absorbing phytochrome
PURE	Protein synthesis using recombinant elements
RNA	Ribonucleic acid
ROI	Region of interest
rpm	Round per minute

rt	Room temperature
RTK	Receptor Tyrosine Kinase
SDS-PAGE	Sodium dodecyl sulfide-polyacrylamide gel electrophoresis
SNARE	Soluble NSF(N-ethylmaleimide-sensitive factor) Attachment Protein Receptor
SUV	Small Unilamellar Vesicle
TEMED	N,N,N',N'-Tetranethyl-ethylrnrdiamine
TetR	Tetracycline repressor
TEV	Tobacco Etch Virus
TRIS	Tris(hydroxymethyl)aminomethane
trisNTA-Suc-DODA	N-succinyldioctadecylamine with three NTA groups
TRITC	Tetramethylrhodamine
UV	Ultraviolet
Vis	Visible light
VVD	Vivid

List of Figures

List of Tables

Contents

Chapter 1: Introduction

1.1 Approaches to minimal synthetic cells

Over centuries both scientists and theologists have been debating over the definition of life. Among other theories life is thought to be initially wired by the self-organization of molecules followed by an increase in complexity within the systems.[1] To date, despite a variety of existing definitions, it is generally agreed that there are a few major functions that living systems have in common. First of all, the system should have defined borders separating it from the environment, i.e. they should be compartmentalized. This allows different chemical reactions to proceed within the boundaries and retains all the components of the system together.[2-3] Secondly, the system should be able to communicate with its environment as well as contain and be able to transfer information. In nature this is possible by encoding the information into DNA, which is a robust biopolymer that acts as a universal code. It allows translating the information into a multitude of proteins that can perform a variety of functions (catalyze different chemical reactions, signaling function, transport function etc.).[3-4] Next, there should be energy and nutrients exchange between the system and its environment to sustain the operation of the system and keep it out of equilibrium.[3-6] And last but not least, the system should be able to grow and self-reproduce using the dynamic self-assembly of its components.[2-4, 6] These essential life processes are difficult to study even in simplest living cells due to their inherent complexity and ambiguity gained over the course of evolution.[3, 7-8]

The construction of a minimal synthetic cell is a relatively new direction in synthetic biology that lies on the border of biology, chemistry, physics and biotechnology as well as computational design.[4] The main goal of synthetic biology is to create a well-defined and controlled minimal functioning unit, which is a minimal synthetic cell, and that can perform at least one of the essential functions of life.[3, 9] There are two distinct ways to approach the task of creating a minimal synthetic cell: the top-down and the bottom-up approach to

synthetic biology (Figure 1.1).[1, 10] The top-down approach to synthetic biology has been pursued more widely until now. In this approach, one starts from a living matter, a cell, and by applying modifications to it and reducing its genome investigates, what would be the minimal set of genes that is sufficient to perform all the functions of a living unit. As genomes of all living organisms have a certain degree of redundancy due to evolution, there has been a substantial amount of work done on creating a "minimal genome" through careful engineering. In one example it has been possible to produce viable synthetic bacteria using only the DNA sequence as a blueprint (*Mycoplasma mycoides*) and transplant this genome into another *Mycoplasma* species, *Mycoplasma capricolum*.[11-12] The acceptor species that are controlled only by a synthetic genome exhibit the expected phenotype and are capable of continuous replication. However, even for this small genome the functions of 28% of essential protein-coding genes are still unknown.[13] Therefore, despite having an advantage of using the host cell co-factors, metabolites and other components, the complexity of the top-down approach is still very high.[10, 14] Due to its inherent ambiguity in living cells, it is questionable if, in the end, this approach is suitable for identification of the smallest possible configuration of a living system.[3, 12]

The more recent approach to synthetic biology is the bottom-up approach. In this approach the aim is to define minimal set of elements and functions needed to build a life-like system *de novo*.[3] This approach starts at the molecular level and non-living matter, i.e. pure chemical components, and in some cases purified components extracted from living cells. Inspired by engineering, bottom-up synthetic biology follows the modularity approach, in which first all the separate components and their interactions with each other are thoroughly characterized under well-defined conditions as it is important to then be able to assemble them into functioning parts.[3, 15-16] Parts are in turn incorporated into modules and modules into systems to build up a minimal synthetic cell that performs the above-mentioned functions.[3] The modular approach of bottom-up synthetic biology allows defining the boundaries, in which biological functions are predictable and can be controlled.[16] All these functions, i.e. life-like

processes, can be synthesized and studied separately to gain exquisite control and understanding over the each of them.

There has been a great amount of work done towards replicating each of the processes separately. For example, to mimic the continuous energy supply in synthetic cells an ATP regeneration module, also called an artificial mitochondrion, has been developed by reconstituting ATP synthase and a thermal oxidase into either graft copolymer or hybrid graft copolymer/lipid nanocontainers.[3, 17] The growth process has been mimicked in protocells either by acquiring material from the outside or by fusing cell-like compartment together.[3] In particular, compartment growth of lipid vesicles through fusion has been controlled with light using photosensitive azobenzene-containing surfactants or with electric pulses.[3, 18-19] Towards mimicking the metabolism it is already possible to encapsulate functional enzymes within vesicles.[3, 20] The further challenge would be to reconstitute the whole complex metabolic pathway within such synthetic compartments.[3]

Further, the production of functional proteins in a cell-free manner has also been one of the focuses of bottom-up synthetic biology as these proteins are important building blocks in assembly of artificial cells.[3-5] In these systems the translation machinery of *E. coli* or wheat germ are encapsulated into synthetic vesicles, often into phospholipid ones, of a cell-comparable size of tens of micrometers. Once the energy/nutrition supply limitations were figured out, it was possible to produce relatively large quantities of proteins (30 μM per compartment) *in vitro* over the course of several days.[4-5] The cell-free protein expression systems are a good example for a technology that has also been transferred to the field of biotechnology. The PURE system (protein synthesis using recombinant elements) has been commercialized due to its robust, efficient and better controlled protein production.[21]

In summary, bottom-up approach to synthetic biology allows for a well-defined and detailed investigation on how each of the components in a minimal synthetic cell contributes to its function. This detailed understanding allows creating novel modular life-like systems with well-engineered properties.[3, 12, 22]

Synthetic biology is pursuing two main goals. The application driven goal is to manipulate cells for engineering and biotechnological applications. This would enable us to use synthetic cells for a multitude of compelling applications, such as personalized therapies, novel materials, diagnostics and even biofuels.[22] The more fundamental goal pursues the intellectual curiosity and has emerged from a desire to understand the origin of life and the way living systems function.[23] It aims to overcome the biggest challenge in studying biological systems, which lies in their complexity gained over the course of evolution. Such simplified synthetic cells, where all the components can be well understood and controlled separately, represent a big opportunity.[10] This would allow us to create novel living systems with desirable set of properties and to better understand the functions of life.

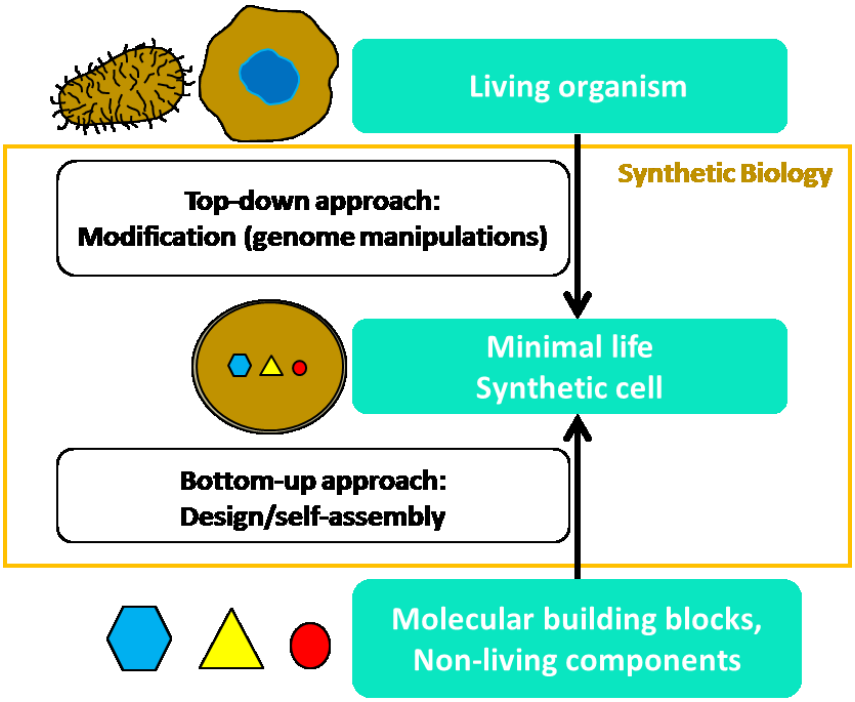

Figure 1.1 Synthetic biology approaches. Figure is adapted and modified from reference[1]. Copyright @ 1999 Elsevier. Reprinted with permission from Current Opinion in Colloid & Interface Science.

1.2 Compartmentalization and multicellularity

Compartmentalization of biochemical reactions is believed to have been a crucial step in the origin of life and allowed early cells to form a barrier with its environment.[24] A major bottleneck when attempting to create a protocell out of non-living components is the fact that only a few reactions can occur in one

space without interference.[20] For example, the rate of enzyme-catalyzed reactions strongly depends on the pH and ions in the environment. Therefore, it might not be possible to operate multiple enzymes in the same compartment.[25] In nature this problem was solved during evolution by separating incompatible reactions into organelles within a cell and by building up multicellular organisms from cells with different functions.[26] This compartmentalization helps the regulation of the metabolic pathways by making them more targeted and accurate and preventing their interference with each other. Overall, both the intracellular compartmentalization into organelles and the emergence of multicellular organisms lead to a big increase in life complexity and diversity.[27]

In multicellular organisms the complexity arises not only from the complexity of individual cells but also from the arrangements of the cells in respect to each other. The arrangements of cells determine the efficiency of material exchange, communication, and hence function. The arrangement of different compartments is a result of the precise control over the interactions between compartments within the cell as well as the interactions between the cells within a tissue.[27] Essential features of these interactions are the precise spatiotemporal control, high specificity in order to work in complex mixtures, and reversibility to facilitate dynamic adjustment to the changing environment. Therefore, it is also of a great interest to find a way to precisely modulate interactions between synthetic compartments and minimal synthetic cells to regulate their self-assembly and assemble them into synthetic prototisses with increased complexity. In such prototissues, synthetic cells that house different life-like processes could work together to give rise to emergent properties found in living systems.

1.3 Giant unilamellar vesicles as artificial cell models

One of the cell's most ingenious features is the compartmentalization.[26, 28-29] It allows cells to physically and chemically separate from its environment and run many different processes in parallel without them intervening with each other. In bottom-up synthetic biology there is a big variety of compartments that are used as simplified cell models. The most frequently used compartment types

are lipid vesicles of various sizes, polymersomes, coacervates, proteinosomes (protein-polymer conjugates) and various kinds of micro-droplets.[20, 30-32]

Lipid-based vesicles are the most frequently used simplified models of cells in bottom-up synthetic biology as they resemble the most the cellular membranes, which are also composed of lipid bilayers as well as a variety of associated biomolecules, for example transmembrane proteins.[33] Unilamellar vesicles can be prepared in sizes from small to large and giant (SUVs (<50 nm), LUVs (~100 nm) and GUVs (tens of μm)), which makes it possible to study the compartmentalization at different levels.[33] GUVs are often used as protocells due to their comparable size to the mammalian cell (typically tens of micrometers). Their sizes also make it possible to observe them by optical microscopy at a single vesicle level.[29] Moreover, the low membrane curvature of GUVs is considered to be significantly flat for studying nanoscale processes, such as interactions with proteins. GUVs have been used to study interactions of various biomolecules (such as DNA, RNA, peptides, and proteins) with lipid membranes and mechanical properties of membranes (ex. fluidity) and encapsulating capabilities of the vesicles.[28-29] All of the above-mentioned GUV characteristics and a variety of preparation methods (lipid film hydration, emulsions, electroformation, microfluidics etc.) that provide big flexibility in the production of GUVs, make GUVs an excellent choice as a cell mimic.[28-29, 33-34]

1.4 Colloidal self-assembly

Colloids are widely used as models to study the self-assembly of nanometer and micrometer sized particles into higher order structures, and can provide insight on the self-assembly of prototissues from protocells, which are also nano- and micro sized objects.[30-32, 35-38] Various external triggers, such as temperature or light, have been used to regulate the self-assembly within such colloidal systems.

1.4.1 Temperature-dependent colloidal self-assembly

One of the most widely established thermo-responsive self-assembling approaches that has been established in the 1990s is based on DNA-decorated colloids.[39-40] In this approach nano- and micrometer sized colloidal particles,

either gold- or polymer-based, are decorated with short single-stranded oligonucleotides with complementary "sticky ends" through the covalent binding. Upon heating of the DNA decorated colloids above the melting temperature of the DNA strands and cooling them down, the DNA strands on different colloids anneal with each other and result in the self-assembly of the colloids. Such a biologically inspired approach offers great specificity due specificity of the Watson-Crick base pairing.[41-42] Moreover, it offers a large variety of possible binding motifs and adjustable melting temperatures depending on the design of the single-stranded DNA to fit the application. This approach has been used in a variety of both nano- and micrometer sized colloids to form different colloidal amorphous and crystal structures.[43-49] However, despite having all the above mentioned advantages, this approach has few disadvantages. First of all, being temperature-responsive the system lacks the high spatiotemporal control and is in some cases inapplicable with biological conditions due to the high melting temperatures. Secondly, DNA based colloidal assemblies can be reversed with DNAase enzymes and with increased temperature but the majority are irreversible. Next, micron-sized colloids involve a large number of DNA interactions in the process, making it more difficult to fine-tune the system for the micrometer-sized objects compared to the nanoparticles.[43, 47]

Temperature-responsive self-assembly of colloidal particles has also been achieved using the temperature dependent hydrophilic-hydrophobic phase transition of peptides (such as elastin-like peptides, ELPs) and polymers (such as a copolymer of *N*-isopropylacrylamide and acrylamide).[50-51] Such peptides/polymers grafted on the colloidal particles are hydrophilic at low temperatures and become hydrophobic upon the temperature increase, which leads to particle aggregation. These approaches provide good reversibility and the ability to fine-tune the peptides/polymers to adjust the transition temperatures. However, these self-assembly strategies rely on unspecific hydrophobic interactions. Higher specificity and a big variety of different recognition motifs with a range of binding affinities has been achieved by decorating colloids with coiled-coil leucine zipper peptides. Nonetheless, the

use of temperature as an external trigger is still not ideal to achieve the high spatial and temporal control over self-assembly and is limited by high transition temperatures.[52]

1.4.2 Light-dependent colloidal self-assembly

Light is an attractive trigger to control self-assembly in colloidal systems with high spatiotemporal resolution. Moreover, light is easy to deliver both continuously at different intensities and in pulses to tune interactions. Moreover, different wavelengths can be used to address different functionalities specifically. In general, visible light is non-invasive and does not damage biomolecules. Yet, most described light responsive assembly methods respond to UV light as a trigger reducing their biocompatibility. Nonetheless, UV light responsive setups still provide important insight into light controlled self-assembly.

One way to control colloidal self-assembly with light is to decorate colloidal particles with small molecules that undergo light-induced changes in polarity, such as azobenzenes[53-54] and spiropyrans[55-56], or light induced dimerization such as coumarins[57]. All of these light induced changes are reversible in the dark or under blue light illumination, which also makes also the colloidal self-assemblies reversible.

So far, these approaches are mostly used on nanometer-sized colloids rather than micrometer-sized particles, which have comparable sizes to cells. Another limitation is that the self-assembly is not specific.

It is also possible to trigger self-assembly with light using specific and reversible supramolecular interactions based on host-guest interactions between cyclodextrines/azobenzenes and curcubit[8]urils/methyl viologen (or azobenzenes).[58-63] The cyclodextrines/azobenzenes host/guest interaction is based on the azobenzene in *trans*-conformation fitting into the cavity of cyclodextrines (α-, β- or γ-cyclodextrine). The cyclodextrines/azobenzenes complex reversibly dissociates upon UV irradiation, when azobenzene switches into its *cis*-state.[58-59] This interaction has been used to assemble Janus particles (colloidal particles whose surfaces have asymmetric properties) into

superstructures.[60, 64] The curcubit[8]urils are able to host simultaneously two guest molecules, such as methyl viologen or *trans*-azobenzene, inside their cavity. This supramolecular interaction has been used in order to obtain photoresponsive hybrid raspberry-like colloids and to reversibly self-assemble nanoparticles.[61-63] However, these light-dependent host-guest interactions used for the self-assembly are mostly formed in organic solvents reducing their biocompatibility. Overall, to the best of our knowledge, a way to reversibly self-assemble colloids into higher order architectures with high spatiotemporal control using visible light and under biocompatible conditions is still missing.

1.4.3 Self-sorting within colloidal systems

In biological systems it does not just suffice to self-assemble cells but they have to self-sort into different families with precise arrangements in order to work together. Therefore, also in synthetic systems there is a need to mimic such sorting behavior.[65] Self-sorting is defined by the ability to distinguish between self and non-self, which allows assemblies of one component to coexist with assemblies of another component without interacting with each other.[65-66] The self-sorting within a colloidal mixture can have different sorting modes depending on the type of interactions between the colloidal particles (Figure 1.2).[58, 65, 67]

i) Indiscriminate sorting: Weak and unspecific interactions, such as electrostatic or hydrophilic/hydrophobic interactions, lead to indiscriminate sorting in which all types of colloids assemble into one aggregate. For example, the self-assembly based on hydrophilic-hydrophobic phase transition of peptides or polymers enables all particles in the mixture to self-assemble into indiscriminate aggregates.[50-51]

ii) Asocial sorting: Self-complementary interactions cause narcissistic, or asocial, sorting in which each type of colloids assembles into isolated aggregates. For example, it has been shown with azobenzene-functionalized nanoparticles.[54] Two populations were functionalized with differently substituted azobenzenes, which undergo conformational change either under UV or blue light. Therefore, it was possible to selectively self-sort particular

population of nanoparticles within one mixture by applying light of a certain wavelength.[54] Asocial sorting has also been shown on micrometer-sized particles, namely silica microparticles.[67] For this two different types of self-complementary moieties that interact with each other through hydrogen bonds formation were tethered onto the particles. The self-sorting within one mixture was enabled by the UV-induced removal of protecting groups. Nonetheless, only one of the subpopulations could self-sort reversibly and could disperse upon addition of a competitive binder.[67]

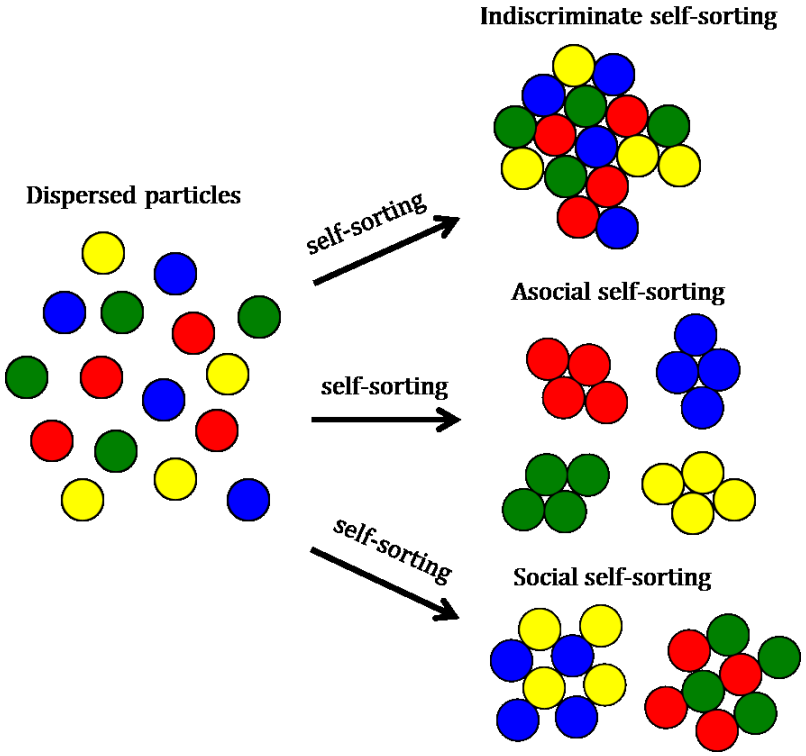

Figure 1.2 Different types of colloidal self-sorting. Figure is adapted and modified from reference[58]. Copyright @ 2017 John Wiley and Sons. Reprinted with permission from Angewandte Chemie International Edition.

iii) Social sorting: Complementary and orthogonal interactions allow achieving social self-sorting leading to the formation of separate and independent colloidal families within one mixture.[58, 65] Social self-sorting has been achieved by decorating one population of micrometer-sized colloids with α-cyclodextrines and azobenzenes and another population with β-cyclodextrines and ferrocene. This enabled first pair to interact with each other in the dark when the azobenzenes are in the *trans*-conformation and fit into the cavity of cyclodextrines. These complexes reversibly dissociate upon UV irradiation,

when azobenzene switches into its *cis*-state. The second pair can be reversibly switched by redox chemistry where the oxidized ferrocenium turns hydrophilic and is expelled from the β-cyclodextrine. These orthogonal interactions have been used to self-sort four populations of micrometer-sized particles into two distinct families of aggregates within one mixture.[58-59] Therefore, social self-sorting allows achieving high level of complexity within synthetic systems under tight control and is a promising approach to enable the assembly of protocells into prototissues with high complexity.

1.5 Protein patterns

Self-organized protein patterns and protein gradients control basic life processes, such as cell polarization or cell division.[68-70] An important feature of such protein patterns in nature is that they are highly dynamic and precisely regulated in space and time.[68-71] For example, in *E. coli* Min proteins regulate the cytokinesis by oscillating between the cell poles and creating protein gradients that localize the division machinery to the middle of the cell.[68-70] Another important example of protein gradients is the distribution of morphogens (Bicoid protein) along the anterior-posterior axis of the early *Drosophila* embryos. This gradient gives rise to the head and thorax formation.[72-73] Attempting to reconstitute such protein patterns as well as protein gradients in synthetic systems is, therefore, also of a great interest. Using minimal synthetic cells as a model allow to precisely control the parameters within the investigated system.[69]

Various methods have been established to produce such dynamic protein patterns *in vitro* in order to control and understand the underlying processes. However, most of the classical approaches to pattern molecules, such as lithography, micro-contact printing and chemical vapor deposition require multiple steps, harsh conditions, such as high temperature, UV light or non-physiological pH as well as the use of chemicals, which makes these methods not biocompatible.[74-76]

Light is the most promising stimulus as it has the advantage of providing the highest spatial and temporal resolution. Further, it is bio-orthogonal and

biocompatible in most wavelengths. Therefore, using light-responsive approaches for protein patterning is particularly promising.

There are several approaches that utilize unspecific adsorption of proteins to produce photopatterns on substrates. For example, it is possible to unspecifically photopattern proteins on solid substrates by locally heating and collapsing the thermoresposive polymer poly(N-isopropylacrylamid) (PNIPAM) with a beam of visible light.[77] This method provides high spatiotemporal control due to the nature of light. However, it does not provide high specificity as any proteins can adsorb on the surface when the PNIPAM is collapsed. Moreover, despite light being used as a stimulus, polymer actually collapses due to the temperature change caused by the light-to-heat conversion. This requires the use of high light absorbing material as a substrate, which makes the setup more complex.[77] Another protein patterning approach utilizing unspecific adsorption is based on decomposing ruthenium complexes with upconverting nanoparticles that convert near-infrared light into UV and visible light. This upconverted light can then induce cleavage of the ruthenium complexes, therefore, releasing the adsorbed proteins from the substrate.[78] However, the biggest drawback of this photon upconversion lithography method is its irreversible nature.

Other approaches utilize specific interactions to patter proteins with light. One of them is based on photocleavable nitrobenzyl caging groups. Photocleavable nitrobenzyl linkers have been used to block the Ni^{2+}-NTA (N-nitrilotriacetic acid) groups on the surface from interacting with His-tagged proteins. Upon UV light illumination the linker was cleaved allowing the His-tagged proteins to specifically bind to the Ni^{2+}-NTA groups.[79] Another Ni^{2+}-NTA-His-tag based approach uses multivalent derivative of NTA, so called trisNTA, that has been modified to be photoactivatable (PA-trisNTA).[80] Like in all the methods that rely on the de-caging of nitrobenzyl groups, the use of UV light is cytotoxic and the de-caging is irreversible, which does not allow for alteration of the protein patterns once formed.

The highly specific biotin-streptavidin interaction has been used to photopattern labeling agents directly on living cells.[81] For this photocaged

biotins were developed, which have reduced affinity for streptavidin in the dark but recover the affinity upon UV irradiation. These photocaged biotins allow fluorescent labeling of cells by illuminating the cells that were pre-labeled with this caged biotin in presence of streptavidin-conjugated fluorophores. Despite being highly specific, the limitations of de-caging methods are also true here, which limits their use in biological studies.

Further, azobenzenes and their derivatives have been used to produce reversible protein photopatterns based on the change in surface properties upon *cis-trans* isomerization.[82-83] For example, protein adsorption can be reversibly switched by light irradiation through the change in wettability of the substrate. Wettability is altered due to the difference in dipole moments between *trans* and *cis* conformations.[82] Yet, also these azobenzenes require UV light for the *trans* to *cis* isomerization (with the rare exception of red-shifted substituted azobenzenes)[84] and protein adsorption is unspecific.

In summary, a variety of methods to pattern proteins with light is already established. However, all these methods have drawbacks of either responding to UV light, which is damaging to biological molecules, or being unspecific or irreversible. Thus, there is still a need for a reversible, specific and biocompatible way to produce such protein patterns with high spatial and temporal precision.

1.6 Light sensitive proteins for optogenetic control

Light is crucial to life on Earth and is an essential resource for organisms throughout all kingdoms.[85] In nature, different living organisms have evolved a variety of photosensitive proteins in order to respond to changing light conditions. The field of optogenetics uses the broad spectrum of properties such light-sensitive proteins provide to control processes in cells using light as external stimulus.[85-87] Control with light provides not only outstanding spatial resolution due to its nature but also high temporal precision, which allows keeping up with the fast pace of biological processes.

There is a class of optogenetic proteins that utilizes light-induced dimerization or multimerization (based either on homo- or heterophilic interactions) as

their mode of action. These interactions are specific and for most of the proteins reversible, which provides dynamic switchability. There has been a substantial amount of work done on engineering the kinetic properties as well as broadening the range of binding affinities between such proteins. This offers high tunability and a wide selection of tools to control processes within the cells. Moreover, these light-sensitive proteins react to a particular colour/wavelength of light: blue (~470 nm), green (~530 nm), red (~650 nm), and far-red (~750 nm).[85-86, 88] Such particular activation windows provide orthogonality between these proteins, which allows addressing them selectively to activate a certain process. For example, the orthogonality of blue and red light sensitive proteins has been used to independently control the translocation from the cytoplasm to the plasma membrane and consequent activation of several classes of proteins within one cell on demand[89] or to selectively mediate cell-material contacts in the presence of other cells[90].

Despite neuronal optogenetics being an important field of its own, for example making use of light-sensitive ion channels opsins to regulate neural and muscle activity, it was not the focus of this thesis and will not be covered in the following chapters.[87, 91-94] In context of this thesis several light-sensitive dimerizing proteins from plants, fungi and cyanobacteria were used and, therefore, will be covered in the following sections.

1.6.1 Red light-responsive optogenetic proteins

1.6.1.1 PhyB/PIF protein pair

Phytochromes (Phy) are red/far-red absorbing photoreceptors (650 nm/750 nm respectively) from the plant *Arabidopsis thaliana*.[95-96] In plants phytochromes (PhyA-PhyE) regulate growth and development in response to changes in light conditions as well as circadian rhythms.[97-98] Phytochromes detect light through the photoisomerization of a covalently-bound chromophore. In nature this chromophore is phytochromobilin, however it is often being substituted by a commercially available related tetrapyrrolle such as phytocyanobilin (PCB). Phy can exist in two different states: Pr (red light absorbing) and Pfr (far-red light absorbing). In the Pfr form the protein can heterodimerize with members of the basic helix-loop-helix

family of transcription factors, called phytochrome interaction factors (PIFs). The Pfr form can be reversed to the Pr form upon far-red light irradiation, which also leads to the dissociation from PIFs (Figure 1.3).[85, 99]

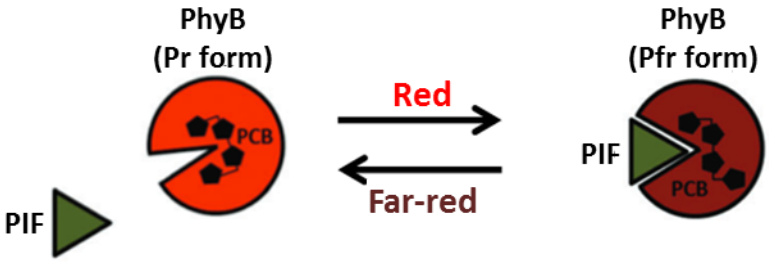

Figure 1.3 Schematic representation of red light induced interactions (PhyB /PIF system). Upon red light irradiation chromophore (PCB) undergoes a conformational change that causes switching from Pr (red light sensing form) that does not interact with the PIF to Pfr (far-red light sensing form) that can interact with the PIF. Figure is adapted and modified from reference[85]. Copyright @ 2013 Royal Society of Chemistry. Reprinted with permission from Molecular BioSystems.

The interaction between PhyB and PIF6 (phytochrome interacting factor 6, residues 1-100) has been used in a variety of organisms to control different processes with red light. Firstly, PhyB and PIF6 have been used to control the localization of proteins[89, 99-103], organelles[104] or even nuclear translocation of viruses[105] inside mammalian and yeast cells as well as in zebrafish. The light controlled localization can be used to activate and deactivate signalling pathways and protein function. For example, the localization of the guanine nucleotide exchange factors (GEFs) was controlled by fussing it to PIF6 and tethering PhyB to the plasma membrane. The localization of GEFs to the plasma membrane with red light led to the activation of the small G-proteins of the Rho-family, which in turn generated morphological changes in mammalian cells.[99] Secondly, the PhyB/PIF6 interaction has been used to regulate gene expression in mammalian[106-109] and yeast[110-113] cells as well as in zebrafish[106] and in plants[114]. For example, nuclear-targeted PhyB was fused to the VP16 transactivation domain and PIF6 to the rest of the split transcription factor consisting of tetracycline repressor TetR. Upon red light irradiation the transcription factor was reversibly reconstituted, triggering reporter expression.[85, 107] Next, this light-switchable interaction has been used to control

and study the signal transmission in the mitogen-activated protein kinase (MAPK) cascade. When fusing PhyB/PIF to the signaling proteins, it was possible to control their recruitment and activate isolated signalling nodes within the cascade to observe their specific influence on it.[115] Further, the PhyB/PIF6 interaction has recently been used in combination with a blue light switchable protein pair (cryptochrome2 with its specific interaction partner) as a contact mediator to orthogonally mediate reversible cell-substrate contacts.[90]

1.6.1.2 Cph1 protein

Cph1 is a phytochrome-like protein from cyanobacteria *Synechocystis*. It is a red/far-red light absorbing protein that can be converted between red light absorbing Pr state and far-red light absorbing Pfr state. Similarly to plant phytochromes, apo-Cph1 assembles with the tetrapyrrole phycocyanobilin (PCB) resulting in a holoprotein that homodimerizes upon red light irradiation (Figure 1.4). Upon far-red illumination dimers disassemble back to monomers.[116-117]

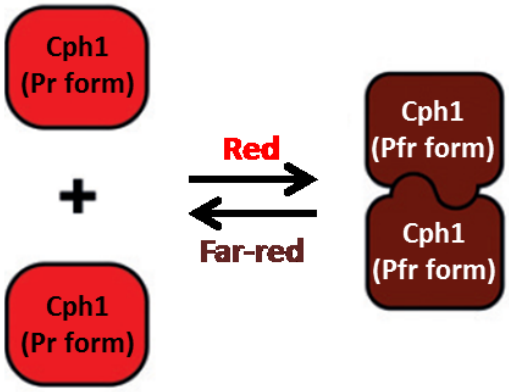

Figure 1.4 Schematic representation of the Cph1 homodimerization. Upon red light irradiation a mainly monomeric Pr form is converted to a mainly homodimeric Pfr form. Figure is adapted and modified from reference[116]. Copyright @ 2016 John Wiley and Sons. Reprinted with permission from Angewandte Chemie International Edition.

Cph1 has mostly been used in *E. coli* to control the gene expression[100, 118-119] and protein interactions[120] with light. For example, Cph1 has been used to selectively activate bacterial gene expression in biofilms gaining complex chemical images on them with high spatiotemporal resolution.[100] Cph1 can also be used in mammalian cells to control signaling pathways with red light.[116] As it was demonstrated before, for many receptor tyrosine kinases (RTK) homodimerization is required to initiate associated downstream signaling.[121]

Therefore, Cph1 was fused to a C-terminal of the murine fibroblast growth factor receptor 1 (mFGFR1), which was missing its natural ligand binding domain to yield a red light activatable RTK. Strong pathway activation was observed upon red light illumination.[116]

1.6.2 Blue light-responsive optogenetic proteins

Light-oxygen-voltage (LOV) domain is a common blue light responsive domain from the phototropin protein family that can be found in bacteria, fungi, algae or plants (such as *Arabidopsis thaliana* and *Avena sativa*).[85, 122-123] Blue light illumination of the LOV domain leads to a covalent bond formation between an embedded flavin cofactor and the key cysteine residue that leads to a reversible conformational change within the protein. Different LOV domain variants were engineered to broaden and optimize the kinetic rage as well as the difference between the activated and non-activated states.[124-127]

1.6.2.1 iLID/Nano protein pair

The improved light-inducible dimer (iLID) has been engineered from a naturally occurring LOV2 domain of phototropin1 from the plant *Avena sativa* (*As*LOV2). *As*LOV2 consists of a core per-arnt-sim (PAS) fold with an α-helix on each of the N- and C-termini. Under blue light illumination, a specific cysteine residue in the core of *As*LOV2 forms a covalent bond to the flavin mononucleotide cofactor (FMN). This reaction causes structural change in the PAS fold and leads to the unfolding of the C-terminal α-helix (called Jα-helix). The bond to the cofactor breaks and the helix refolds spontaneously within seconds to hours in the dark.[124, 128] The re-engineered version of *As*LOV2 domain, iLID, contains a naturally occurring peptide, SsrA, form *E. coli* (seven amino acids) in its Jα-helix that can bind an adaptor protein, SspB. In the dark the SsrA peptide is hidden in the Jα-helix of *As*LOV2, and the binding of SspB is sterically hindered. Blue light irradiation (488 nm) results in the unfolding of the Jα helix and allows the interaction to occur, yielding a light-inducible dimerization pair (LID).[124] Further engineering led to the development of an improved version of LID (improved light-inducible dimer, iLID) that has larger difference between the binding affinity to SspB in dark and upon blue light

illumination. There are three variants of SspB interaction partner: SspB-Nano (wild type SspB), which switches its binding affinity to iLID from 132 nM under blue light to 4.7 μM in the dark (36-fold change); SspB-Micro (point mutation R37Q in wild type SspB), which switches from 800 nM under blue light to 47 μM in the dark (58-fold change); and SspB-Milli (point mutation A58V in SspB-Micro), which switches from 3 μM under blue light to 125 μM in the dark (42-fold change). All of the interaction pairs revert to dark state within minutes (Figure 1.5).[124, 126, 129]

iLID with its interaction partners have been used to control protein localization[126, 129-132], activate signaling pathways[133] and transcription[134], induce cell migration[135-136] as well as to self-assemble oligomeric enzymes[137] and mimic RNA granules by forming protein hydrogels[138]. For example, iLID/Micro dimerization has been used to regulate the GTPase signaling through the translocation of guanine nucleotide exchange factors (GEFs) to the plasma membrane.[126] Active Cdc42 (a small GTPase from a Rho family) is responsible for bundled actin formation and filopodial morphology. When fusing the Cdc42-activating GEFs, such as diffuse B-cell lymphoma homology (DH) and Pleckstrin homology (PH) domains, to SspB it was possible to recruit them to the membrane-tethered iLID.[126, 139] This led to the Cdc42 activation and consequent ruffling and lamellipodia formation upon blue light illumination. This example shows that the iLID/Nano interaction can be used for local activation of GTPase signaling that leads to a change in actin cytoskeleton dynamics and cell morphology.[126] Further, asymmetric light-induced localization and activation of Cdc42 on one side of the cell was used to generate polarized signaling, which led to consequent cell migration.[135] Moreover, iLID/Micro interaction has also been used to reversibly self-assemble oligomeric enzymes, such as nitralases, in a scaffold-free manner. For this iLID-fused nitralase was mixed (*in vitro*) or co-expressed (*in vivo*) with Micro protein. Upon blue light illumination, optogenetic proteins dimerized causing the nitralase to assemble into supramolecular structures both *in vitro* in a cell-free solution and *in vivo* in *E. coli*.[137]

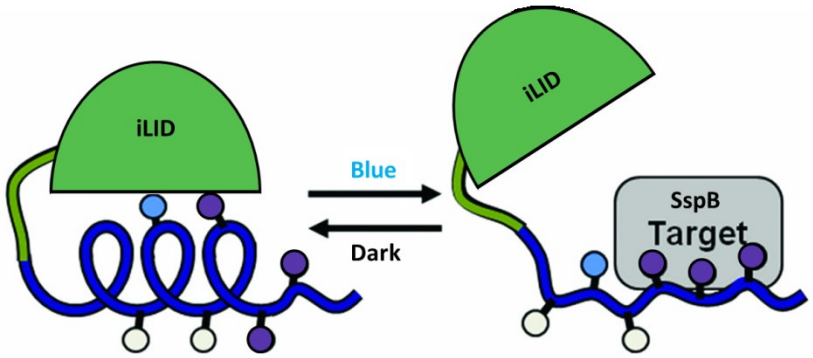

Figure 1.5 Schematic representation of improved light-induced dimer based on AsLOV2 domain. Residues important for Jα helix interactions with the core are depicted in cyan; residues important for SsrA/SspB interaction are depicted in purple (SsrA peptide). Upon blue light irradiation the Jα helix unfolds and SsrA peptide is available to interact with the adaptor protein SspB. Figure is adapted and modified from reference[124]. Copyright @ 2012 Elsevier. Reprinted with permission from Chemistry & Biology.

1.6.2.2 Magnets and Vivid proteins

The proteins nMagHigh and pMagHigh heterodimerize under blue light and have been engineered from the Vivid (VVD) protein.[125] VVD is a small fungal photoreceptor from *Neurospora crassa* that is composed of a LOV domain and uses flavin adenine dinucleotide (FAD) as a cofactor. VVD can reversibly homodimerize under blue light.[125,128] To gain a heterodimerizer out of VVD, at first, positive and negatively charged amino acids were introduced into its homodimer interface (from Ile47 to Asn56, called Ncap). This adds electrostatic interactions to the protein-protein interactions and as proteins of opposite charge preferentially interact, they were named Magnets.[125] Proteins with negatively charged amino acids were called nMag (I52R/M55R) and positively charged amino acids were called pMag (I52D/M55G). Mutations in the PAS core can alter the interactions strength and dynamics of VVD protein variants. The mutations M135I and M165I, called nMagHigh and pMagHigh respectively, slow down the dark reversion ($t_{1/2}$=1.8 hours for nMag/pMag vs. $t_{1/2}$=4.7 hours for nMagHigh/pMagHigh) and have higher binding affinities to each other under blue light compared to nMag/pMag (K_d=1.1*10^{-4} for nMag/pMag vs. K_d=4.1*10^{-5} for nMagHigh/pMagHigh) (Figure 1.6 a-b). Other mutations have also been introduced to shorten the reversion kinetics of the Magnets

(I85V, $t_{1/2}$=4.2 minutes, K_d=2.7*10^{-3} for nMagFast1/pMagFast1 and I74V/I85V, $t_{1/2}$=25 seconds, K_d=2.8*10^{-2} for nMagFast2/pMagFast2 versions). The light-induced dimerization of all these variants can be reversed in the dark.[125]

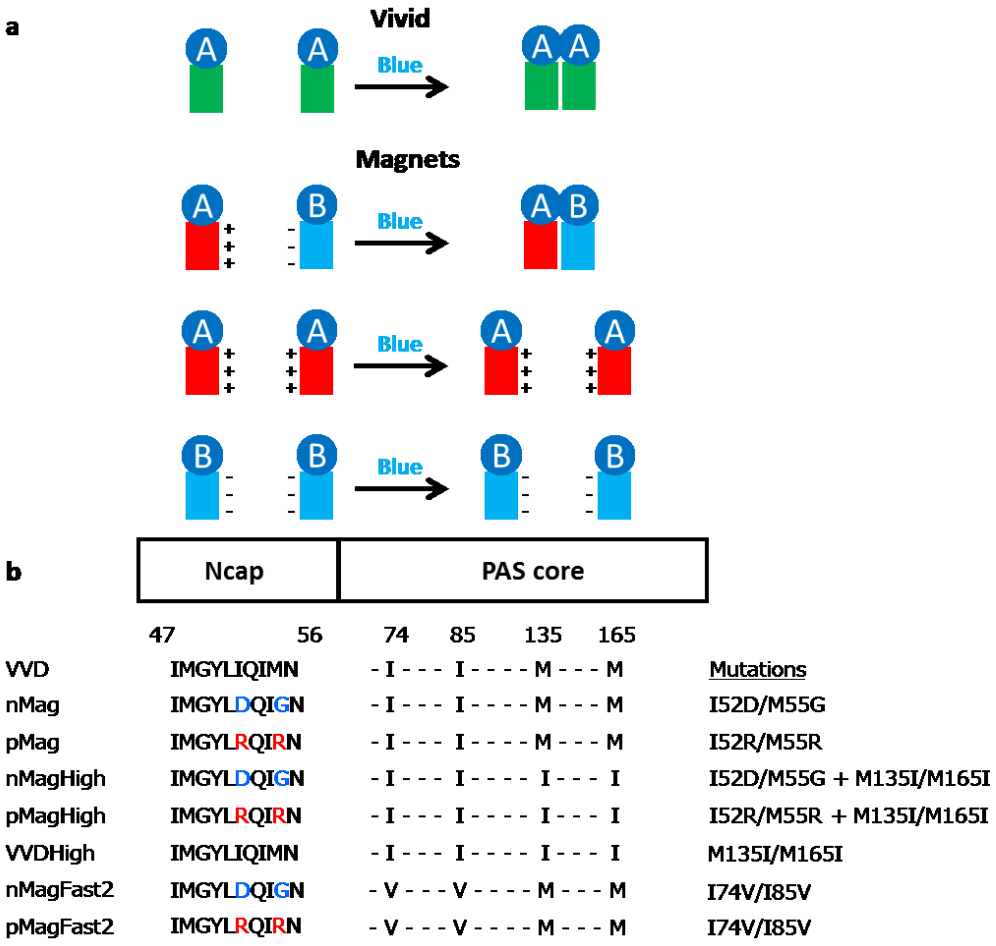

Figure 1.6 Schematic representation of: a) the interactions between VVD proteins and Magnet proteins; b) the mutations introduced into VVD to gain heterodimerizing proteins called Magnets and improved homodimerizing protein called VVDHigh. Figure is adapted and modified from reference[125]. Copyright @ 2015 Springer Nature. Reprinted with permission from Nature Communications.

VVD homodimerization has been extensively used to control the gene expression by either inducing the recruitment of transactivators to promoters[109, 140-143] or by using polymerase-based switches[144] in mammalian, bacterial and fungal cells as well as in mice. For example, by fusing split units of T7 RNA polymerase to VVD it was possible to induce the gene expression in *E. coli* with blue light.[144] Further, VVD protein has also been used to control the protein activation in mammalian cells.[145-146] Notch protein activity has been

induced in an oscillating manner with pulses of blue light to control the differentiation of neural progenitors.[146]

Magnet proteins have been successfully used to optogenetically control the transcription activation[147], genome editing[148-149] and to activate proteins[89] in mammalian cells and in mice. For example, Magnets were used to regulate CRISPR-Cas9 genome editing in human cells.[148] For this an engineered photoactivatable Cas9 (paCas9) that consists of two split Cas9 fragments fused to Magnets was produced and the Cas9 could be reconstituted in response to blue light. paCas9 could be used to induced targeted genome sequence modifications and withdrawing the blue light switched the genome editing activity off.[148] Further, Magnets in combination with an orthogonal red light sensitive protein dimerizer PhyB/PIF6 have been used to control the plasma membrane recruitment of the Gα proteins from the cytosol through the heterodimerization of the optogenetic proteins. This translocation led to the selective activation of two classes of proteins with light of a certain wavelength: either phospholipase C-beta activation leading to the cytosolic Ca^{2+} release or adenylyl cyclase activation that led to the conversion of adenosine triphosphate into cyclic adenosine monophosphate and pyrophosphate.[89] Recently, Magnets have also been employed as contact mediators to control the bacterial adhesion to the substrates with light.[150]

Table 1.1 Light-induced switching of optogenetic proteins. Table is adapted and modified from reference[86]. Copyright @ 2017 Elsevier. Reprinted with permission from Biochimica et Biophysica Acta (BBA) - Molecular Cell Research.

Photosensitive Proteins	Activation	Relaxation	Cofactor	Activation time	Inactivation time
iLID	Blue light (470 nm)	Thermal (dark)	FMN	seconds	seconds to minutes (variants available)
VVD	Blue light (470 nm)	Thermal (dark)	FAD	seconds	hours
Magnets	Blue light (470 nm)	Thermal (dark)	FAD	seconds	seconds to hours (variants available)
PhyB	Red light (650 nm)	Far-red light (750 nm)	PCB	milliseconds	milliseconds
Cph1	Red light (650 nm)	Far-red light (750 nm)	PCB	milliseconds	milliseconds

In summary, optogenetics offers a wide range of light-sensitive proteins that reversibly interact upon illumination with light of different wavelength (Table 1.1). These proteins overcome the majority of the drawbacks that are present in the existing stimuli-responsive systems (Table 1.2). Therefore, these proteins are a promising and versatile tool in the synthetic biology toolbox that can be implemented in order to control various processes within the synthetic cell as well as the interactions between different synthetic cell-mimics with high spatiotemporal resolution.

Table 1.2 Characteristics of different stimuli-responsive strategies.

Characteristics	Optogenetic proteins	Thermo-responsive strategies (DNA-glue; peptide/polymer-based)	Light-responsive strategies (small molecules)	Light-responsive strategies (host/guest)
High spatial control	Yes	No	Yes	Yes
High temporal control	Yes	No	Yes	Yes
Reversibility	Yes	Yes	Yes	Yes
Bio-orthogonality and biocompatibility	Yes	No	No	No
Specificity	Yes	Yes/No	No	Yes
Aqueous environment	Yes	Yes	No	No

Chapter 2: Results and Discussion

2.1 Part I: Light-controlled self-assembly of cell-like compartments

Parts of the results and discussion in the following chapter are published by Chervyachkova, E. and Wegner, S. V. (*ACS Synth. Biol.* 7, 1817-1824, 2018)

2.1.1 Motivation and Objectives

The goal of this study was to use various photoswitchable proteins to control the self-assembly and self-sorting of colloidal cell mimics with light. In nature the self-assembly process is dynamic, reversible and precisely controlled in time and space. The aim was to capture these fundamental features of interactions between cells in a synthetic system. The idea to use these photoswitchable proteins comes from the field of optogenetics, where a number of such light sensitive proteins have recently been developed to control various processes inside a cell, such as gene activation, protein localization, enzyme activity, protein clustering etc., using visible light.[85, 99, 126, 151-152] For this purpose first two specific photoswitchable protein pairs were used, namely iLID/Nano and nMagHigh/pMagHigh. These two protein pairs interact under blue light of low intensity, dissociate from each other in the dark and operate in biocompatible conditions. Our hypothesis was that, when immobilized on colloidal cell-mimics, the orthogonality and high specificity of these protein interactions would enable the social self-sorting of micrometer-sized protocells in a four-component mixture under blue light control.

The next objective was to expand the portfolio of assembly modes and develop self-assemblies that respond to different wavelengths of light using photoswitchable proteins that respond to red/far-red light, such as PhyB/PIF6, and have a different dimerization mode (homodimerization), using the proteins VVDHigh and Cph1. These proteins can be used to control the self-assembly of colloidal cell-mimics and potentially combined together to further increase complexity in synthetic setups (Figure 2.1.1).

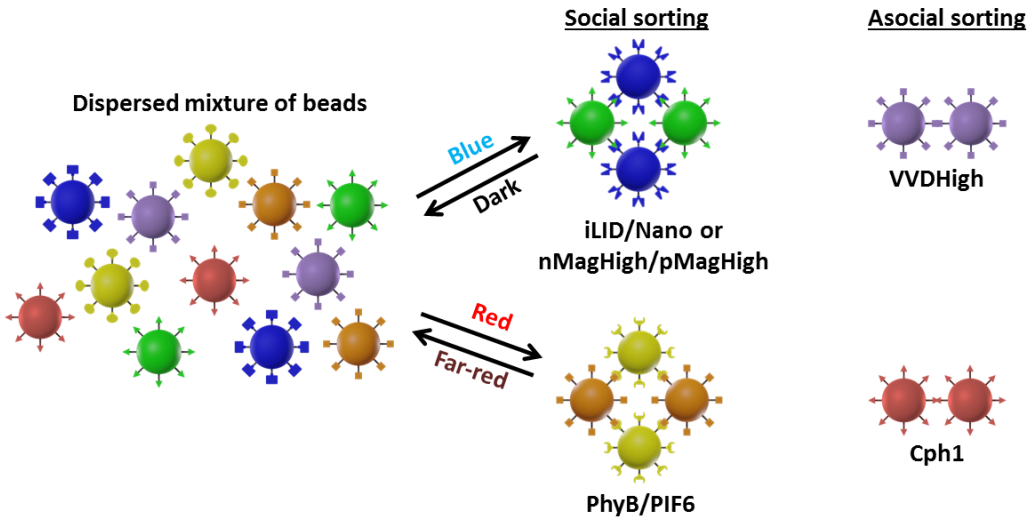

Figure 2.1.1 Schematic representation of the project's objectives.

2.1.2 Blue light-dependent self-assembly of colloids based on heterodimerizing proteins iLID/Nano and nMagHigh/pMagHigh

The light-dependent self-assembly of synthetic protocells using iLID/Nano and nMagHigh/pMagHigh protein pairs was first studied. Despite these proteins being used to control various processes with light in living cells,[89, 125-126] they have not yet been used to induce light-dependent self-assembly of particles in synthetic systems. All the proteins were recombinantly expressed and purified from *E. coli* and contained a His6-tag, which allowed immobilizing them on 2 µm in diameter Ni^{2+}-NTA functionalized polystyrene beads. First, using His-tagged green fluorescent protein (His-GFP) as a model the number of proteins per bead was calculated to be between 200 and 300 using two different methods (Figure 2.1.2 b-c). In the first method, His-GFP was immobilized on the beads, the beads were spun down and the fluorescence intensity of His-GFP in the supernatant was measured using the microplate reader. From this the amount of His-GFP bound on the beads and the number of proteins per beads was calculated using a calibration curve with known His-GFP concentrations (Figure 2.1.2 b). In the second method, His-GFP was first immobilized on the beads, and then everything that was bound on them was denatured and run on an SDS-PAGE together with known His-GFP concentrations. Using ImageJ software the intensity of the bands was evaluated and the amount of His-GFP bound on the beads and the number of proteins per beads was calculated (Figure 2.1.2 c). Moreover, flow cytometry experiments showed a single

population of His-GFP functionalized beads with a significantly higher fluorescence signal compared to non-functionalized beads, showing a homogenous functionalization of the colloids (Figure 2.1.2 a).

Next, the ability of two different blue light sensitive protein pairs, iLID/Nano and nMagHigh/pMagHigh, to independently induce aggregation of micrometer-sized colloids was investigated (Figure 2.1.3 a). To do this, Ni^{2+}-NTA functionalized beads (Figure A1) were functionalized separately with each of the purified proteins through their His-tags (Figure A2). To study the light-dependent self-assembly, bead populations of iLID and Nano functionalized beads as well as populations of nMagHigh and pMagHigh functionalized beads were mixed in equal proportions and incubated either in the dark or under blue light (460 nm) under low agitation (50 rpm) to prevent beads from settling. The samples were fixed with 10% (w/v) paraformaldehyde (PFA) prior to imaging them using the bright field microscopy (40x magnification). There was significantly more clustering in the samples that were exposed to blue light for 2 hours compared to the samples that were kept in the dark (Figure 2.1.3 b-c).

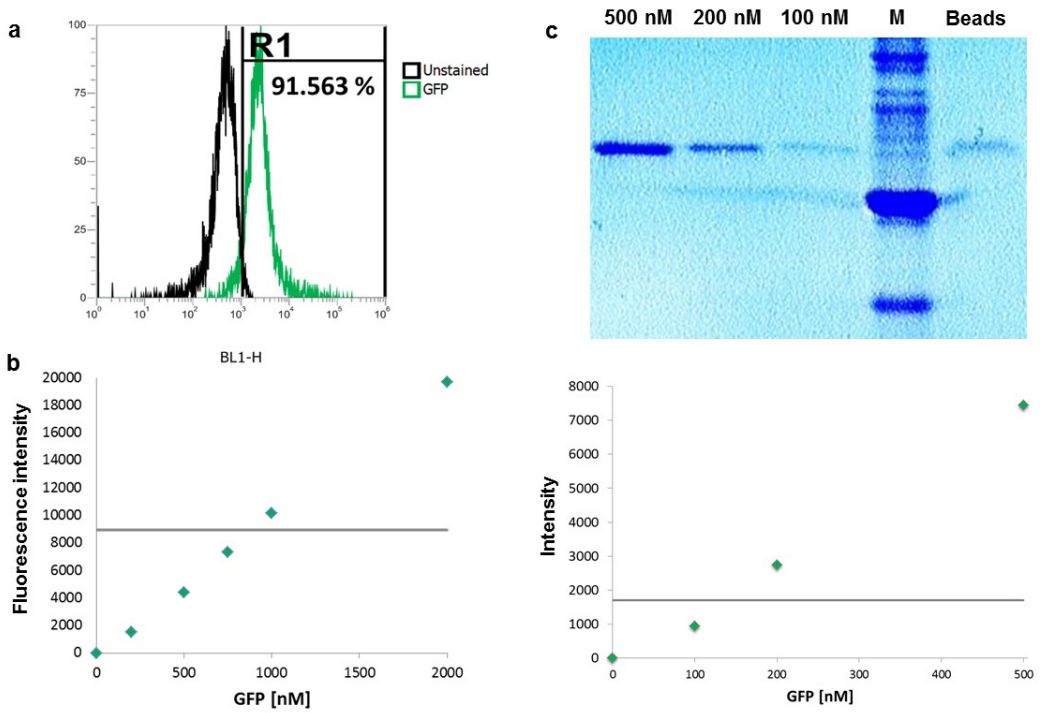

	Protein in the supernatant [nM]	Protein bound [nM]	Number of proteins per bead
Beads	918	82	≈ 220

	Protein bound [nM]	Number of proteins per bead
Beads	130	≈ 320

Figure 2.1.2 Characterization of the bead functionalization with proteins using His-GFP as model protein: (a) Shift in fluorescence intensity for GFP-functionalized beads measured using flow cytometry. (b) Quantification of the number of proteins per bead through the fluorescence intensity of the unbound His-GFP protein (grey line) measured using the microplate reader. (c) Quantification of the number of proteins per bead through the protein band intensity on the SDS-PAGE. The intensity of the protein bound on beads is depicted by grey line; the intensity of the calibration bands is depicted by green rhombus.

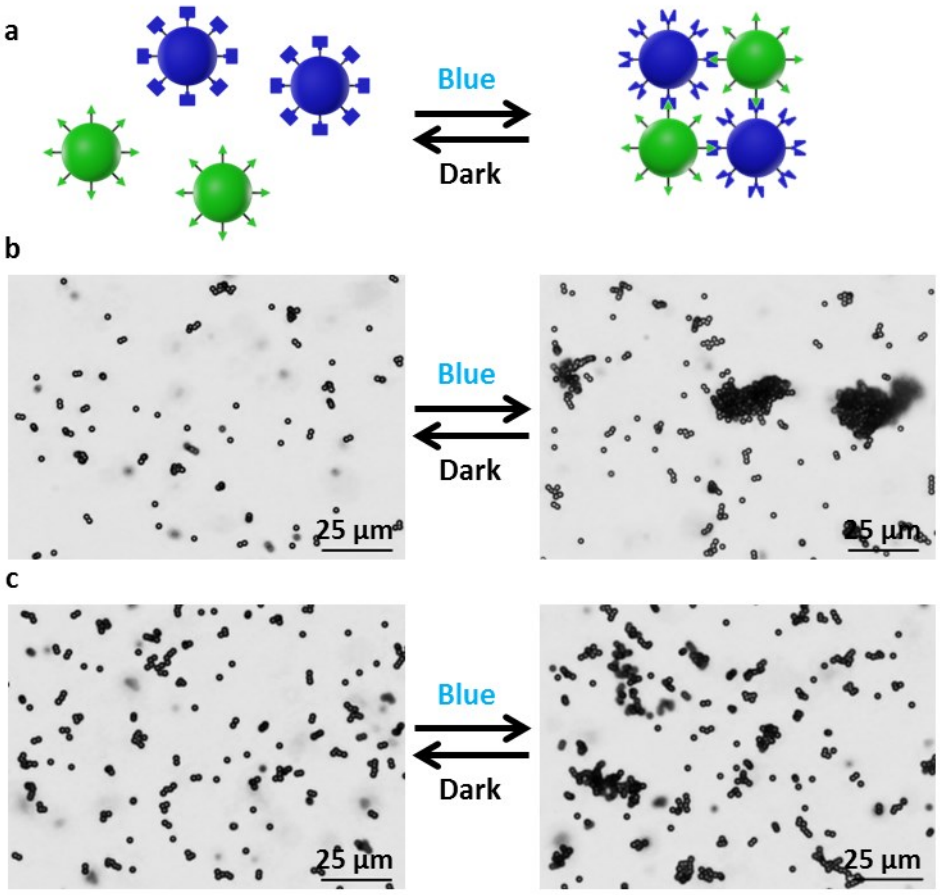

Figure 2.1.3 Blue light-dependent self-assembly of polystyrene beads. (a) iLID (or nMagHigh) functionalized beads (blue) and Nano (or pMagHigh) functionalized beads (green) self-assemble under blue light due to the blue light-dependent heterodimerization of these proteins. (b) Bright field images of a 1:1 mixture of iLID and Nano functionalized beads in the dark and under blue light. (c) Bright field images of a mixture of nMagHigh and pMagHigh functionalized beads in the dark and under blue light.

It was previously reported that both of the protein pairs iLID/Nano and nMagHigh/pMagHigh, when used to control protein interactions in the cell, interact with each other within a few minutes when exposed to blue light.[125-126] However, both the immobilization of the proteins on the beads as well as the self-assembly process itself can change the dynamics. As we expected that protein immobilization leads to slower dynamics, the aggregation ratios were compared between the samples incubated in the dark or exposed to the blue light at different time points ranging from 15 minutes to 2 hours for both of the protein pairs (Figure 2.1.4 a-b). For all the conditions the aggregation ratio was

calculated by dividing the area of clusters (aggregates with a projected area bigger than 10 beads) by the total area of all beads in the same bright field image.[153] After 30 minutes both iLID/Nano as well as nMagHigh/pMagHigh functionalized bead mixtures showed no difference in clustering. However, after 1 hour significantly more clusters were formed under blue light compared to the dark. After 2 hours the aggregation levels were reaching a plateau; therefore, the 2 hour time point was chosen as an analysis point for the future experiments. One should note that the protein functionalization of beads has an effect on the bead aggregation. First, beads aggregate to a certain extent (aggregation ratio ≈ 17%) as soon as they are functionalized with proteins independent of the type of protein on the bead, indicating unspecific interactions between the proteins on the beads (Figure 2.1.4 a-b). Second, the non-functionalized beads do not aggregate significantly and remain dispersed in buffer over time, demonstrating their colloidal stability and proving that the observed aggregation is due to the protein functionalization (Figure 2.1.4, orange line). As both iLID/Nano as well as nMagHigh/pMagHigh also have some affinity to each other in the dark (which increases under blue light illumination 36- and 17- fold, respectively),[125-126] the beads functionalized with complementary interaction partners also aggregate to some extent in the dark over the 2 hours incubation, although significantly less and slower than under the blue light.

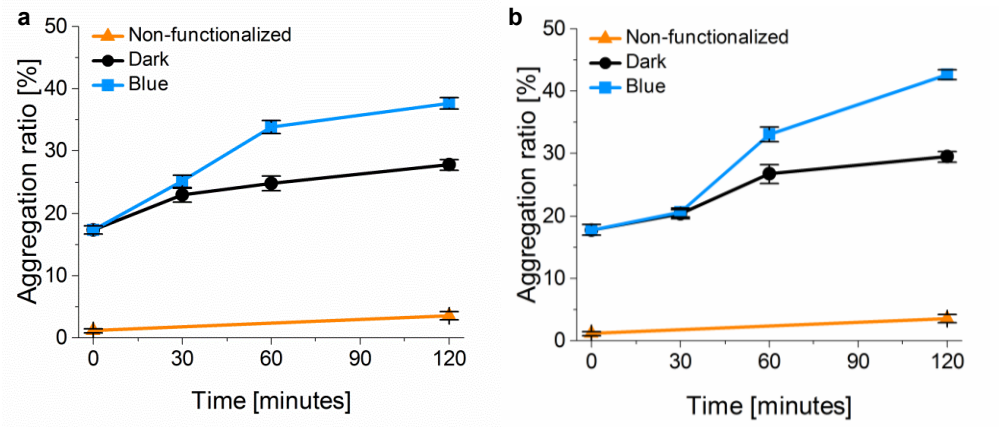

Figure 2.1.4 Bead aggregation dynamics of: a) iLID/Nano and b) nMagHigh/pMagHigh protein functionalized beads. Samples kept in the dark are depicted in black; samples kept under blue light are depicted in blue; non-functionalized beads are depicted in orange. Error bars are the standard error of the mean from > 30 images.

At the time point t=2 hours both protein pairs show higher aggregation ratios under blue light than in the dark. The aggregation ratio of the iLID/Nano pair increased from 27% in the dark to 37% under blue light (10% difference), while for the nMagHigh/pMagHigh pair the aggregation ratio increased from 30% in the dark to 42% under blue light (12% difference) (Figure 2.1.5 a-b). This shows that the blue light-dependent interactions between iLID and Nano as well as nMagHigh and pMagHigh are sufficiently strong to induce light-dependent self-assembly of micrometer-sized beads. In addition, the number of clusters and their average size was calculated for both of the protein pairs after 2 hours of aggregation either in the dark or under the blue light. Both of these parameters separately indicate the clustering degree. For both protein pairs the number of clusters as well as their average size was significantly higher under blue light illumination than in dark (Figure 2.1.5 c-f). Moreover, the blue light-dependent self-assembly mediated by these two blue light switchable protein pairs exhibits comparable aggregation behavior, despite the differences in the interactions between proteins.

For both of the blue light-sensitive proteins iLID and nMagHigh other interaction partners with lower binding affinities are described in the literature.[125-126] For iLID protein there is an interaction partner called Micro, which switches from 800 nM under blue light to 47 µM in the dark (compared to Nano that switches from 132 nM under blue light to 4.7 µM in the dark).[126] Likewise for nMagHigh protein there is an interaction partner called pMag, which has lower affinity and faster dissociation kinetics compared to pMagHigh.[125] The blue light dependent interaction pairs iLID/Micro and the nMagHigh/pMag were also studied to understand if these interactions are sufficiently strong to induce the bead aggregation. However, in both cases no significant light-induced bead aggregation was observed, which is probably due to the lower protein affinities to each other.

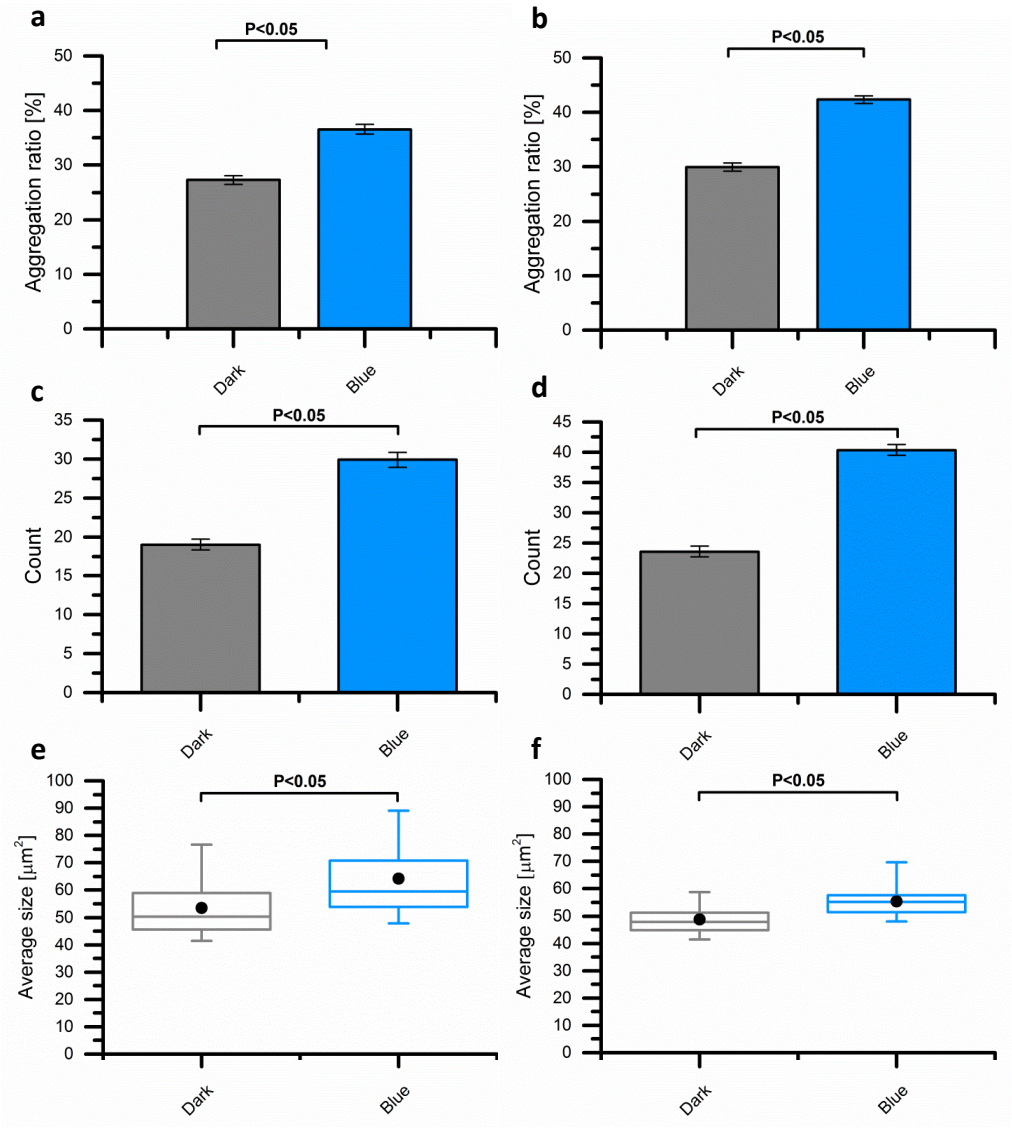

Figure 2.1.5 a-b) Light-induced aggregation of the beads functionalized with: a) iLID/Nano protein pair and b) nMagHigh/pMagHigh protein pair. c-d) Cluster number for: c) iLID/Nano protein pair and d) nMagHigh/pMagHigh protein pair. e-f) Average cluster size for: e) iLID/Nano protein pair and f) nMagHigh/pMagHigh protein pair. Samples kept in the dark are depicted in grey; samples kept under blue light are depicted in blue. Mann-Whitney test (significance level 0.05) was performed to analyze the statistical difference. Error bars are the standard error of the mean from > 60 images.

As the extent of protein interaction also depends on the intensity of blue light, its effect on the bead aggregation was investigated (Figure 2.1.6 a-b). For this, the mixtures of iLID/Nano and nMagHigh/pMagHigh were incubated for 2 hours under different intensities of blue light (adjusted by using neutral density filters). The blue light intensity of 0.7 mW/cm^2 was sufficient for both protein pairs to achieve maximal aggregation but already at 0.5 mW/cm^2 the blue light

dependent aggregation decreased. Increasing the light intensity up to 1.0 mW/cm² did not lead to an increase in bead aggregation. This shows the tight light control and confirms that non-toxic low intensities are enough to induce bead self-assembly. By working in this tight range it is possible to control the aggregation by modulating the light intensities.

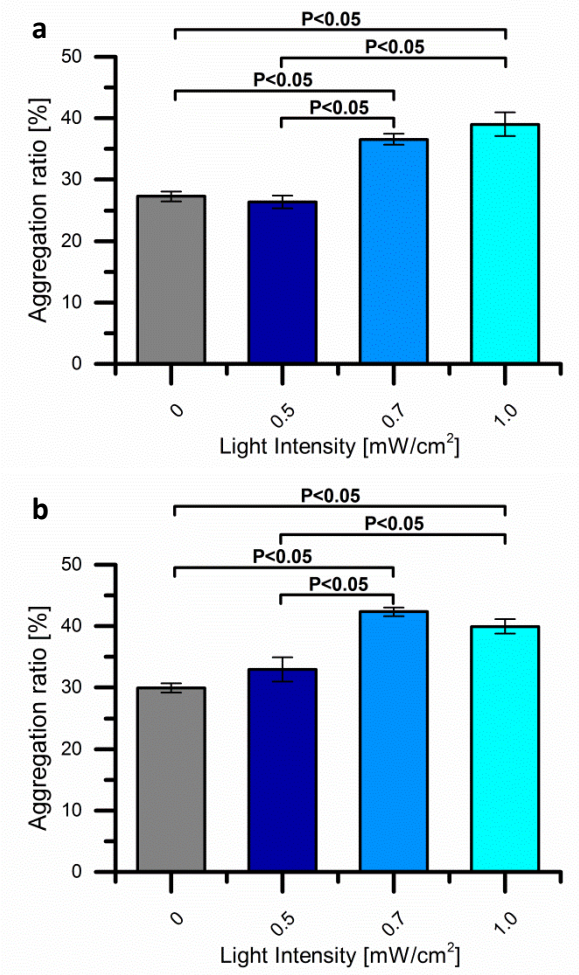

Figure 2.1.6 Bead aggregation dependence on the intensity of blue light: a) iLID/Nano protein pair and b) nMagHigh/pMagHigh protein pair. The standard blue light intensity used in all other experiments is 0.7 mW/cm². One-Way ANOVA test (significance level 0.05) was performed to analyze the statistical difference followed by Dunn-Sidak post hoc test (significance level 0.05). Error bars are the standard error of the mean from > 15 images.

2.1.3 Light-dependent self-assembly is based on specific heterodimerization

As one of the main goal of this work was to achieve the social self-sorting in mixtures beads that each display one of the four proteins, it was important to

prove that self-assembly induced by both of the protein pairs is based on the specific heterodimerization and not homodimerization. To distinguish, which of the two interaction modes is responsible for the self-assembly, complementary proteins were immobilized on fluorescently pre-labeled green (Nano or pMagHigh) and red (iLID or nMagHigh) polystyrene beads through the His-tag-Ni^{2+}-NTA interaction. The aggregation behavior of each of the protein pairs was then investigated as described above (chapter 2.1.2). Confocal microscopy showed that for both photoswitchable protein pairs, green and red fluorescently labeled beads strongly intermixed and formed heterogeneous clusters, demonstrating that heterodimerization is responsible for the blue light-dependent self-assembly (Figure 2.1.7 a-b). Moreover, the light-dependent self-assembly of beads that were functionalized with only one protein at a time was quantified to assess the protein homodimerization (Figure 2.1.7 c-f). For all the proteins the aggregation ratio of the samples exposed to blue light was comparable to the aggregation ratio in the dark and there was no blue light-dependent bead aggregation.

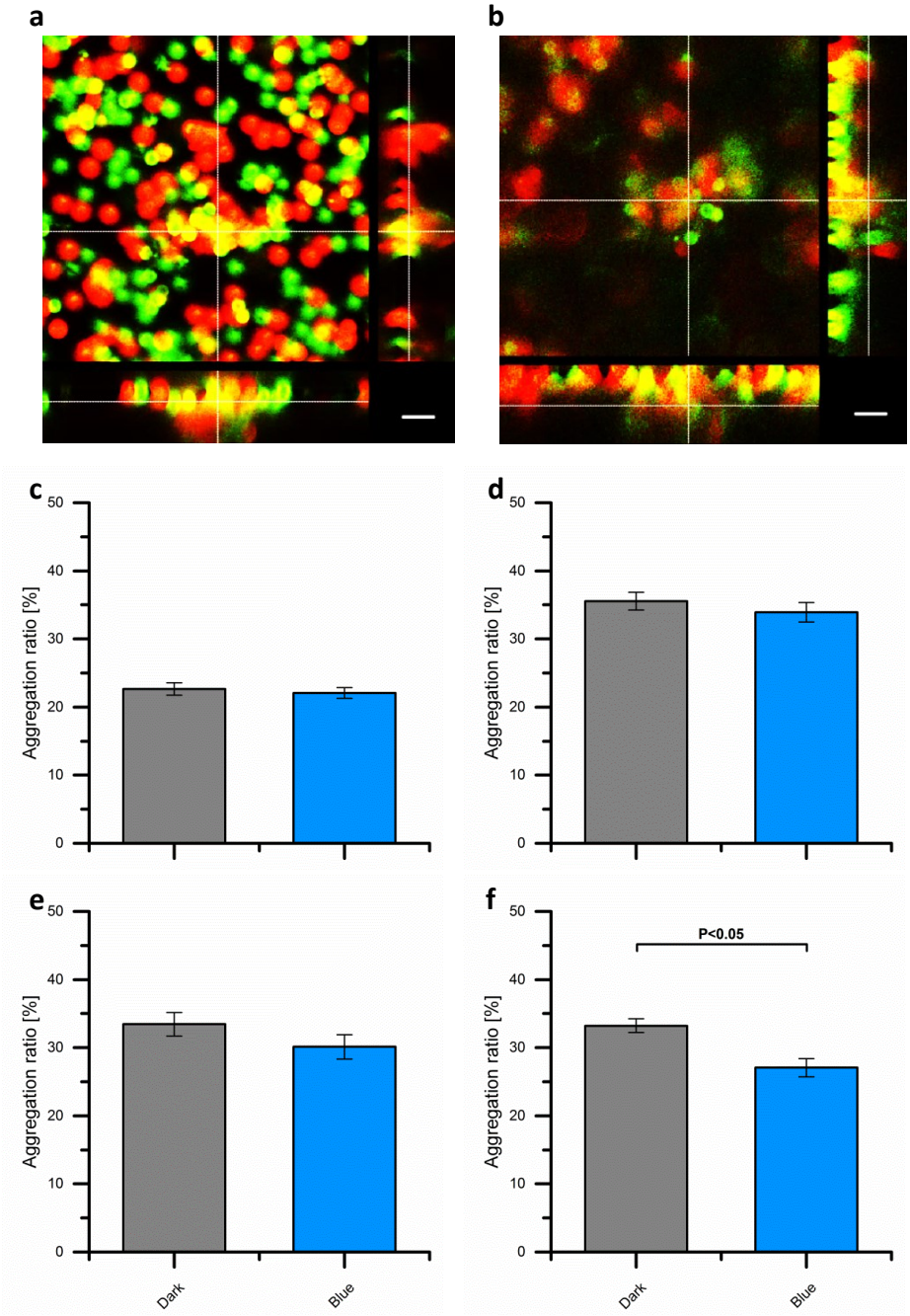

Figure 2.1.7 a-b) Confocal fluorescence microscopy images: a) 3D clusters formed under blue light with iLID (red) and Nano (green) functionalized beads and b) nMagHigh (red) and pMagHigh (green) functionalized beads. The scale bars are 5 µm. c-f) Homodimerization of: c) iLID; d) Nano; e) nMagHigh and f) pMagHigh functionalized beads. Mann-Whitney test (significance level 0.05) was performed to analyze the statistical difference. Error bars are the standard error of the mean from > 40 images.

To assure that the light dependent self-assembly of beads is due to the specific interaction of the blue light depended interaction partners, the competitive binding to the soluble protein was investigated in order to see if it can prevent the bead aggregation. For this the bead aggregation behavior after 2 hours was studied for both protein pairs in presence of an excess of soluble protein (1 µM of interaction partner in each case). Indeed, when iLID or Nano protein was added to the iLID/Nano bead mixture and nMagHigh or pMagHigh was added to the nMagHigh/pMagHigh bead mixture, light dependent aggregation was ceased (Figure 2.1.8 a-d). In conclusion, for both protein pairs the blue light-dependent self-assembly is a result of the specific heterodimerization of the protein pairs and occurs not due to the unspecific homodimerization.

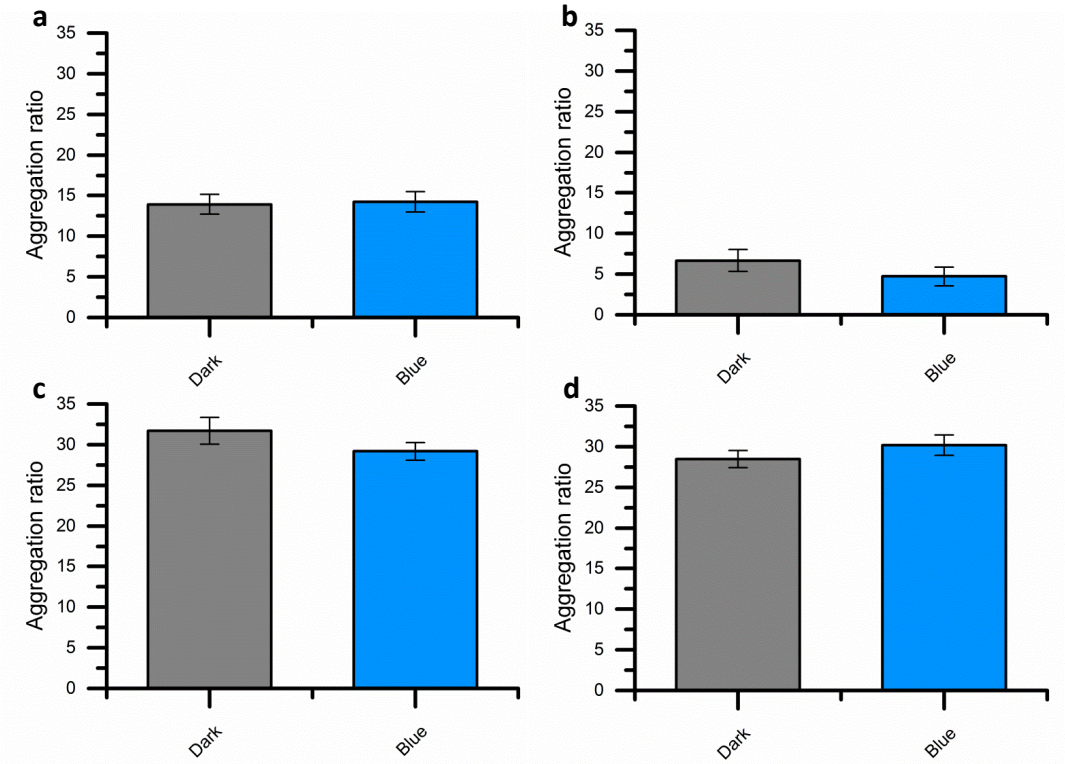

Figure 2.1.8 Competitive light-dependent aggregation in presence of soluble protein binding partners: a) iLID/Nano in 1µM iLID solution; b) iLID/Nano in 1µM Nano solution; c) nMagHigh/pMagHigh in 1µM nMagHigh solution; d) nMagHigh/pMagHigh in 1µM pMagHigh solution. Mann-Whitney test (significance level 0.05) was performed to analyze the statistical difference, no significant difference was found. Error bars are the standard error of the mean from 15 images.

The use of blocking agents can prevent the bead aggregation. Already low concentrations (0.2% w/v) of such blocking agents as bovine serum albumin (BSA) or Pluronic® F-127 completely obliterated the bead aggregation for both

iLID/Nano and nMagHigh/pMagHigh interactions in the dark as well as under blue light (Figure 2.1.9 a-d). This is probably due to an excess of blocking agent in the solution that blocks the protein binding interactions.

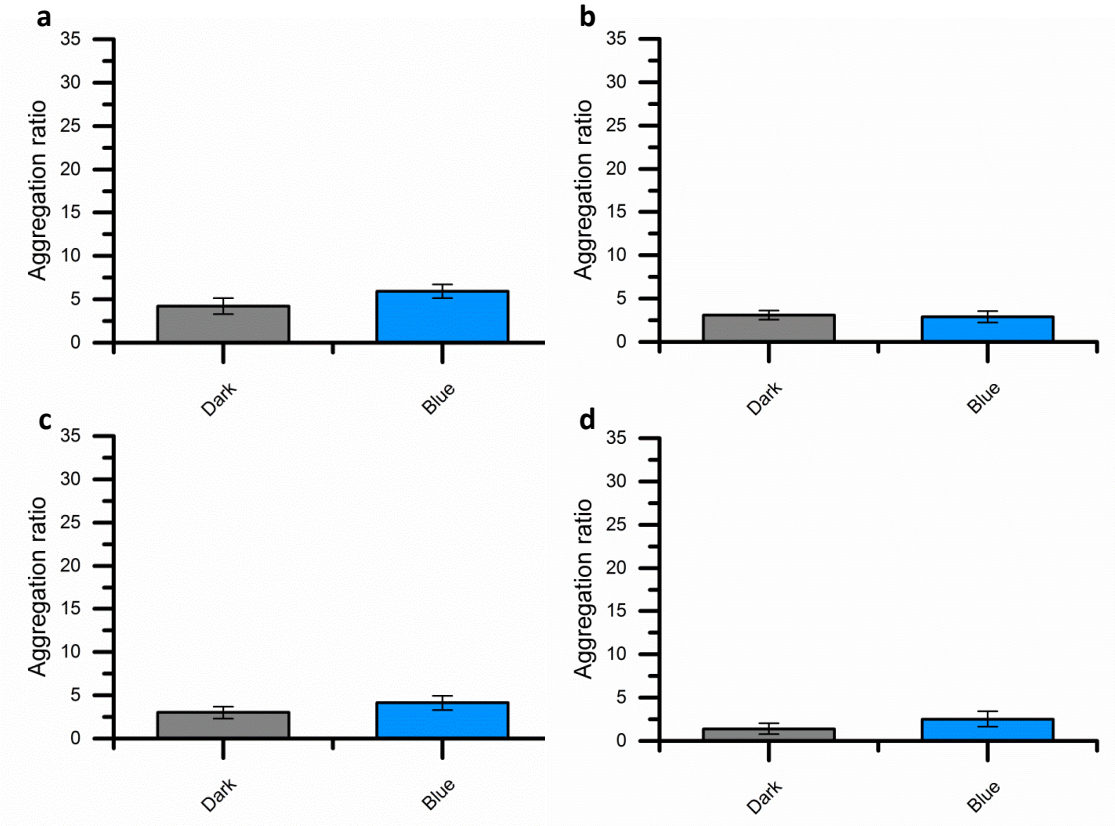

Figure 2.1.9 Light-dependent aggregation in presence of blocking agents: a) iLID/Nano in 0.2% (w/v) BSA; b) nMagHigh/pMagHigh in 0.2% (w/v) BSA; c) iLID/Nano in 0.2% (w/v) Pluronic® F-127; d) nMagHigh/pMagHigh in 0.2% (w/v) Pluronic® F-127. Mann-Whitney test (significance level 0.05) was performed to analyze the statistical difference, no significant difference was found. Error bars are the standard error of the mean from 15 images.

2.1.4 Reversibility of blue light-dependent self-assembly

In nature self-assembly is a highly dynamic, reversible and precisely regulated process. Therefore, it is also important to understand how the dynamics and reversibility work in synthetic systems. Both protein pairs can reversibly dissociate from each other in the dark, which should also lead to the disassembly of the light-induced bead aggregates in the dark. To investigate the light-dependent bead disassembly, the aggregation ratios of bead mixtures kept in the dark or under blue light for 2 hours were compared with beads that were first kept under blue light for 2 hours and then placed in the dark for 1 hour

(reversed) (Figure 2.1.10 a-b). For both of the protein pairs the aggregation ratios decreased upon withdrawal of the blue light. For the iLID/Nano pair the aggregation ratio decreased from 37% under blue light to 29% in the reversed sample (comparable to the dark value of 27% after 2 hours of aggregation). For the nMagHigh/pMagHigh pair, the aggregation ratio decreased from 42% under blue light to 32% in the reversed sample (comparable to the dark value of 30% after 2 hours of aggregation). In parallel, the number of clusters as well as their average size has also decreased upon blue light withdrawal for both protein pairs (Figure 2.1.10 c-f).

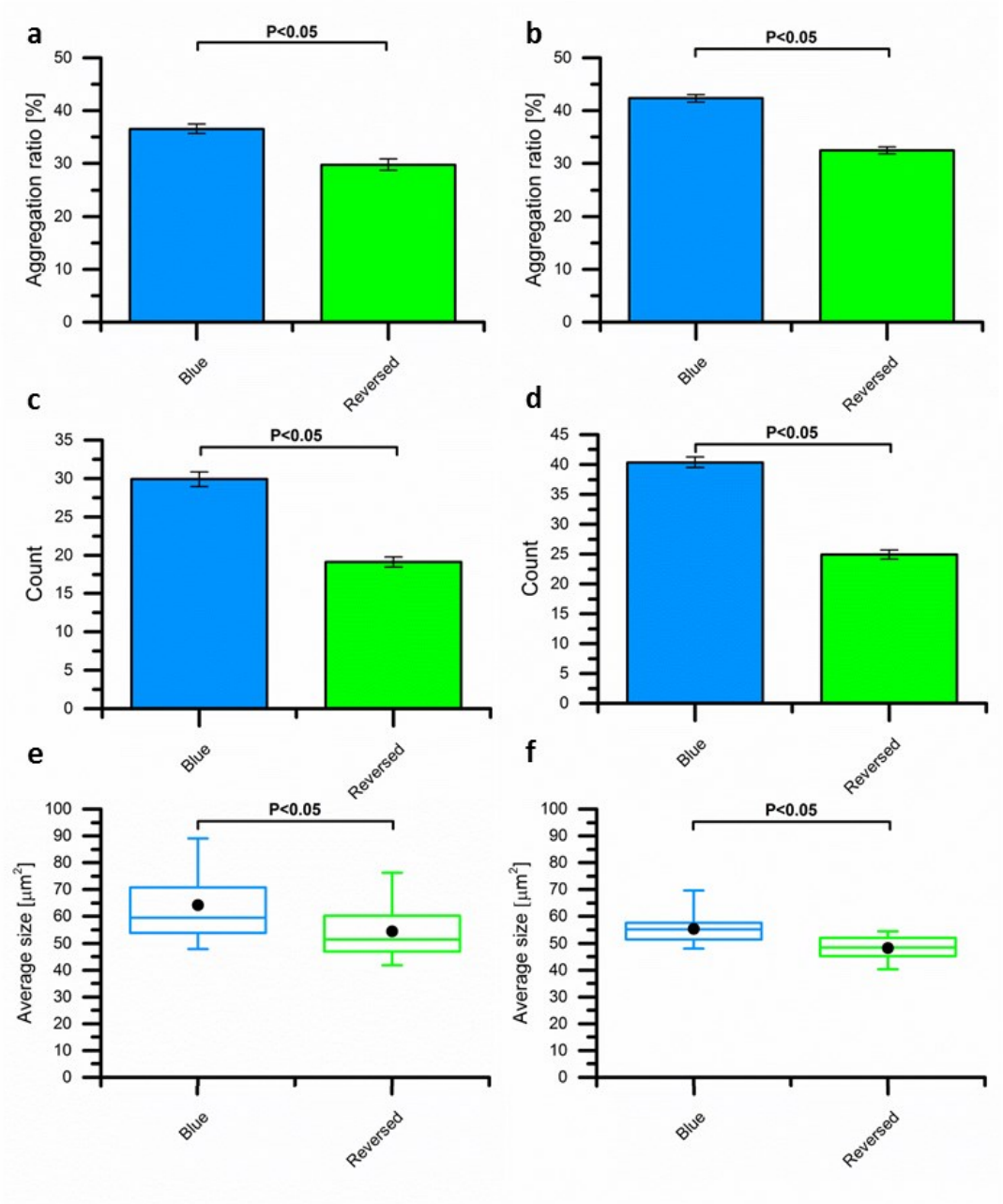

Figure 2.1.10 a-b) Reversion of light-induced aggregation of the beads functionalized with: a) iLID/Nano protein pair and b) nMagHigh/pMagHigh protein pair. c-d) Cluster number for: c) iLID/Nano protein pair and d) nMagHigh/pMagHigh protein pair. e-f) Average cluster size for: e) iLID/Nano protein pair and f) nMagHigh/pMagHigh protein pair. Samples kept under blue light are depicted in blue; samples that were reversed are depicted in green. Mann-Whitney test (significance level 0.05) was performed to analyze the statistical difference. Error bars are the standard error of the mean from > 60 images.

2.1.5 Reversion kinetics

The dissociation of proteins from each other is a dynamic process. Therefore, kinetics of the bead disassembly in the dark was investigated along with the repeated switchability of the protein interactions. For the reversibility studies, mixtures of iLID/Nano or nMagHigh/pMagHigh functionalized beads were first aggregated under blue light for 2 hours before placing them in the dark while slowly agitating them at 50 rpm. The aggregation ratio of the samples was quantified at different time points. While 15 minutes in the dark were not sufficient to significantly reduce the aggregation ratios, already after 30 minutes in the dark the aggregation was reversed by ≈ 80% for both of the protein pairs (Figure 2.1.11 a-b). As the blue-light dependent interactions between both proteins pairs can be switched on and off multiple times, consequently the bead aggregation can be also induced several times in blue light/dark cycles. For the iLID/Nano pair the aggregation ratio changed in two cycles of 1 hour under blue light and 30 minutes in the dark form 36% to 22% to 42% and back to 28% (Figure 2.1.11 c). Likewise, the beads functionalized with the nMagHigh/pMagHigh pair changed aggregation ratio from 32% to 20% to 41% and back to 28% in repeated blue light/dark cycles (Figure 2.1.11 d). The aggregation ratios increased from the first cycle to the second due to the general increase in the bead aggregation over time. These results showed that it is possible to use both of these blue light switchable protein pairs to repeatedly induce reversible self-assembly of micrometer-sized beads.

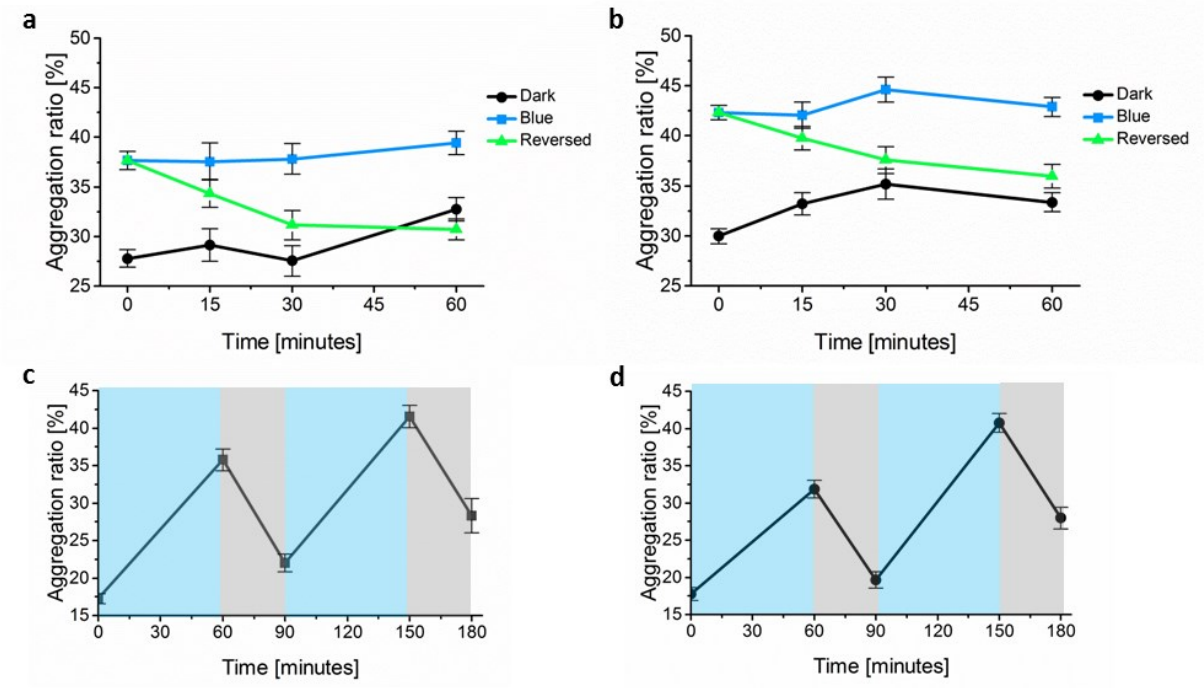

Figure 2.1.11 a-b) Reversion kinetics of blue light dependent bead aggregation in the dark for: a) the iLID/Nano protein pair and b) the nMagHigh/pMagHigh protein pair. Reversed samples (green line) were kept under blue light illumination for 2 hours before placing them into the dark. The dark (black line) and blue (blue line) samples were analyzed at the same time points as the reversed samples. Error bars are the standard error of the mean from > 30 images. c-d) Switching cycles of bead aggregation for: c) iLID/Nano protein pair and d) nMagHigh/pMagHigh protein pair. Periods when samples were kept under blue light are marked in blue; periods when samples were kept in the dark are marked in grey. Error bars are the standard error of the mean from 30 images.

2.1.6 Stoichiometry controlled self-assembly

In social self-sorting it is possible to control respective arrangements of building blocks and cluster sizes by adjusting their stoichiometry in the mixture.[58] In order to demonstrate this, red fluorescent beads functionalized with iLID (or nMagHigh) and green fluorescent beads functionalized with Nano (or pMagHigh) were mixed in 1:5 and 5:1 ratios and incubated under blue light for 2 hours. Under the fluorescent microscope a corona of 5 to 8 beads of the prevalent bead type surrounding the complementary bead type was observed (Figure 2.1.12 a-b). Thus, it is possible to use different stoichiometries between the building blocks in order to control the respective arrangement of building blocks to each other.

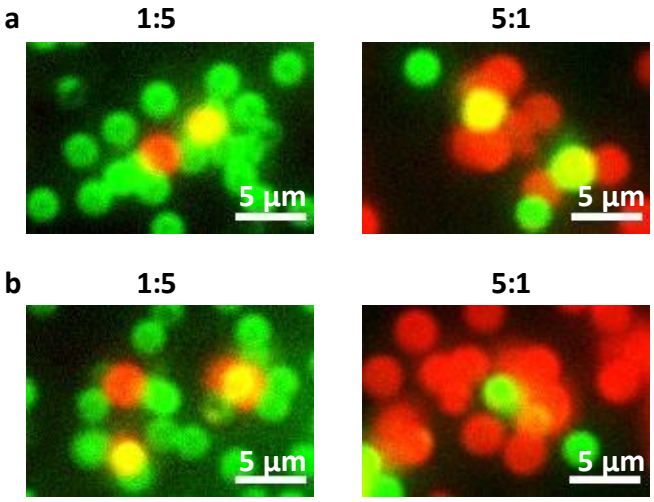

Figure 2.1.12 Fluorescence microscopy images with different arrangements of: a) iLID (red) and Nano (green); b) nMagHigh (red) and pMagHigh (green) mixed in 1:5 and 5:1 ratios under blue light. The scale bars are 5 µm.

2.1.7 Social self-sorting in a four component mixture

Social self-sorting requires two orthogonal and specific heterodimerization partners on the colloidal particles, which sort into two families of aggregates.[58] In order to show that the two blue light switchable protein pairs can be used to achieve the social self-sorting, four different bead subpopulations (each functionalized with one of the proteins) were mixed in equal ratios and incubated under blue light for 2 hours at 50 rpm (Figure 2.1.13 a). iLID and Nano (which are expected to sort into one family) were each immobilized on red fluorescent beads while nMagHigh and pMagHigh (which are expected to sort into the second family) were each immobilized on green fluorescent beads. After 2 hours of blue light exposure discrete families of distinct red or green beads were observed in this four component mixture (Figure 2.1.13 b). In the 3D cross-section confocal images one can see that the separate clusters containing only one family of beads (red: iLID/Nano, green: nMagHigh/pMagHigh), were formed. No intermixed clusters were observed (Figure 2.1.13 d-e). Furthermore, the reversibility of such a social self-sorting was investigated by placing the self-sorted under blue light for 2 hours samples in the dark for 1 hour. This led to the disassembly of the clusters and reversion

of the social-sorting (Figure 2.1.13 b-c). The calculated aggregation ratio for these samples increased from 16% in the dark to 32% after 2 hours under blue light illumination, while subsequently decreasing back to 20% upon withdrawal of the blue light for 1 hour (Figure 2.1.13 c).

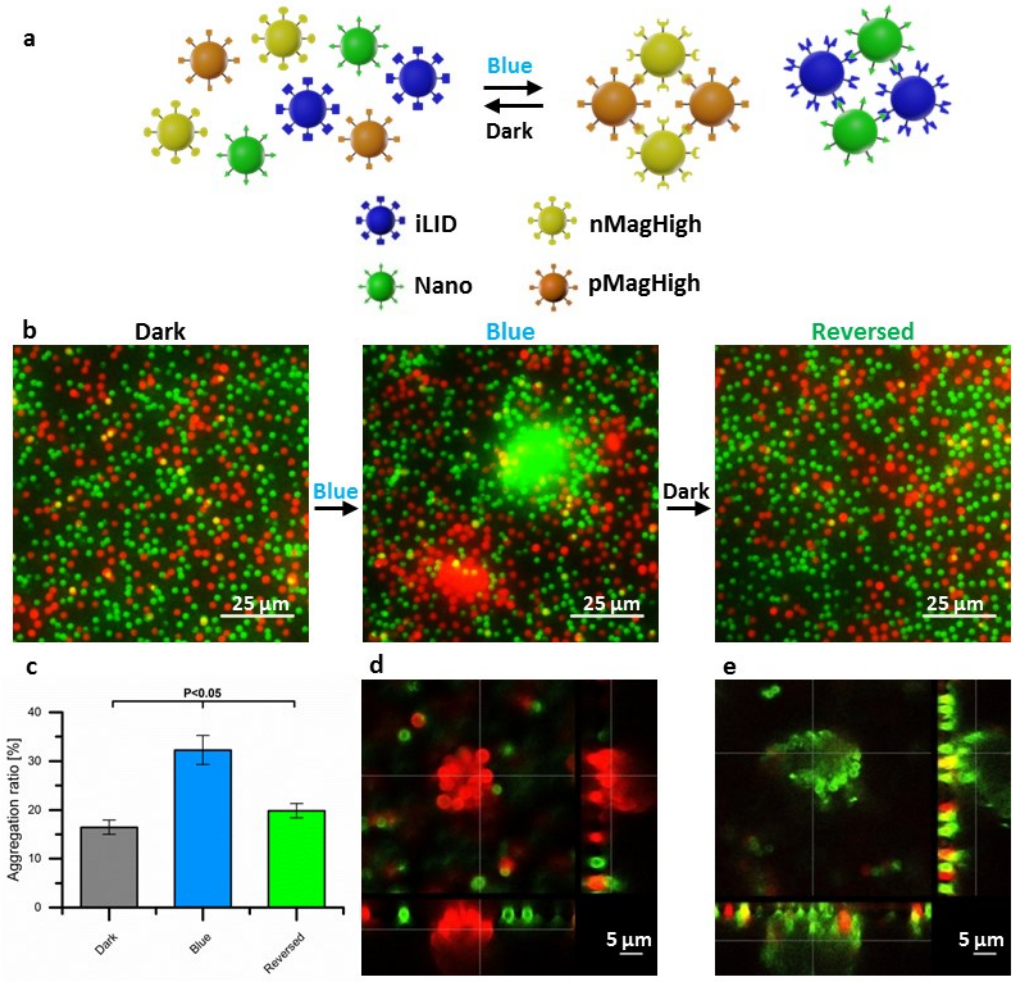

Figure 2.1.13 Blue light-induced reversible social self-sorting. a) A schematic representation of the social self-sorting of four components using two blue light sensitive protein pairs. b) Fluorescence microscopy images of 4 different bead populations that reversibly sort into two families: iLID/Nano (red) and nMagHigh/pMagHigh (green). c) Social sorting aggregation quantification: samples kept in the dark (grey); samples kept under blue light (blue); samples that were reversed (green). One-Way ANOVA test (significance level 0.05) was performed to analyze the statistical difference followed by Dunn-Sidak post hoc test (significance level 0.05). Error bars are the standard error of the mean from 15 images. d-e) Confocal microscopy images of the exemplary 3D clusters formed by: d) the iLID/Nano protein pair (red); e) the nMagHigh/pMagHigh protein pair (green).

In summary, the two blue light switchable protein pairs (iLID/Nano and nMagHigh/pMagHigh) have proven to be orthogonal to each other and highly specific. Hence, these interactions can be used as the basis to achieve the social self-sorting of four different populations of compartments into two separate families with blue light under biocompatible conditions.

2.1.8 Red light-dependent self-assembly based on heterodimerizing proteins PhyB/ PIF6

To self-assemble multicompartment synthetic prototissues of higher complexity, there is a further need to investigate a greater variety of photoswitchable proteins that can be used for this purpose and can be addressed orthogonally. For this purpose light responsive proteins that respond to light of different wavelengths were used to trigger the self-assembly in more complex mixtures with different colors of light. As red/far-red light responsive heterodimerizing protein pair we used the PhyB and its specific phytochrome interaction partner PIF6 to control the self-aggregation of colloids. First, the ability of this protein pair to induce aggregation of colloidal particles was investigated as for the blue light responsive proteins above and PhyB and PIF6 fluorescently labeled with GFP were immobilized onto 2 µm colloids. In contrast to the blue light responsive proteins, the PhyB/PIF6 samples were incubated either under far-red light and blue light, where the proteins should not interact (730 nm and 460 nm) or under red light (630 nm) under low agitation (50 rpm). When comparing the samples that were kept under these two different conditions for 2 hours, the samples that were exposed to red light showed higher aggregation ratios than in the samples that were kept under far-red (+blue) light (Figure 2.1.14 a-b). However, there was significantly more clustering also under far-red/blue light, when comparing to the previously discussed blue light responsive proteins in the dark (chapter 2.1.2).

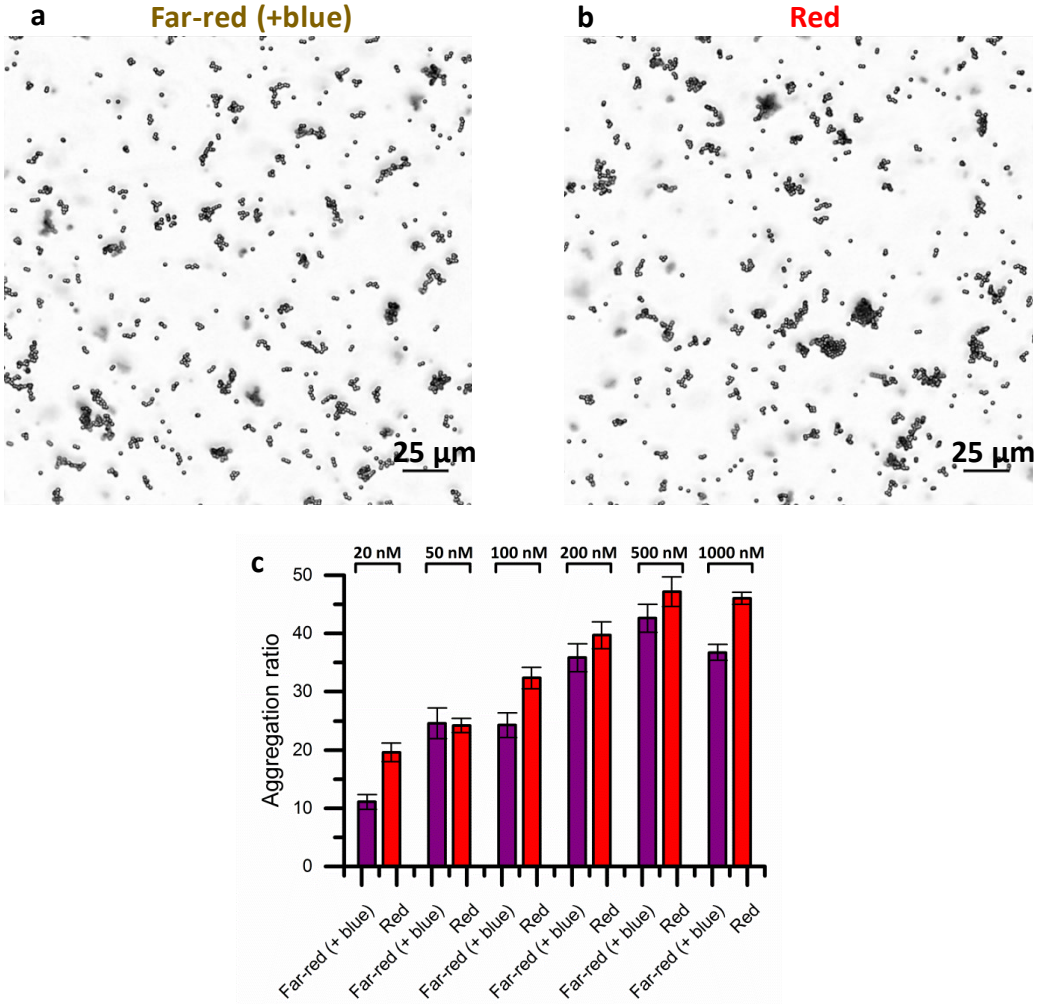

Figure 2.1.14 Bright field images of a mixture of PhyB and PIF6-GFP functionalized 2 µm polystyrene beads: a) co-illumination with far-red and blue light and b) under red light. c) Optimization of the bead functionalization with PhyB. PIF6-GFP concentration during the bead-functionalization with protein was kept 1 µM. Samples kept under far-red/blue light are depicted in purple; samples kept under red light are depicted in red. Error bars are the standard error of the mean from > 15 images.

Therefore, the protein functionalization density on the beads was optimized to find the parameters that would allow the bead aggregation to be in the comparable range with the blue light sensitive proteins. It was important to do so as in the future this would allow to combine red and blue light responsive self-assembly and trigger self-sorting orthogonally with different colors of light. To optimize the protein density, polystyrene beads were functionalized with different concentrations of PhyB protein (20 nM, 50 nM, 100 nM, 200 nM, 500 nM and 1 µM), while the concentration of PIF6-GFP was kept the same (1 µM as for the other proteins). By adjusting the protein concentration it was possible to tune the aggregation ratio of the samples as well as to adjust its

range (Figure 2.1.14 c). Under far-red/blue light the aggregation range changed from ≈10% for 20 nM functionalization to ≈40% for 500nM functionalization, while under the red light it changed from ≈20% for 20 nM to ≈45% for 500nM. As the aggregation ratios of both of the blue light sensitive protein pairs (iLID/Nano and nMagHigh/pMagHigh) were changing from about 30% in the dark to about 40% under blue light, 100 nM concentration of PhyB was selected for further experiments.

At first, the aggregation ratios were compared between the samples incubated under far-red/blue or red light at different time points ranging from 15 minutes to 2 hours to investigate bead aggregation dynamics (Figure 2.1.15 a). After 30 minutes there was little difference between the samples; however, after 1 hour there was significantly more clusters under red light compared to the sample kept under far-red/blue light. After 2 hours the aggregation levels were reaching a plateau as it was also observed for the blue light sensitive protein pairs described above; therefore 2 hour time point was chosen as an analysis point for the future experiments. At the time point t=2 hours the aggregation ratio was significantly higher (9% difference) under red light (36%) than under the far-red/blue (27%) light (Figure 2.1.15 b). This shows that the red light-dependent interaction between PhyB and PIF6-GFP is sufficiently strong to induce light-dependent self-assembly of micrometer-sized beads. Moreover, the reversion of this light-induced bead aggregation was investigated by first keeping the samples under red light for 2 hours and then placing them under far-red/blue light for another hour. This led to a decrease in the aggregation ratio from 36% under red light to 32% in the reversed samples (Figure 2.1.15 b). Despite a statistical difference between samples kept under red light and the reversed samples (Mann-Whitney test, significance level 0.05), the reversion is not fully complete as the aggregation does not go down to the observed ratio under far-red/blue light. Further, the number of clusters as well as their average size was calculated after 2 hours of aggregation under the far-red/blue light and under red light as well as for the reversed samples (Figure 2.1.15 c-d). Significantly more clusters were formed under red light compared to the far-red/blue light and they were bigger in size. Likewise, the

number and size of clusters also decreased in the reversed samples compared to the red light sample but not to the full extent as in the dark sample.

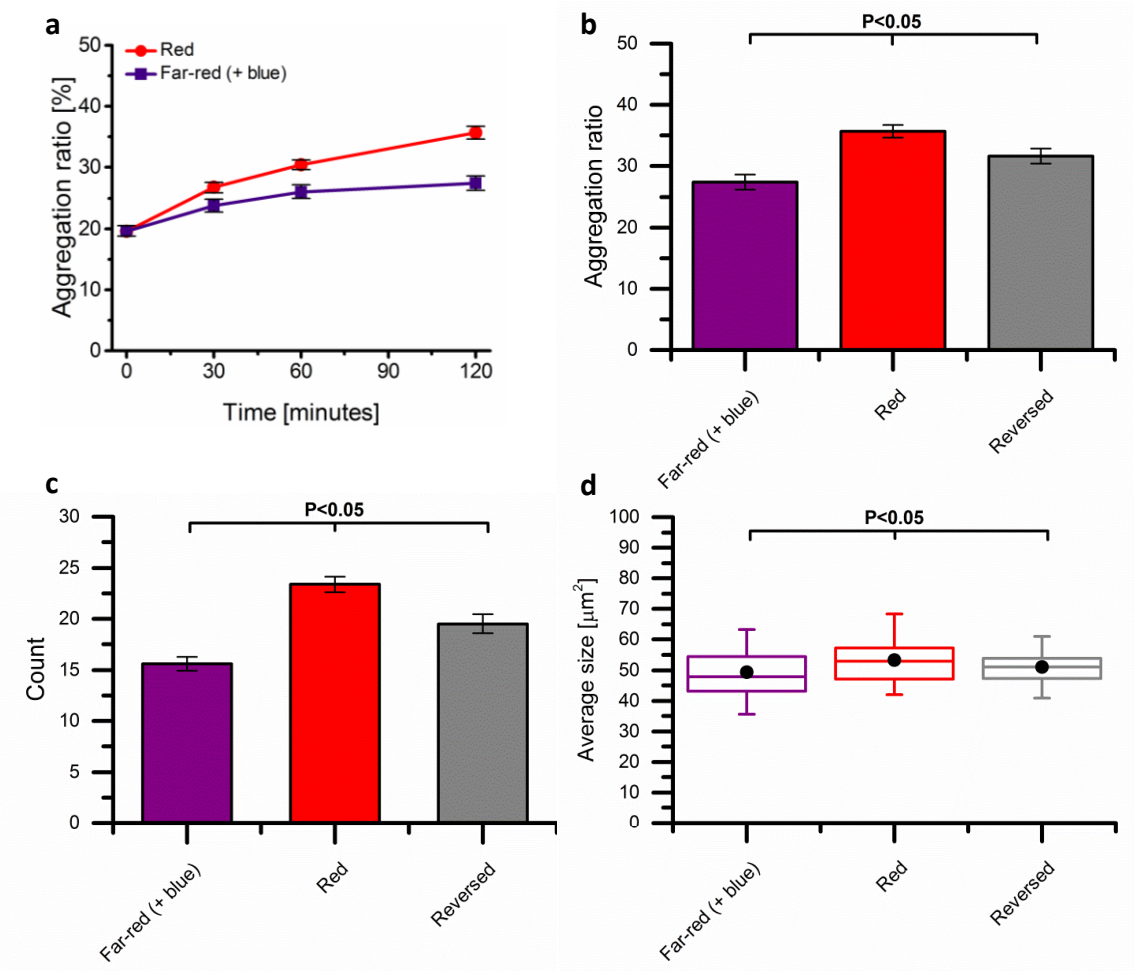

Figure 2.1.15 PhyB (100 nM)/PIF6-GFP (1 µM) protein functionalized beads: a) Bead aggregation dynamics. Error bars are the standard error of the mean from > 30 images. b) Light-induced aggregation and reversion. c) Cluster number. d) Average cluster size. Samples kept under far-red/blue light are depicted in purple; samples kept under red light are depicted in red, reversed samples are depicted in grey. One-Way ANOVA test (significance level 0.05) was performed to analyze the statistical difference followed by Dunn-Sidak post hoc test (significance level 0.05). Error bars are the standard error of the mean from > 45 images.

It was important to prove that the red light triggered self-assembly is based on the specific heterodimerization between the PhyB and PIF6-GFP and is not due to the homodimerization as we aim to use this protein pair for social self-sorting in the future. For this, the far-red/blue and red light-dependent self-assembly of beads just functionalized with one protein at a time, PhyB or PIF6-

GFP, was quantified (Figure 2.1.16 a-b). For both of the proteins the aggregation ratio of the samples exposed to red light was comparable to the aggregation ratio under the far-red/blue light and the bead aggregation was not light-dependent. PhyB functionalized beads appeared to be stickier than PIF6-GFP functionalized ones and showed higher aggregation ratio overall. Nonetheless, this clustering was not light-dependent. The stickiness of PhyB can be a possible reason, why the reversion of bead clustering was incomplete for this protein pair.

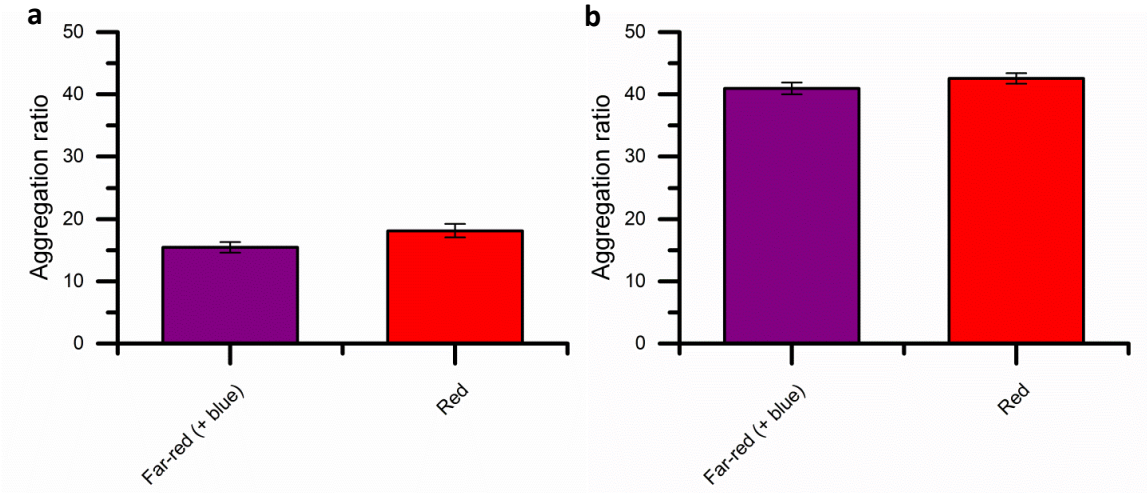

Figure 2.1.16 Homodimerization of: a) PIF6-GFP (1 μM) and b) PhyB (100 nM) protein functionalized beads. Mann-Whitney test (significance level 0.05) was performed to analyze the statistical difference, no significant difference was found. Error bars are the standard error of the mean from > 45 images.

2.1.9 Blue and red light-dependent self-assembly of colloids based on homodimerizing proteins VVDHigh and Cph1

Another light-activated dimerization mode, namely homodimerization, can be also utilized in order to bring together compartments of the same type, achieving so called asocial sorting.[58, 65] Two homodimerizing proteins, one blue light sensitive (LOV domain-based, namely VVDHigh) and one red/far-red light sensitive (phytochrome-like, namely Cph1), were used to control reversible self-assembly of solid colloidal particles of the same type.

As for the above described systems, first the ability of both protein pairs to induce aggregation of colloidal micrometer-sized beads was investigated. The beads functionalized with VVDHigh protein were incubated either under blue light (460 nm) or red (630 nm) light and the beads with Cph1 protein were

incubated under far-red/blue (730 nm+460 nm) or red (630 nm) under low agitation (50 rpm). Such illumination conditions were chosen to prove that the proteins VVDHigh and CphI orthogonally respond to the light of different wavelengths and are only activated by light of a specific color (blue for the VVDHigh protein and red for the Cph1 protein). This would allow us to combine these two protein interactions to achieve wavelength-dependent asocial self-sorting within colloidal mixtures. For simplicity, the red samples for the VVDHigh protein experiments will be referred to as "dark" from now on.

Firstly, the light dependent aggregation of VVDHigh based interactions was characterized. Comparable to all the protein based self-assemblies described above, no difference between the samples kept in the dark or under blue light was observed after 30 minutes incubation. The maximum difference was reached after 1 hour and did not increase from then on (Figure 2.1.17 a). However, as for the other systems 2 hours were chosen as the time point for the further investigation. After 2 hours incubation, the aggregation ratio increased from 20% in the dark to 28% under blue light (8% difference) (Figure 2.1.17 b). This shows that blue light-dependent homodimerization of VVDHigh protein is sufficiently strong to induce light-dependent self-assembly of micrometer-sized beads. Moreover, the reversion of this light-induced bead aggregation was investigated as before. One hour in the dark led to full reversion of the aggregation and a decrease in the aggregation ratio from 28% to 16% (Figure 2.1.17 b). The number of clusters and their size was also analyzed after 2 hours in the dark or under the blue light as well as for the reversed samples. There were significantly more clusters and they were bigger under blue light compared to the dark and reversed samples (Figure 2.1.17 c-d).

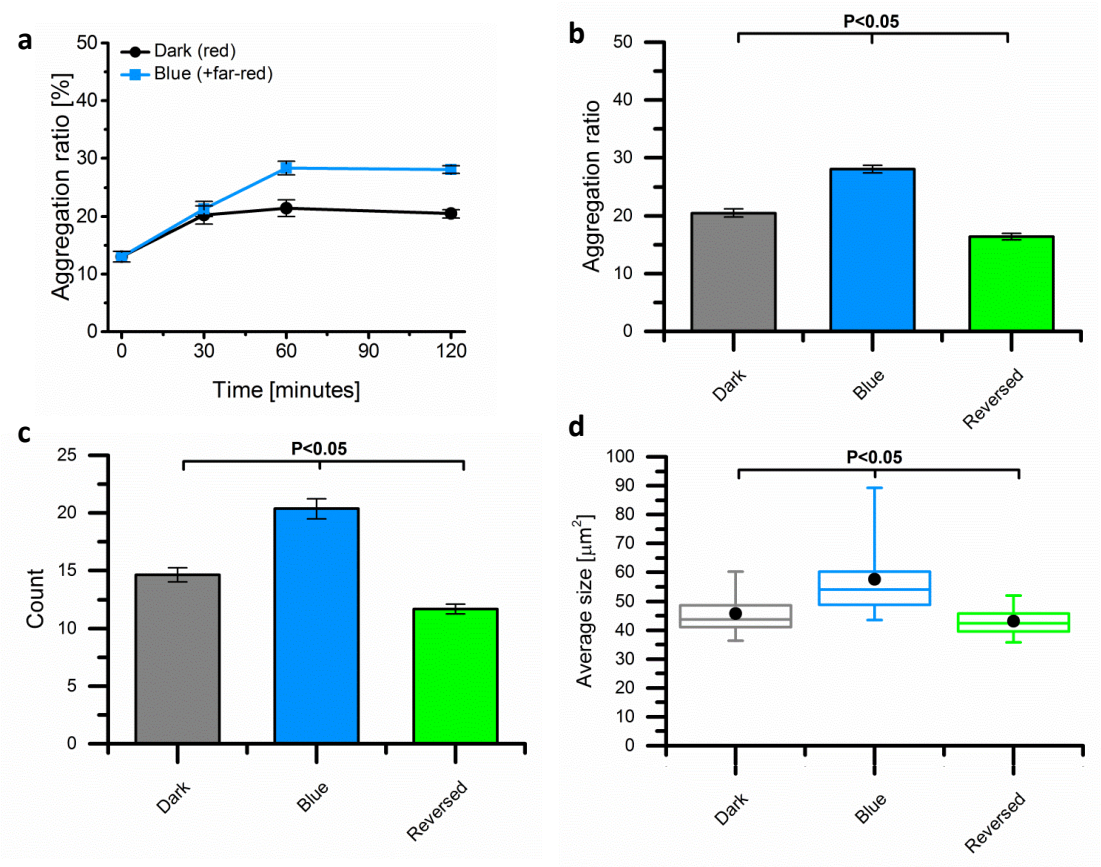

Figure 2.1.17 VVDHigh protein functionalized beads: a) Bead aggregation dynamics. Error bars are the standard error of the mean from > 30 images. b) Light-induced aggregation and reversion. c) Cluster number. d) Average cluster size. Samples kept in the dark (under red light) are depicted in grey; samples kept under far-red/blue light are depicted in blue; reversed samples are depicted in green. One-Way ANOVA test (significance level 0.05) was performed to analyze the statistical difference followed by Dunn-Sidak post hoc test (significance level 0.05). Error bars are the standard error of the mean from > 75 images.

Next the aggregation behavior for the Cph1 mediated interactions was characterized as it was done for the other proteins before. No difference between the samples was observed after 30 minutes incubation. The difference increased after 1 hour incubation and reached the maximum after 2 hours incubation (Figure 2.1.18 a). At the time point t=2 hours, the aggregation ratio was 29% under the far-red/blue light and 41% under red light (12% difference) proving that light-dependent homodimerization of Cph1 protein is strong enough to induce self-assembly of micrometer-sized beads (Figure 2.1.18 b). Further, the reversion of this light-induced bead aggregation was investigated by first keeping the samples under red light for 2 hours and

then placing them under far-red/blue for another hour. A decrease in the aggregation ratio from 41% under red light to 28% in the reversed sample was observed (Figure 2.1.18 b). Finally, the number of clusters and their size was analyzed after 2 hours for the light-activated, dark and reversed samples. More and bigger clusters were observed under red light compared to the far-red/blue and reversed samples (Figure 2.1.18 c-d).

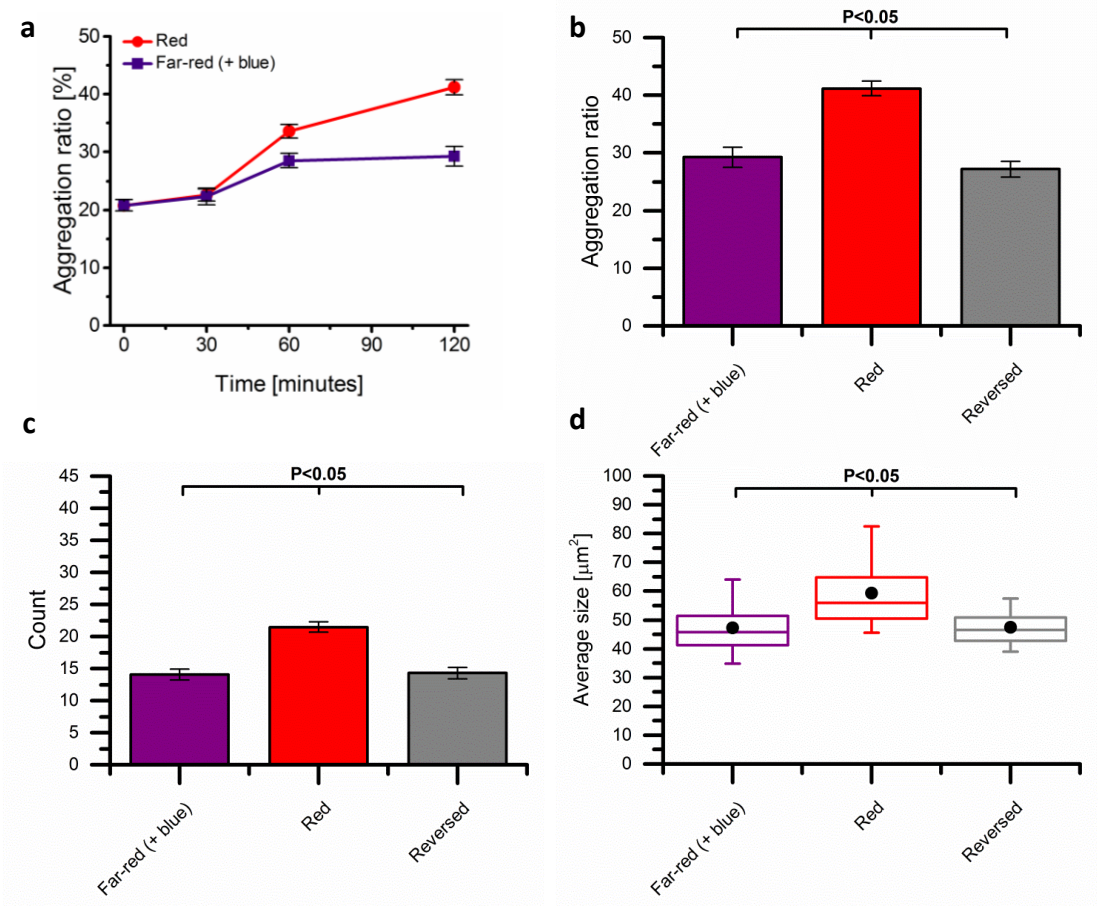

Figure 2.1.18 Cph1 protein functionalized beads: a) Bead aggregation dynamics. Samples kept under far-red (+blue) light are depicted in purple; samples kept under red light are depicted in red. Error bars are the standard error of the mean from > 30 images. b) Light-induced aggregation and reversion. c) Cluster number. d) Average cluster size. Samples kept under far-red (+blue) light are depicted in purple; samples kept under red light are depicted in red, reversed samples are depicted in grey. One-Way ANOVA test (significance level 0.05) was performed to analyze the statistical difference followed by Dunn-Sidak post hoc test (significance level 0.05). Error bars are the standard error of the mean from > 45 images.

2.1.10 Blue light-dependent sedimentation of colloids

The beads used this far were 2 µm in diameter, which is approximately the size of an *E. coli* bacteria. Considering that mammalian cells are larger, it was also of interest to investigate if light dependent protein interactions can bring together bigger objects. To analyze the light induced aggregation of larger colloids of 12 µm in diameter we investigated their sedimentation time as the method used for 2 µm beads was not suitable for such large beads because they are heavier and settle too fast.

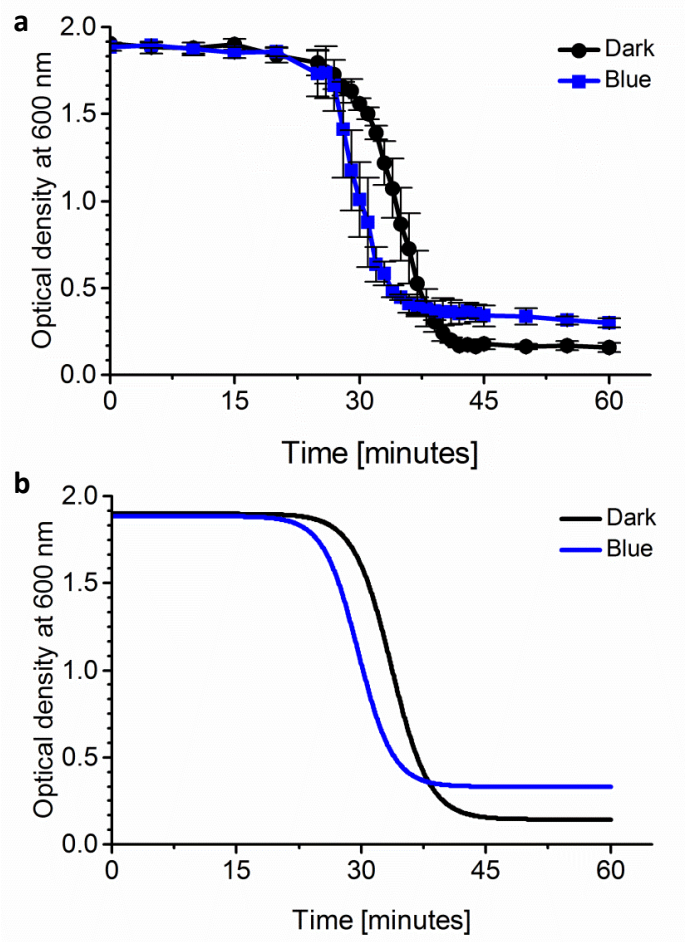

Half-time of sedimentation:	
Dark	$x_{1/2}$ = 33.64 minutes
Blue	$x_{1/2}$ = 29.64 minutes

Figure 2.1.19 Sedimentation of the nMagHigh/pMagHigh protein functionalized 12 µm beads. a) Actual sedimentation curves. Error bars are the standard deviation from 3 independent measurements. b) Boltzmann sigmoidal fits. Samples kept in the dark are depicted in black; samples kept under blue light are depicted in blue.

For such sedimentation experiments 12 µm in diameter Ni^{2+}-NTA functionalized polystyrene beads were functionalized with either nMagHigh or pMagHigh protein through their His-tags. Bead populations with complementary interaction partners were mixed in equal proportions in a cuvette and incubated either in the dark or under blue light, while continuously measuring the optical density of the samples at 600 nm (OD_{600}). The hypothesis was that as more clusters are formed under blue light, the samples would settle faster because the aggregates are heavier than single beads. Indeed, when comparing the times, at which OD_{600} has decreased by half ($t_{1/2}$), the samples in the dark settled slower ($t_{1/2}$≈34 minutes) compared to the samples under blue light ($t_{1/2}$≈30 minutes) (Figure 2.1.19). This has proven that the protein interactions between nMagHigh and pMagHigh are also sufficiently strong to induce self-assembly of bigger colloidal particles with sizes comparable to mammalian cells. Therefore, other proteins can be potentially also implemented on colloidal cell-mimics with sizes of tens of micrometers.

In summary, blue and red light dependent homo- and heterodimerization of light switchable proteins have proven themselves effective to induce the self-assembly of micrometer-sized colloidal beads that were used as synthetic cell-mimics. This provides great flexibility in terms of independently triggering self-assembly with blue or red light and selectively bringing together colloids of the same or different type. The fact that all the light responsive protein interactions required about 2 hours to self-assemble colloids shows that it is not the photoswitching of proteins, which takes place on the timescale of seconds, but the self-assembly itself that is the rate determining step. All the light triggered aggregates are fully reversible, except the PhyB/PIF6 mediated ones, which allows for dynamic assembly and disassembly. Such a variety of proteins offers many possibilities to address self-assembly and asocial or social self-sorting in multi-component mixtures of protocells into prototissues.

2.2 Part II: Dynamic blue light switchable protein patterns on giant unilamellar vesicles

The results and discussion in this chapter are published by S. M. Bartelt*, E. Chervyachkova*, J. Steinkühler, J. Ricken, R. Wieneke, R. Tampé, R. Dimova and S. V. Wegner. (*Chem. Commun.*, 54, 948-951, 2018)
* These authors contributed to the work equally.

Contribution

This work was a tight collaboration with Solveig M. Bartelt. We contributed equally to the protein recruitment to the whole GUV (including recruitment to a single GUV in presence of others), protein recruitment to the region of interest and to the data analysis as well as paper writing. I performed all the reversibility experiments as well as light intensity dependence experiments. Solveig M. Bartelt performed the light wavelength orthogonality experiments, the membrane fluidity dependence experiments and the patterning on the GUV carpets experiments.

2.2.1 Motivation and Objectives

Protein patterns are observed in many different contexts in nature. As part of their function, protein patterns are dynamic and precisely regulated in biological systems. To replicate the biological phenomena that are associated to dynamic protein patterns in synthetic cells, there is a need for a specific, biocompatible, and reversible way to form protein patterns *in vitro* with the desired spatiotemporal precision. The goal in this part of the thesis was to create protein patterns on synthetic cells by using photoswitchable protein heterodimers from the field of optogenetics. For this purpose, we used the iLID protein (an engineered version of the LOV2 domain from *Avena sativa*, with an incorporated SsrA peptide), which specifically binds to the Nano protein (wild-type SspB peptide) upon blue light illumination.[124, 126] This interaction is reversible and proteins dissociate from each other in the dark.

In our approach, first the iLID protein was anchored to the outer membrane of GUVs. Subsequently, we investigated the recruitment of a protein fused to Nano, in this case fluorescent protein mOrange, to the GUV membrane *in situ*

upon blue light illumination and the reversibility of this recruitment in the dark. In addition, we explored the spatial and temporal control over protein patterns that could be achieved with this approach.

2.2.2 Protein recruitment to giant unilamellar vesicles (GUVs)

In nature protein patterns and protein gradients on cell membranes are important during many biological processes, such as cell division, migration and signalling.[154-155] Therefore, it is important to be able to mimic such dynamic protein patterns on cell-mimicking compartments *in vitro* to understand and control underlying processes. To produce protein patterns on membranes of GUVs with high spatiotemporal control we used protein heterodimerizers from the field of optogenetics, namely iLID protein and its specific interaction partner Nano with a fluorescent tag (mOrange-Nano protein). For this His-tagged iLID protein was anchored to the outer lipid membrane of GUVs (lipid composition: palmitoyl-2-oleoylphosphatidylcholine (POPC) with 10 mol% POPG + 0.1 mol% DGS-NTA-Ni^{2+} + 1 mol% DiD dye) through the Ni^{2+}-NTA-His-tag interaction. mOrange protein fused to Nano was then recruited *in situ* to the GUV membrane from the solution upon blue light illumination (Figure 2.2.1 a). GUV membranes immediately showed some initial fluorescence when put into the solution of mOrange-Nano protein in the dark but this fluorescence did not increase over time. This was probably due to the fact that there is also some interaction between iLID and Nano in the dark.[126] However, within 15 minutes after turning on the blue laser (Argon laser, 488 nm) a gradual and substantial increase of the GUV membrane fluorescence intensity was observed (Figure 2.2.1 b). This increase was quantified by comparing the membrane fluorescence intensity before and after illumination (Figure 2.2.1 c). After approximately 15 minutes the fluorescence intensity was reaching a plateau.

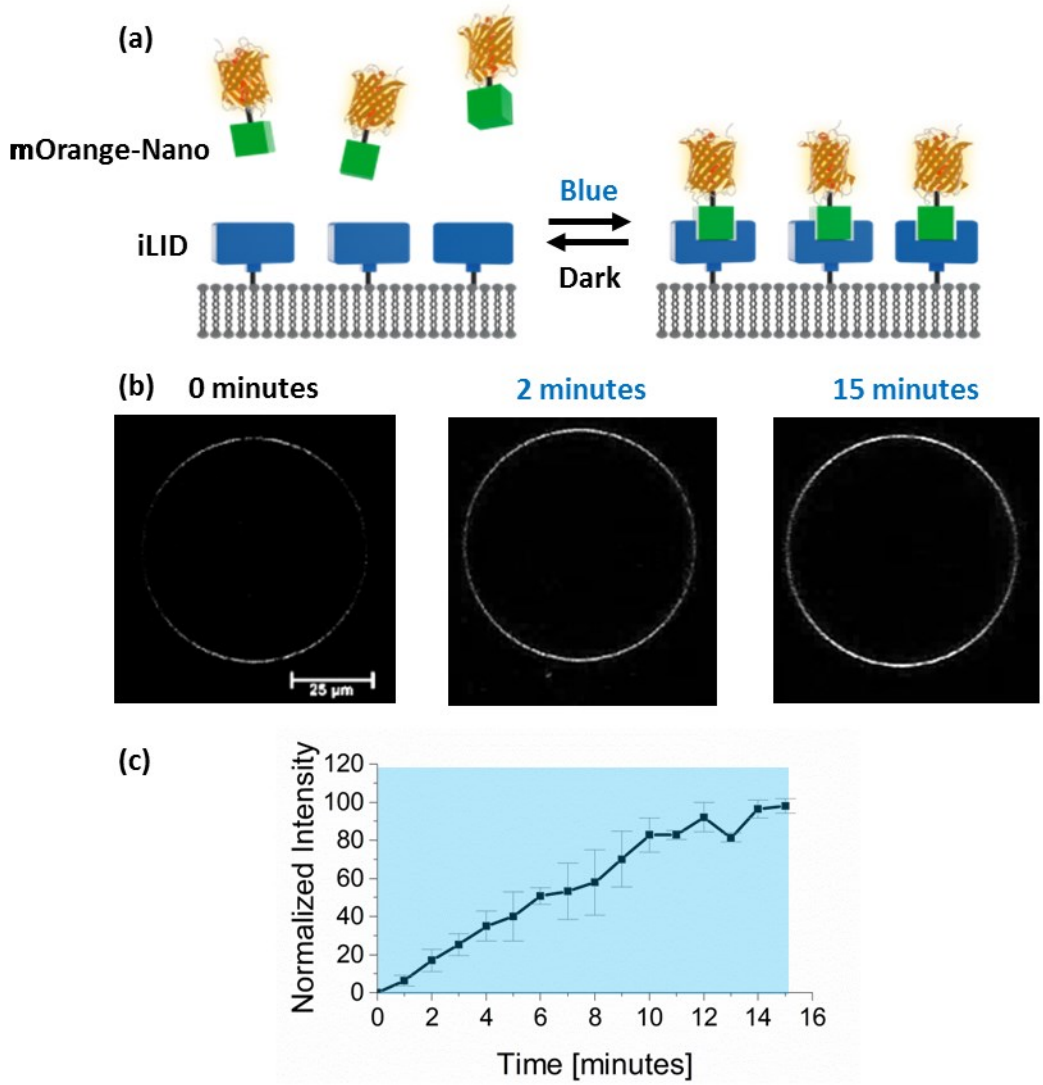

Figure 2.2.1 a) A schematic representation of reversible mOrange-Nano recruitment to iLID-functionalized lipid membrane under blue light illumination. b) Fluorescence images of iLID-functionalized GUVs in the presence of mOrange-Nano in the dark (0 minutes) and under blue light illumination (5 % laser power: 575.5 ± 21 nW, 488 nm). The scale bar is 25 µm. c) mOrange-Nano recruitment to GUV membrane under blue light. Error bars show the standard deviation from 3 independent experiments.

The amount of protein that was recruited to the GUV membrane can be controlled by adjusting the intensity of the blue light (Argon laser, 488 nm). Laser power of 70 nW through a 63x water objective (corresponds to 1% of the laser power) was already sufficient to partially activate iLID and recruit mOrange-Nano to the GUV. When increasing the power up to 6.3 µW (corresponds to 20% of the laser power) both the amount of the recruited protein and the recruitment rate increased. Laser

powers higher than that did not lead to further protein recruitment probably either due to the full activation of iLID and achieving the photostationary state or the photo-bleaching of the fluorescent protein (Figure 2.2.2 a).

Moreover, the interaction between iLID and Nano was selectively activated by blue light and not by light of other wavelengths. All the samples were prepared under the red light LED lamp (633 nm) and mOrange-Nano protein did not recruit to an iLID-functionalized GUV membrane under these conditions (Figure 2.2.2 b, labelled as "dark"). Further, a green light laser (561 nm) was used to excite mOrange for the fluorescence imaging during the experiments and similarly the protein did not recruit to the GUV membrane (labelled as "dark"). Moreover, illumination with the far-red light (750 nm) also did not lead to mOrange-Nano recruitment to the membrane (Figure 2.2.2 b). This proves the iLID/Nano interaction selectively responds to blue light and is orthogonal to light of different wavelengths. This is a great advantage for the future, when combining multiple light-sensitive proteins to selectively recruit different proteins on demand.

Additionally, different lipid compositions (1,2-Dioleoyl-sn-glycero-3-phosphocholine, DOPC, vs. POPC) and membrane fluidity (POPC + 20-40 mol% cholesterol) did not lead to changes in the mOrange-Nano protein recruitment to GUVs under the blue light illumination (Figure 2.2.2 c).

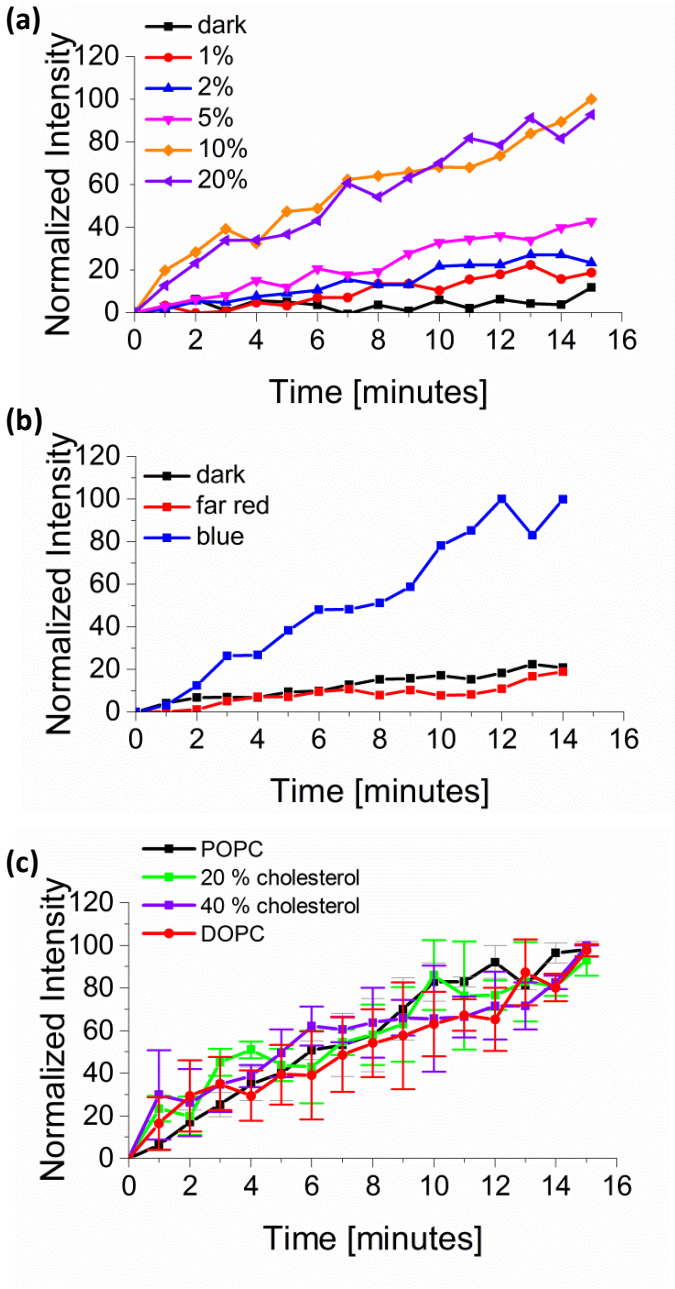

Figure 2.2.2 a) mOrange-Nano recruitment to iLID-functionalized GUVs depending on the intensity of the blue light laser; b) mOrange-Nano recruitment to iLID-functionalized GUVs depending on the illumination wavelengths; c) mOrange-Nano recruitment to iLID-functionalized GUVs depending on the lipid composition and membrane fluidity. POPC-GUVs were used in all other protein recruitment to GUVs experiments. The error bars show standard deviation from 3 different experiments.

2.2.3 Reversion of the protein recruitment

As the interaction between iLID and Nano is reversible in the dark, it was possible to form reversible and dynamic protein patterns on the lipid membranes. When GUVs were first placed under the blue light for

15 minutes and then removed into darkness, the fluorescence intensity at the membrane decreased, showing the reversibility of the mOrange-Nano recruitment to the GUV. About 70% of the recruited mOrange-Nano dissociated from the iLID-functionalized GUVs within 15 minutes in the dark. After 30 minutes in the dark the fluorescence intensity of the membrane decreased by approximately 95% (Figure 2.2.3). Moreover, the recruitment of mOrange-Nano protein was achieved repeatedly by alternating cycles of blue light and periods of darkness (Figure 2.2.3). Another 15 minutes of blue light illumination led to the fluorescence intensity increase at the GUV membrane, reaching the same intensity level as after the first cycle. Therefore, the reversible photoswitchable interaction between iLID and Nano can be used to repeatedly recruit proteins fused to Nano to the membranes of iLID-functionalized GUVs.

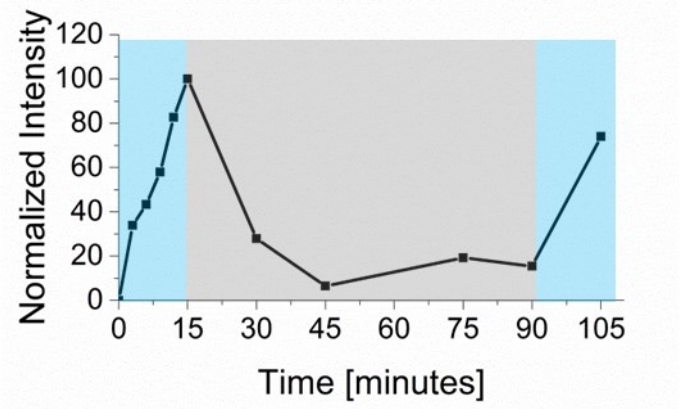

Figure 2.2.3 Repeated mOrange-Nano recruitment to the iLID-functionalized GUV under blue light (488 nm, marked in blue) and its reversion in the dark (marked in grey).

2.2.4 Protein recruitment to the region of interest

Light can be delivered with high spatiotemporal control; therefore, it can be used not only to induce the protein recruitment to the whole GUV membrane but also to recruit the protein only to a small region of interest (ROI) on the membrane. Despite the high fluidity of the lipid membrane, it was possible to observe a local fluorescence intensity increase when illuminating a small ROI on one side of an iLID-functionalized GUV, while continuously imaging mOrange-Nano recruitment (Figure 2.2.4 a-b). This increase was quantified by comparing the fluorescence intensity of the

ROI to the intensity of the region on the opposite side of the GUV with the same area (Figure 2.2.4 c). The fluorescence intensity of the illuminated ROI was consistently higher compared to the intensity of the area on the opposite side of the GUV (Figure 2.2.4 c).

High lipid membrane fluidity leads to the diffusion of proteins from the ROI at the pole of the GUV throughout the whole membrane creating a gradient. Therefore, there was a gradual fluoresce intensity increase of the whole GUV membrane over time, while illuminating it only locally. However, this increase was slower than when illuminating the whole GUV.

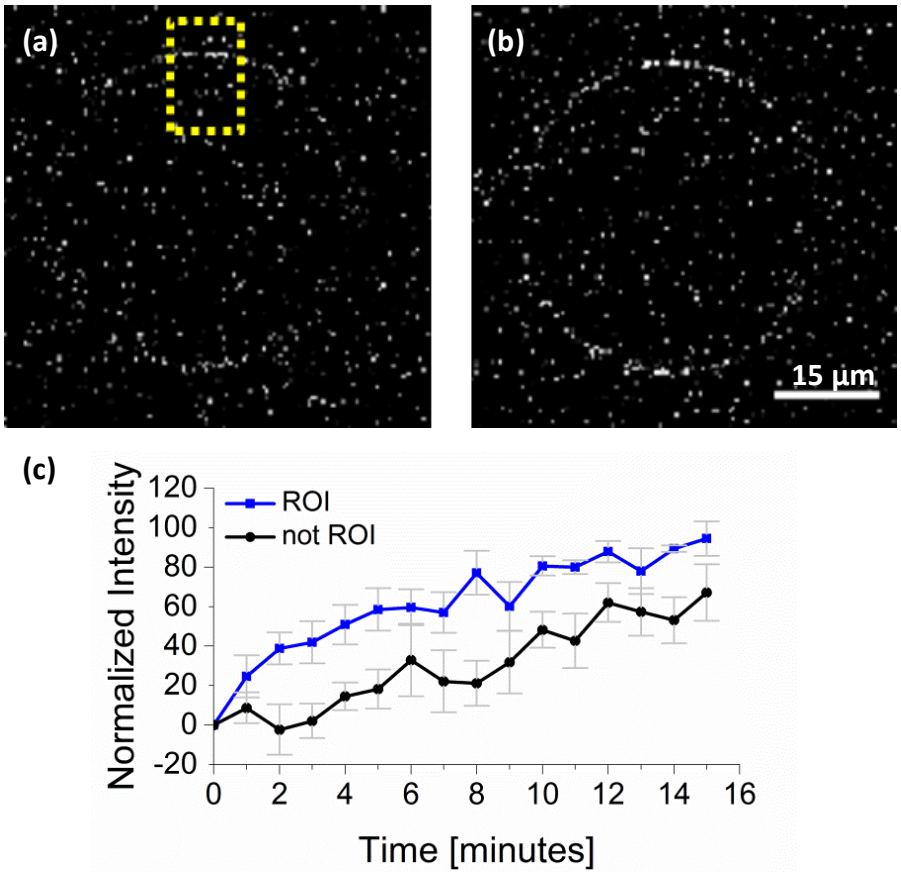

Figure 2.2.4 Local recruitment of mOrange-Nano from the solution to a ROI on a GUV membrane. a) Fluorescence images of iLID-functionalized GUVs in the presence of mOrange-Nano before the local illumination with blue light (488 nm Argon Laser) at the ROI (yellow rectangle). b) Fluorescence images of iLID-functionalized GUVs in presence of mOrange-Nano after the local illumination with blue light at the ROI for 15 minutes. The scale bar is 15 µm. c) Quantification of the local recruitment of mOrange-Nano to the ROI (indicated in blue) and to the opposite side of the GUV (indicated in black). The error bars show the standard error of mean from 5 independent experiments.

2.2.5 Protein recruitment to a single GUV and protein patterning on tissue-like GUV carpets

As light provides tight spatiotemporal control, it was also possible to selectively activate a single GUV in the presence of other GUVs staying not activated. When selecting a field of view with several GUVs and illuminating only a single one of them, mOrange-Nano protein was recruited selectively to the illuminated GUV (Figure 2.2.5 a-b). No fluorescence intensity increase was observed for the unilluminated GUV.

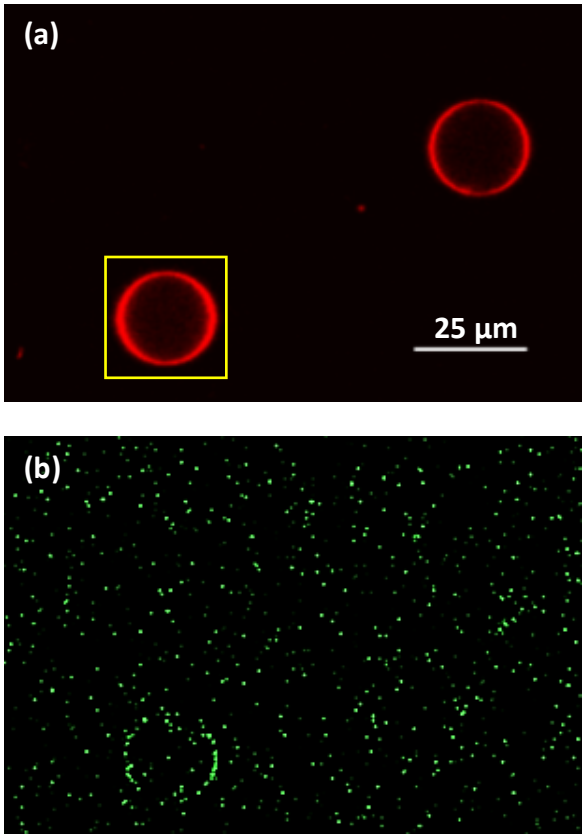

Figure 2.2.5 Selective single GUV activation. a) Fluorescent image (DID dye) of two GUVs located close to each other. The yellow rectangle indicates the GUV that was illuminated with blue light. b) Fluorescence intensity increase after locally recruiting mOrange-Nano to a single GUV by targeted blue light illumination. The scale bar is 25 µm.

In nature protein patterns often are formed over multiple cells; therefore, it was of interest to mimic such patterns by recruiting proteins at the scale of multiple GUVs.[156] For this a carpet of GUVs (lipid composition: POPC + 10 mol% POGP + 1 mol% trisNTA-Suc-DODA) formed on a polyvinyl alcohol

(PVA) substrate was used as a tissue-like substrate, reducing the mobility of the GUVs (Figure 2.2.6 a-b). First, it was possible to recruit mOrange-Nano to the whole GUV carpet under blue light illumination within minutes (Figure 2.2.6 c). Further, it was possible to induce the protein recruitment not only to the whole tissue-like carpet by illuminating the whole field of view but also to the selected ROI by locally illuminating only a region (Figure 2.2.6 d).

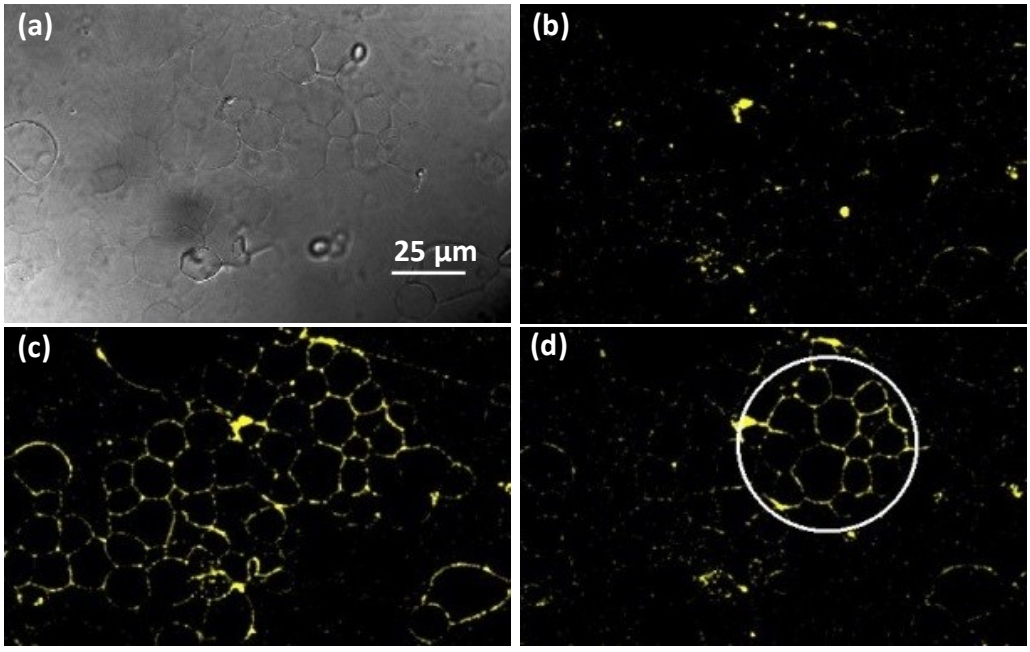

Figure 2.2.6 mOrange-Nano protein patterning on iLID-functionalized GUV carpets. a) DIC image of the PVA substrate-supported GUVs; b) Fluorescence images of the GUV carpet in the dark; c) Fluorescence images of the GUV carpet fully activated with blue light (488 nm); d) Fluorescence images of the GUV carpet locally activated in a ROI with blue light (488 nm) for 1 minute. The circle indicates the illuminated region. The scale bar is 25 µm.

Next, it was also possible to reverse the protein recruitment to the GUV carpet by withdrawing the blue light and keeping the sample for a few minutes in the dark (Figure 2.2.7 a-c).

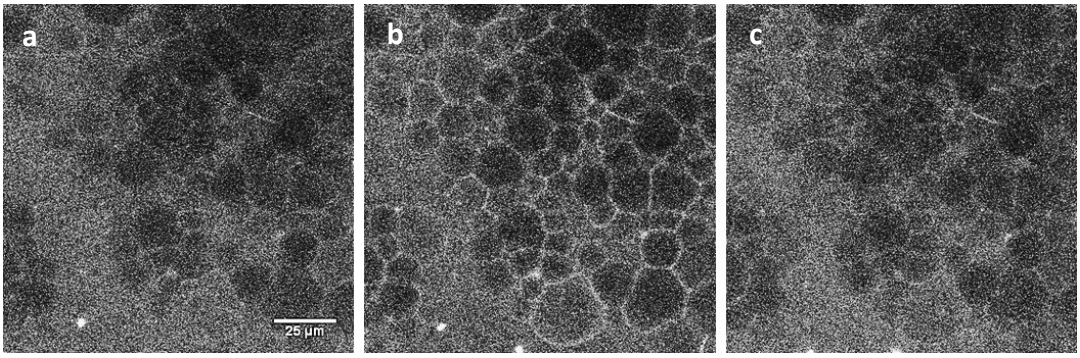

Figure 2.2.7 Reversibility of protein patterns on GUV carpet. a) GUV carpet before blue light illumination; b) GUV carpet after blue light illumination (488 nm) for approx. 1 second; c) GUV carpet after reversing the protein recruitment for approx. 3 minutes in the dark. The scale bar is 25 µm.

Membrane fluidity led to the protein recruitment to the membranes of neighbouring GUVs that were in contact with the illuminated ones. Despite that, it was possible to scale the size of the activated region by adjusting the illuminated area (Figure 2.2.8).

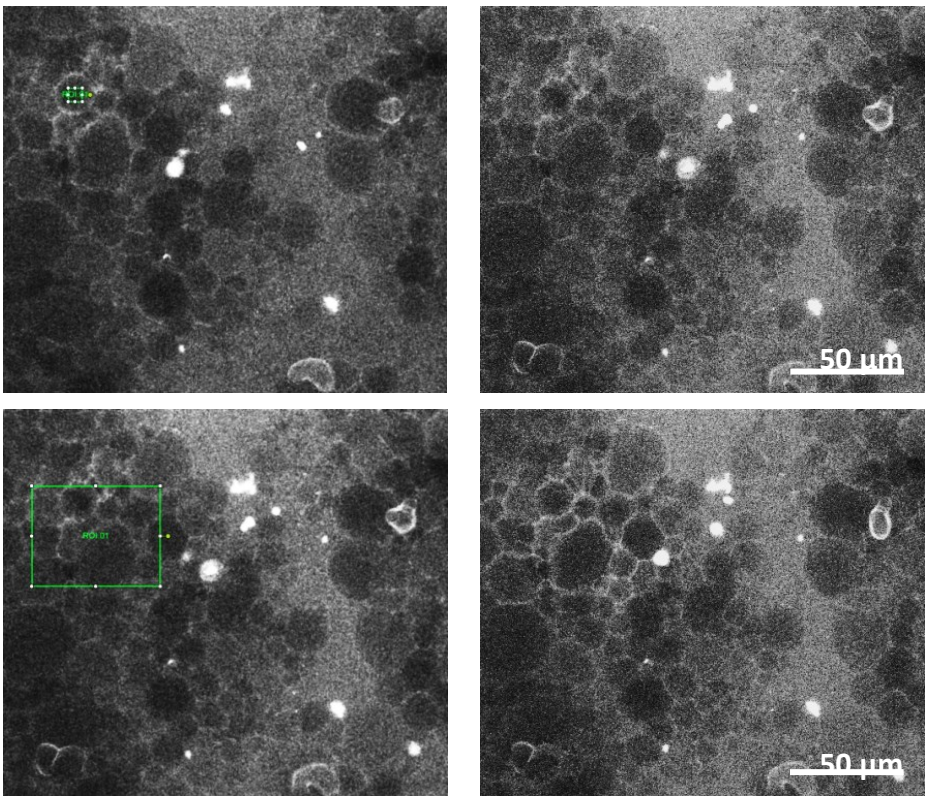

Figure 2.2.8 Illumination of ROIs with different sizes on a GUV carpet. Left panel shows the area and size of the illuminated region. Right panel shows the mOrange-Nano protein recruitment to the GUV carpet membrane after blue light (488 nm) illumination of the ROI.

In summary, in this part of the thesis we were able to selectively and reversibly pattern proteins on GUV membranes using light-dependent interactions between iLID and Nano proteins. We created protein gradients as well as recruited proteins to the whole GUV. Protein recruitment was easily tunable by controlling the light intensity. Further, it was possible to reversibly pattern proteins on single GUVs, at level of a few GUVs and on a whole tissue-like GUV carpet. These patterns over multiple GUVs were easily scalable in size due to the high spatiotemporal resolution. Overall, optogenetic proteins offer a versatile, reversible, dynamic, and non-invasive method to photopattern proteins with high spatiotemporal control that operates under mild conditions.

Chapter 3: Summary and Outlook

Controlling the interactions between synthetic cell-like compartments is essential for their self-assembly and self-sorting into prototissues where different compartments work together and perform complex functions. Although different approaches to control the self-assembly of particles into precise multi-compartmental structures exist, it remains a challenge to dynamically control interactions between colloids with high spatiotemporal resolution. The first aim of this thesis was to achieve self-assembly and self-sorting within complex mixtures of micrometer-sized colloids used as cell-mimics with visible light, mediated by photoswitchable proteins. The control with visible light provides the desired spatiotemporal and dynamic resolution.

In the first part of this thesis, blue light triggered reversible self-assembly and social self-sorting of four populations of colloids into two discrete families was achieved by immobilizing two pairs of blue light switchable proteins, iLID/Nano and nMagHigh/pMagHigh, on solid colloidal particles. The high specificity of iLID/Nano and nMagHigh/pMagHigh protein interactions and the orthogonality of these two protein pairs to each other have made this tight control possible. Together with the reversible nature of these interactions it allowed to overcome the limitations of currently established approaches in colloidal self-assembly. Moreover, the conformational state of these proteins can be switched with low intensities of blue light making this self-assembly strategy biocompatible.

In the future, this concept can be transferred to assemble prototissues using different types of compartments as protocells. For this the photoswitchable proteins can be immobilized on surfaces of different compartments like GUVs, polymersomes or proteinosomes. The interaction between the His-tags of the photoswitchable proteins and the Ni^{2+}-NTA groups on the colloids can also be used to readily functionalize different types of protocells with similar surface chemistry. The limitation of the colloids used as a model for synthetic cells is the inability to encapsulate substances inside them. Expanding the here established photoswitchable self-assembly and self-sorting principles to GUVs

would allow to encapsulate polysaccharides,[31] DNA,[31, 157-158] gene-expression systems,[158] proteins[158] or drugs[159] inside the GUVs. Similarly, various biomolecules, such as DNA and proteins, have been encapsulated into polymersomes[160] and proteinosomes[161-162]. Weiss and colleagues have shown a strategy to encapsulate lipid vesicles into copolymer-stabilized droplets.[20] In the future, using diverse types of cell-mimics would allow bringing together compartments that house different reactions. Regulating the proximity of such hollow compartments is a means to control communication and material exchange between the protocells. For example, Tang and colleagues were already able to show the chemically induced communication between lipid vesicles and proteinosomes.[32] The optogenetic proteins provide a new way to induce the communication between the protocells and would allow regulating it with high spatiotemporal precision.

As there is a wide variety of proteins that have evolved in nature to respond to light of different wavelengths, it is possible to further expand this optogenetic approach using different photoreceptors. As part of this thesis, the heterodimerizing red/far-red light sensitive protein pair PhyB/PIF6 and the blue light sensitive protein pairs iLID/Nano and nMagHigh/pMagHigh were employed to control the self-assembly of colloidal particles of opposite types. This offers further exciting possibilities to combine the red/far-red and the blue light sensitive proteins to achieve self-sorting selectively activated by light of a particular wavelength in multicomponent mixtures. Furthermore, a different interaction mode, namely homodimerization, can be used to bring together compartments of the same type. As part of this thesis, two homodimerizing proteins, one blue (VVDHigh) and one red/far-red (Cph1) light sensitive, were used to achieve the reversible self-assembly of colloids. This offers a capacity to reproduce asocial self-sorting or even more complex sorting modes in colloidal mixtures by utilizing all the described proteins in various combinations. This makes photoswitchable proteins an important building block in the synthetic biology toolbox with the potential to assemble protocells that house different functionalities into prototissues. Finally, these photoswitchable protein interactions can be used to assemble different types of minimal synthetic cells

into complex multi-compartment consortia to mimic processes occurring in nature.

In the second part of this thesis, the application of iLID/Nano protein interaction was extended to form protein patterns on lipid vesicles used as cell-mimics. By functionalizing GUV membranes with iLID protein the recruitment of mOrange fluorescent protein fused to Nano was controlled using blue light with high spatial and temporal precision. The main advantage of the described method compared to the existing protein patterning strategies is that iLID/Nano interaction is highly specific, dynamic and reversible. Blue light at low intensities is not damaging and the protein patterning operates in physiological buffers instead of organic solvents. This would allow using this setup in complex microenvironments with multiple biomolecules. Moreover, the use of light to pattern proteins allows forming the patterns with high spatial and temporal resolution, which is highly relevant to biological systems. Another important advantage of using light as stimulus is that the size of the pattern can be easily scaled up or down from the level of a protein cluster on the GUV membrane to the whole GUV and further to the level of a GUV carpet, providing exceptionally versatile approach.

This strategy is not limited to lipid or colloidal interphases and can be extended to any Ni^{2+}-NTA-functionalized substrate to immobilize one of the His-tagged partners and to any protein of interest that can be fused to its complementary interaction partner. Furthermore, as there is a variety of proteins that respond to light of different wavelengths, this strategy can be expanded to combine different light responsive interactions and simultaneously pattern multiple proteins with high specificity and complexity in a tightly controlled manner.

Chapter 4: Materials and Methods

4.1 Materials

4.1.1 General laboratory equipment

AccuBlock Digital Dry Bath Labnet	Labnet International Inc., Edison, USA
Cell Density Meter CO8000	Biochrom Ltd., Cambourne, England
Centrifuges:	
Avanti J-26S XP (rotors: JA-10 and JA-25.50)	Beckman Coulter Inc., Brea, USA
VWR Micro Star 17	VWR International GmbH, Darmstadt, Germany
Rotixa 50 RS	Andreas Hettich GmbH & Co.KG
Electroporator (MicroPulser™)	Bio-Rad Laboratories GmbH, Munich, Germany
Gel electrophoresis	Bio-Rad Laboratories GmbH, Munich, Germany
HPLC-ÄKTA Explorer 10	GE Healthcare Europe GmbH, Freiburg, Germany
Incubators:	
INCU-Line ® ILS6	VWR International GmbH, Darmstadt, Germany
Innova ® 44	New Brunswick Scientific Co., Inc., Enfield, USA
Lamps:	
Bulbs (blue, red, far-red), 15 Watts	Osram GmbH, Munich, Germany
Blue light panel Albrillo LL-GL003	Albrillo
Red light panel Albrillo LL-GL002	Albrillo
Magnetic stirring hotplate Heidolph MR 3001 K	Sigma Aldrich, Munich, Germany

Milli-Q® Synthesis water purification system with Q-Grad® 2 Purification Cartridge	Merck KGaA, Darmstadt, Germany
NanoDrop 8-sample Spectrophotometer ND-8000	Peqlab Biotechnologie GmbH, Erlangen, Germany
Orbital shaker	Carl Roth GmbH + Co. KG, Karlsruhe, Germany
pH-meter Hanna HI 208	Sigma Aldrich, Munich, Germany
Pipetteboy accu-jet® pro	Brand GmbH + Co KG, Wertheim, Germany
Plate Reader (TECAN SPARK)	Tecan Group Ltd., Männedorf, Switzerland
Protein purification columns:	
Affinity columns HisTrap™ HP (1 mL and 5 mL)	GE Healthcare Europe GmbH, Freiburg, Germany
Scales:	
Mettler PM460 DeltaRange	Mettler-Toledo GmbH, Gießen, Germany
Kern EMB 1000-2	KERN & SOHN GmbH, Balingen, Germany
Sonication bath	BANDELIN Electronic GmbH & Co. KG, Berlin, Germany
Ultrasonic homogenizer Omni Sonic Ruptor 400	Omni International Inc., Tulsa, USA
UV-VIS spectrometer	Lambda25, Perkin Elmer, Germany
Vortex-Genie 1	Scientific Industries Inc., Bohemia, USA

4.1.2 Microscopes

Confocal microscope Leica SP5 with 63X water lens (NA 1.20)	Leica Microsystems GmbH, Wetzlar, Germany

Fluorescence microscope Leica DMi8 with 40X air lens (NA 0.60)	Leica Microsystems GmbH, Wetzlar, Germany
Hamamatsu digital CMOS camera ORCA-Flash4.0, C11440	Hamamatsu Photonics Deutschland GmbH, Herrsching am Ammersee, Germany

4.1.3 Software

Microsoft office (Word, Excel, Power Point)
OriginPro 9.1
ImageJ 1.49h
Leica Application Suite X
EndNote X8

4.1.4 Chemicals

Acetic acid glacial	VWR International GmbH, Darmstadt, Germany
Acetone	VWR International GmbH, Darmstadt, Germany
40% Acrylamide/Bis Solution	Bio-Rad Laboratories GmbH, Munich, Germany
Agarose	Sigma Aldrich, Munich, Germany
Ammonium persulfate (APS)	Sigma Aldrich, Munich, Germany
Antibiotics:	
Ampicillin	Carl Roth GmbH + Co. KG, Karlsruhe, Germany
Kanamycin	Carl Roth GmbH + Co. KG, Karlsruhe, Germany
Chloramphenicol	Sigma Aldrich, Munich, Germany
Brilliant Blue	Sigma Aldrich, Munich, Germany

Bromophenol Blue	Sigma Aldrich, Munich, Germany
Citric acid	Sigma Aldrich, Munich, Germany
Chloroform	Fisher Scientific UK Ltd, Loughborough, United Kingdom
Cholesterol	Sigma Aldrich, Munich, Germany
Copper(II) sulfate pentahydrate ($CuSO_4x5H_2O$)	Sigma Aldrich, Munich, Germany
Diethyl ether	Sigma Aldrich, Munich, Germany
Dimethyl sulfoxide (DMSO)	Merck KGaA, Darmstadt, Germany
DL-Dithiothreitol (DTT)	Sigma Aldrich, Munich, Germany
Ethylenediaminetetraacetic acid (EDTA)	Sigma Aldrich, Munich, Germany
Ethanol	VWR International GmbH, Darmstadt, Germany
Ethyl acetate	VWR International GmbH, Darmstadt, Germany Honeywell International Inc., New Jersey, United States
α-D-Glucose	Sigma Aldrich, Munich, Germany
Glycerol	Sigma Aldrich, Munich, Germany
Glycine	Carl Roth GmbH + Co. KG, Karlsruhe, Germany
Hydrogen peroxide (35%) (H_2O_2)	Carl Roth GmbH + Co. KG, Karlsruhe, Germany

Hydrochloric acid (37%) (HCl)	VWR International GmbH, Darmstadt, Germany
Imidazole	Sigma Aldrich, Munich, Germany
Isopropyl-β-D-thiogalactopyranoside (IPTG)	Fisher Scientific GmbH, Schwerte,Germany
L-Ascorbic acid	Sigma Aldrich, Munich, Germany
Lipids:	All from Avanti® Polar Lipids, Alabaster USA; Distributed by Sigma Aldrich, Munich, Germany
1,2-Dioleoyl-sn-glycero-3-phosphocholine (DOPC)	
Palmitoyl-2-oleoylphosphatidylcholine (POPC)	
1-palmitoyl-2-oleoyl-sn-glycero-3-phospho-(1'-rac-glycerol) (POPG)	
1,2-dioleoyl-sn-glycero-3-[(N-(5-amino-1-carboxypentyl)iminodiacetic acid) succinyl] (DGS-NTA)	
N-succinyldioctadecylamine with three NTA groups (trisNTA-Suc-DODA)	Gift from Prof. R. Tampé Lab, Institute of Biochemistry, Goethe University Frankfurt, Germany
2-Mercaptoethanol	Sigma Aldrich, Munich, Germany
Methanol	VWR International GmbH, Darmstadt, Germany
Nickel(II) chloride hexahydrate ($NiCl_2x6H_2O$)	Sigma Aldrich, Munich, Germany
Paraformaldehyde (PFA)	Sigma Aldrich, Munich, Germany
Phenylmethylsulfonyl fluoride (PMSF)	Sigma Aldrich, Munich, Germany

Pluronic® F-127	Sigma Aldrich, Munich, Germany
Potassium dihydrogen phosphate (KH_2PO_4)	Sigma Aldrich, Munich, Germany
Potassium hydrozyde (KOH)	Carl Roth GmbH + Co. KG, Karlsruhe, Germany
2-Propanol	Biosolve BV, Valkenswaard, Netherlands Honeywell International Inc., New Jersey, United States
Sodium chloride (NaCl)	Sigma Aldrich, Munich, Germany
Sodium dodecyl sulfate (SDS)	Carl Roth GmbH + Co. KG, Karlsruhe, Germany
Sucrose	Sigma Aldrich, Munich, Germany
Sulfuric acid H_2SO_4 (95-97%)	Sigma Aldrich, Munich, Germany
N,N,N',N'-Tetranethyl-ethylrnrdiamine (TEMED)	Sigma Aldrich, Munich, Germany
3-(Triethozysilyl)propyl isocyanate	Sigma Aldrich, Munich, Germany
Trizma® base (TRIS)	Sigma Aldrich, Munich, Germany

4.1.5 Biochemicals

Bacterial medium:	
Agar	Carl Roth GmbH + Co. KG, Karlsruhe, Germany
Luria-Bertani (LB)	Carl Roth GmbH + Co. KG, Karlsruhe, Germany

Bovine Serum Albumin (BSA)	Sigma Aldrich, Munich, Germany
cOmplete Protease inhibitor cocktail tablets	Roche Diagnostics GmbH, Mannheim, Germany
1,1'-Dioctadecyl-3,3,3',3'-Tetramethylindodicarbo-cyanine (DiD) dye	Thermo Fisher Scientific BV & Co KG, Braunschweig, Germany
Kits:	
MiniPrep	QIAGEN Inc., Hilden, Germany
Site-directed mutagenesis	Agilent Technologies, Santa Clara, CA, USA
Novex™ Prestained Protein Standard	Thermo Fisher Scientific BV & Co KG, Braunschweig, Germany
Plasmids	Addgene, Cambridge, USA Genscript, Piscataway, USA Wombacher Lab (Heidelberg)
Protein loading dye:	
4xProtein loading dye (stored at -20 °C): 40 % glycerol 240 mM TRIS pH 6.8 8 % SDS 0.04 % bromphenol blue 5 % beta-mercaptoethanol	
Protein standards:	
Color Protein Standard Broad Range	NEB GmbH, Frankfurt am Main, Germany
Unstained Protein Standard Broad Range (10 - 200 kDa)	NEB GmbH, Frankfurt am Main, Germany

4.1.6 Disposables

Amicon centrifugal filter units, 15mL (10 kDa, 100 kDa)	Merck KGaA, Darmstadt, Germany

Amicon centrifugal filter units, 50mL (10 kDa, 100 kDa)	Merck KGaA, Darmstadt, Germany
Cellulose filters (0.22 and 0.45 µm)	Carl Roth GmbH + Co. KG, Karlsruhe, Germany
Cover slips (20 x 20 mm and 24 x 60 mm)	Carl Roth GmbH + Co. KG, Karlsruhe, Germany
Electroporation cuvettes (1 mm)	Bio-Rad Laboratories GmbH, Munich, Germany
Eppendorf® tubes (1.5 mL, 2 mL)	Eppendorf AG, Hamburg, Germany
Falcon® tubes (15 mL, 50 mL)	Greiner Bio-One, Frickenhausen, Germany
LoBind Eppendorf® tubes (1.5 mL)	Eppendorf AG, Hamburg, Germany
Nunc® Lab-Tek® Chamber Slide System (8-well)	Thermo Fisher Scientific BV & Co KG, Braunschweig, Germany
Petri dishes (90 mm diameter, 14.2 height)	VWR International GmbH, Darmstadt, Germany
Plastic pipettes (5 mL, 10 mL)	Greiner CELLSTAR®, Sigma Aldrich, Munich, Germany
Pipette tips (10 µL, 100 µL, 1000 µL)	STARLAB GmbH, Hamburg, Germany
UV-VIS semi-micro polystyrene cuvettes	Brand GmbH + Co KG, Wertheim, Germany

4.1.7 Buffers

Buffer A (binding buffer):

50 mM TRIS pH 7.4

300 mM NaCl (add 1 mM DTT right before the purification)

Buffer B (elution buffer):

50 mM TRIS pH 7.4

300 mM NaCl

250 mM Imidazole (add 1 mM DTT right before the purification)

Buffer A minimal (experiments with GUVs):

10 mM TRIS pH 7.4

100 mM NaCl

Coomassie brilliant blue (1 L):

1 g brilliant blue

50 % (v/v) Methanol

10 % (v/v) Acetic Acid

40 % MilliQ water

Destaining buffer:

40 % Methanol

10 % Acetic acid

50 % MilliQ water

Immobilized metal affinity chromatography (IMAC) binding buffer:

50 mM KH_2PO_4

400 mM NaCl

0.5 mM 2- Mercaptoethanol

pH 7.5

IMAC elution buffer:

50 mM KH_2PO_4

400 mM NaCl

0.5 mM 2- Mercaptoethanol

500 mM imidazole

pH 7.5

10xSDS PAGE running buffer:

250 mM TRIS

1,92 M glycine

1 % SDS (w/v) in MilliQ water

TEV binding buffer:

50 mM TRIS HCl pH 7.4

300 mM NaCl

30 mM imidazole

1 mM DTT

20xTEV reaction Buffer:

1 M TRIS HCl pH 8.0

10 mM EDTA

(add 1 mM DTT right before the purification)

4.2 Methods

4.2.1 SDS-Gel

Table 4.2.1 SDS-gel preparation

Component	Stacking gel	Resolving gel (12%)	Resolving gel (10%)
40% Acrylamid	1.48 mL	7.5 mL	6.25 mL
0.5 M TRIS pH=6.8	3.78 mL	-	-
1.5 M TRIS pH=8.8	-	6.25 mL	6.25 mL
10% SDS	150 µL	250 µL	250 µL
H_2O	9.5 mL	10.9 mL	12.1 mL
TEMED	15 µL	12.5 µL	12.5 µL
10% (w/v) APS	75 µL	125 µL	125 µL
Total volume	15 mL	25 mL	25 mL

All components for both stacking and resolving gels were mixed together except for the ammonium persulfate (APS). Then APS was added to the resolving gel, rapidly mixed and poured in between glass plates placed in the holders. The gels were allowed to solidify before adding APS to the stacking gel, mixing and pouring on top of the resolving gel. A comb was then placed in the stacking gel to form the wells. Several gels were prepared in parallel and were stored wrapped in soaked with MilliQ water paper at 4 °C.

SDS-Gels were loaded with 15 µL of protein mixed with 5 µL protein loading dye. Protein marker was run in parallel (5 µL) to be able to identify the protein sizes. 120 mA and 200 V were applied for 37 minutes to run the proteins in the gel. SDS-PAGE was stained with coomassie brilliant blue staining solution, while heating it for 30 seconds in the microwave and allowing soaking for 5 minutes at room temperature. After that, the coomassie staining was removed and destaining solution was added. The gel was left on a shaker for 1 hour or until the gel became transparent and the protein bands became clearly visible. The gels were then scanned for documentation and further analysis.

4.2.2 Starting culture

Luria-Bertani (LB) medium was autoclaved and appropriate antibiotic was added to 10 mL LB medium (50 µg/mL for ampicillin and kanamycin; 35 µm/mL for chloramphenicol). Bacteria were inoculated into the medium and left shaking over night at 200 rpm at 37 °C. A glycerol stock of the bacterial culture was prepared after the overnight incubation by mixing 500 µL of the bacteria culture with 500 µL 80% glycerol solution.

4.2.3 Plasmids

pQE-80L iLID (C530M), pQE-80L MBP-SspB Nano and pQE-80L MBP-SspB Micro were gifts from Brian Kuhlman (Addgene plasmids # 60408, # 60409 and #60410, respectively).[126] pQE-80L iLID (C530M) expresses iLID with an N-terminal His6-tag. pQE-80L MBP-SspB Nano and pQE-80L MBP-SspB Micro express Nano or Micro with N-terminal His6-MBP-TEV tag (His6-MBP-TEV-Nano and His6-MBP-TEV-Micro, respectively). The sequence for nMagHigh was synthesized by the GeneScript and inserted into pET21b between the NdeI and XhoI cutting sites to include a C-terminal His6-tag. The pMagHigh plasmid was obtained through site-directed mutagenesis of nMagHigh (D52R, G55R) and pMag plasmid was obtained through site-directed mutagenesis of pMagHigh (I135M, I165M) (done by S. M. Bartelt). VVDHigh plasmid was obtained through site-directed mutagenesis of pMagHigh (R52I, R55M) (done by Y. Ji).[125] pET His6 GFP TEV LIC cloning vector (1GFP) was a gift from Scott Gradia (Addgene plasmid # 29663). The mOrange-GGS was inserted into the pQE-80L MBP-SspB Nano plasmid after the BamHI cutting site to yield His6-MBP-TEV-

mOrange-Nano. The TEV cutting site was used to cleave the His6-tag after Ni^{2+}-NTA affinity purification to yield Nano and mOrange-Nano. His6-tagged TEV protease originated from the Wombacher Lab (Heidelberg) and was kindly provided as a glycerol stock of *E. coli* BL21 (DE3) co-transformed with pLysS (chloramphenicol) and pET N_TEV234 (kanamycin) plasmids.

The DNA sequence for Cph1 was synthesized by the GeneScript and inserted into pET21b vector between the NdeI and SalI cutting sites to include a C-terminal His6-tag.[116]

The PhyB originated from the Prof. Dr. W. Weber Lab (Center for Biological Systems Analysis, University of Freiburg) and was kindly provided to us as a bacterial pellet co-expressing PhyB and PCB. PIF6-GFP-TEV was synthesized by the GeneScript and inserted into pET21b vector between the NdeI and HindIII cutting sites.

All plasmids were amplified using *E. coli* DH5α electrocompetent bacteria and isolated using QIAprep Spin Miniprep Kit following the manufacturer's instructions. The plasmid concentration was then quantified using NanoDrop Spectrophotometer.

4.2.4 Electroporation

49.5 µL of electrocompetent bacteria (*E. coli,* DH5α strain) and 0.5 µL of plasmid DNA were gently mixed by pipetting. The mixture was transferred into a 0.1 cm electroporation cuvette and a single electrical pulse was given (1.8 kV, preprogrammed settings). 450 µL LB medium were immediately added to the bacteria before transferring it into an Eppendorf tube. The bacteria were allowed to recover at 37 °C at 200 rpm for 1 hour. Then the bacteria were spread on a LB agar plate containing 50 µg/mL of appropriate antibiotic and incubated overnight at 37 °C.

4.2.5 Chemical transformation

48 µL of chemically competent bacteria (*E. coli,* BL21 strain) and 2 µL of plasmid DNA were gently mixed by pipetting. After 30 minutes incubation on ice the bacteria were heat-shocked by putting the Eppendorf tube in a heating

block at 42 °C for 45 seconds before transferring it rapidly on ice for another 2 minutes. Then 450 µL of LB media was added to the bacteria and incubated at 37 °C for 1 hour before spreading the bacteria on a LB agar plate with 50 µg/mL of appropriate antibiotic. The plate was incubated overnight at 37 °C before picking the colonies.

4.2.6 Protein expression and purification

Each plasmid was transformed into *E. coli* BL21 (DE3) and a 10 mL overnight starting culture was grown as described above. The culture was then transferred into 1 L of LB medium with 50 µg/mL appropriate antibiotic and grown at 37 °C at 200 rpm until the OD_{600}=0.4-0.6, before inducing protein expression with 0.5 mM IPTG (isopropyl β-D-1-thiogalactopyranoside). The culture was incubated at 16 °C overnight (with an exception for the TEV protease, which was expressed at room temperature overnight) while continuously being shaken. Then the bacteria was pelleted by centrifugation (6000 rpm, 4 °C, 8 minutes, JA-10 rotor) before resuspending it in Buffer A (50 mM Tris, 300 mM NaCl, pH=7.4) containing 100 µM PMSF in methanol and 1 mM DTT and lysing by sonication (50% frequency, 40% power, 10 minutes). The supernatant was filtered twice through a 0.45 µm cellulose filter. Then the clarified lysate was purified using a Ni^{2+}-NTA affinity column (column volume 5 mL). For this the protein solution was passed over the column twice and first washed with 10 mL Buffer A containing 1 mM DTT and then with 5% Buffer B (47 mL Buffer A + 2.5 mL Elution buffer + 80 µL DTT). In the next step the protein was eluted form the Ni^{2+}-NTA affinity column with 10 mL elution buffer (Buffer B containing 1 mM DTT) and collected into a tube. The protein solution was dialyzed in dialysis bags (3.5 kDa cut-off) in 2 L of Buffer A containing 1 mM DTT overnight at 4 °C. The buffer was replaced twice with a fresh one and stirred for another 3 hours each time at 4 °C. The protein purity was verified by SDS-PAGE (Figures A2 and A4). Proteins were aliquoted and stored at -80 °C.

4.2.6.1 PhyB purification

The PhyB pellet was thawed in 125-130 mL IMAC binding buffer (KH_2PO_4 50 mM, NaCl 400 mM, 2-Mercaptoethanol 0.5 mM, pH 7.5 + 0.5 mM 2-Mercaptoethanol added to the buffer directly before purification) in 37 °C water bath. After thawing, the resuspended pellet was cooled down on ice and homogenized with a stir bar on the magnetic stirrer for 30 minutes. After this 1.25 mL of 100 mM PMSF was added and the bacteria were lysed. For this the mixture was distributed into 30 mL portions and sonicated twice for 10 minutes with 60% frequency while continuously cooling. Lysed bacteria were spun down in the ultracentrifuge for 1 hour at 12000 rpm at 4 °C. The supernatant from all fractions was collected and combined before applying it on the pre-washed with IMAC buffer Ni^{2+}-NTA affinity column. The flow through was collected and washed through the column for 5 times to ensure the maximum saturation of the column resin. Further purification was performed as for all the other proteins with an exception of using IMAC buffer instead of Buffer A and IMAC elution buffer instead of buffer B (KH_2PO_4 50 mM, NaCl 400 mM, BME 0.5 mM, 500 mM imidazole, pH 7.5 + 17 µL Mercaptoethanol added directly before the purification).

4.2.7 Light sources and intensities

The light power was measured using a LabMax-TOP meter with an OP-2 VIS power sensor (8 mm in diameter, Coherent Inc.) at 6.5 cm distance (equals to the distance at which the samples were positioned). For the blue and red light illumination an LED light panels were used (blue: Albrillo LL-GL003, 225 LEDs, 460 nm, 14 W, red: Albrillo LL-GL002, 225 LEDs, 630 nm, 14 W). The light intensity was controlled by using neutral density filters (Tables 4.2.2 and 4.2.3). Far-red light illumination was done with a far-red LED lamp, 15 W, 700-800 nm (10.81 mW/cm^2 at 6.5 cm distance).

Table 4.2.2 Blue LED light intensity.

Number of neutral density filters	**Light intensity, [mW/cm²]**
0	≈ 1.45
1	≈ 1.02
2	≈ 0.71
3	≈ 0.50

For all the experiments, unless specified otherwise, the blue light intensity of 0.71 mW/cm² was used.

Table 4.2.3 Red LED light intensity.

Number of neutral density filters	**Light intensity, [mW/cm²]**
0	≈ 0.89
1	≈ 0.62
2	≈ 0.44
3	≈ 0.30

For all the experiments, unless specified otherwise, the red light intensity of 0.89 mW/cm² was used.

For light activation under the confocal microscope, an argon laser (488 nm) was used to illuminate the samples with the blue light. The light power was measured using a LabMax-TOP meter with an OP-2 VIS power sensor (8 mm in diameter, Coherent Inc.). The sensor was positioned over the microscope objective and the laser power was measured for different power percentages (1%, 2%, 5%, 10% and 20%) through the 63x water objective (Table 4.2.4).

Table 4.2.4. Light power at different laser power percentage of the SP5 confocal microscope.

Laser power percentage	Mean power ± Standard deviation [nW]
1%	70.8 ± 2.7
2%	151.3 ± 5.6
5%	575.5 ± 21
10%	1790 ± 71
20%	6330 ± 238

4.2.8 Microscopy

For the bead self-assembly project all images were either acquired on an inverted fluorescent microscope (DMi8, Leica) through the 40x air objective using bright field, FITC (excitation max: 494 nm; emission max: 520 nm) and TRITC (excitation max: 557 nm; emission max: 576 nm) channels, or on a confocal laser scanning fluorescence microscope (SP5 Leica) through the 63x water objective.

For the dynamic patterning project the imaging was performed either on a Leica SP5 laser scanning confocal microscope (for all the experiments except for the patterning on a GUV carpet) or a Leica SP8 laser scanning confocal microscope with a FRAP (Fluorescence Recovery after Photobleaching) module (for the patterning on a GUV carpet experiments).

4.2.9 Protein immobilization on beads

Polystyrene beads with 2 µm or 12 µm diameter functionalized with the Ni^{2+}-NTA groups (with and without fluorescent labels) were purchased as a water suspension (50 mg/mL, $1.2x10^{10}$ beads/mL, stable in aqueous solutions, methanol, ethanol and DMSO). Fluorescently-labelled beads contain fluorescein (excitation/emission: 485/510 nm) and rhodamine B (excitation/emission: 572/590 nm) derivatives to obtain green and red labeled beads, respectively. Beads were stored at 4 °C in water. For the experiments, water was replaced with Buffer A by spinning the beads down (13000 rpm, 2 minutes), removing the water and resuspending them in Buffer A. The proteins were immobilized

on the Ni^{2+}-NTA-functionalized beads through His-tag-Ni^{2+}-NTA interaction by incubating 5 mg/mL of beads in Buffer A with an excess of 1 µM His-tagged protein at 4 °C for 1 hour. Then the excess protein was washed away by spinning the beads down twice and washing them with Buffer A. Before each experiment the protein functionalized beads were sonicated for 1 minute to properly disperse them.

The number of His-tagged proteins per bead was evaluated by incubating an excess of 1 µM His6-tagged GFP (green fluorescent protein) with 5 mg/mL beads at 4 °C for 1 hour. After spinning down the beads the fluorescence of the GFP that remained in the supernatant was measured in a plate reader and compared to a calibration curve. The number of His6-tagged GFPs was calculated to be approximately 200-300 proteins per bead.

Two different methods were used to evaluate the number of proteins per bead. In the first method, 1 µM excess of His6-tagged GFP (green fluorescent protein) was incubated with 5 mg/mL beads at 4 °C for 1 hour. After spinning down the beads the fluorescence of the GFP that remained in the supernatant was measured in a microplate reader and compared to a calibration curve (0 nM, 200 nM, 500 nM, 750 nM, 1000 nM and 2000 nM). From this the number of His6-tagged GFPs was calculated to be approximately 200 proteins per bead. In the second method, 1 µM excess of His6-tagged GFP was first immobilized on the beads as described above. Then the excess of protein was washed away and all the protein that was bound was denatured from the beads at 95 °C for 10 minutes and run on an SDS-PAGE together with known GFP concentrations (100 nM, 200 nM and 500 nM). Using ImageJ software the intensity of the bands was evaluated using the analyze gels tool and the amount of GFP bound on the beads and the number of proteins per beads was calculated to be approximately 300 proteins per bead.

Furthermore, the functionalization efficiency was estimated by using flow cytometry. For this an excess of 5 µM His6-tagged GPF was incubated with 5 mg/mL beads at 4 °C for 1 hour followed by two washing steps with Buffer A. The samples were then diluted 1:500 in Buffer A and analysed with Attune NxT Acoustic Focusing Cytometer. Bead fluorescence was compared to the

fluorescence of an unfunctionalized bead sample at the same dilution. The fluorescence peaks from unstained and stained beads do not overlap in ≈ 92% of all recorded events.

4.2.10 Bead aggregation assay

For the heterodimerization experiments 25 µL (5 mg/mL) of each bead type were mixed and diluted to a total volume of 300 µL in Buffer A. For the homodimerization experiments 50 µL (5 mg/mL) were diluted to a total volume of 300 µL in Buffer A. The samples were either kept in the dark/far-red or under blue light (460 nm)/ red light (630 nm) for 2 hours, while being gently agitated in LoBind Eppendorf tubes at 50 rpm in an orbital shaker. For the reversibility experiments the samples were first incubated under blue or red light for 2 hours and then kept in the dark or far-red light for 1 hour. Subsequently, the samples were fixed with 300 µL of 10% (w/v) paraformaldehyde (PFA) for 20 minutes, 300 µL of the sample were transferred into an imaging chamber (Lab-Tek®) with a cut pipette tip and allowed to settle for 30 minutes before acquiring 15 images (bright field, FITC channel or TRITC channel) for each sample.

To study the aggregation dynamics, the samples were kept in the orbital shaker at 50 rpm under blue or red light or in the dark or far-red light for 30 minutes, 1 hour, or 2 hours before fixation, transfer into the imaging chamber and imaging. For the time point t=0 the samples were fixed immediately after mixing of the samples in an Eppendorf tube. To study the reversion dynamics, samples were first kept under the blue or red light for 2 hours in an orbital shaker at 50 rpm. Then the samples were put in the dark or far-red light for 15 minutes, 30 minutes or 1 hour before fixation and imaging. At each time point the aggregation ratio of the reversed samples was compared to the aggregation ratios of dark and blue samples that were incubated for exactly the same time.

4.2.11 Data analysis

The microscopy images were analyzed using the ImageJ software. After importing the images into the software, an intensity threshold was applied to select particles. The images were made binary and holes were filled using the

"Fill holes" tool. After this the area occupied by beads was quantified using the "Analyze particle tool". First, to quantify the clusters (projected area > 10 beads) a size limit of 30-infinity μm^2 was applied. Second, all beads in the image were quantified by applying a size limit of 3-infinity μm^2. From this data the aggregation ratio occupied by clusters was calculated by dividing the total area occupied by all the clusters by the total area occupied by all the beads in the same image. The sizes of clusters and their number were also quantified. The data was plotted and statistically analyzed (either Mann-Whitney test (significance level 0.05) or One-Way ANOVA test (significance level 0.05) followed by Dunn-Sidak post hoc test (significance level 0.05)) using OriginPro.

4.2.12 Self-assembly with changing stoichiometry

For the stoichiometry experiments iLID (or nMagHigh) were immobilized on red fluorescent beads and Nano (or pMagHigh) were immobilized on green fluorescent beads as described above. 25 µL of one bead type were mixed with 5 µL of the bead type with the complementary interaction partner (5:1 or 1:5 ratios) and diluted to the total volume of 300 µL in Buffer A. The mixture was incubated in an orbital shaker for 2 hours at 25 rpm directly in the imaging chamber (Lab-Tek®). Afterwards, the samples were fixed with 10% (w/v) PFA and fluorescent images were acquired in the FITC and TRITC channels.

4.2.13 Social self-sorting of beads

For the social self-sorting experiments four different proteins were immobilized on 2 µm in diameter polystyrene beads. At first, iLID and Nano were each immobilized on red fluorescent beads and nMagHigh and pMagHigh were each immobilized on green fluorescent beads as described above. Then all four types of beads were mixed together in equal proportions (12.5 µL each type, 5 mg/mL, total volume 300 µL in Buffer A). The samples were kept under blue light at 25 rpm agitation for 2 hours directly in the imaging chamber before being fixed with 300 µL of 10% (w/v) PFA and imaged in bright field, FITC and TRITC channel.

4.2.14 Sedimentation of 12 µm beads

For the sedimentation experiments two bead populations (12 µm in diameter, Ni^{2+}-NTA functionalized) were functionalized separately with either nMagHigh or pMagHigh protein as described above. Next, 40 µL of each bead type (5 mg/mL) were mixed in the total volume of 800 µL in Buffer A in a UV-VIS cuvette and thoroughly resuspended by pipetting. The samples were then either kept in the dark or under the blue light, while measuring the optical density at 600 nm (OD_{600}) every minute for 1 hour (during the measurement itself the light was shortly switched off). For the data analysis the curves were fitted with a sigmoidal Boltzmann fit in OriginPro software. Time points at which the OD_{600} has decreased by half were calculated from these fits.

4.2.15 Removal of His-tags through TEV protease cleavage

The proteins containing a TEV protease cleavage site were mixed with the TEV protease in 50:1 ratio in an Eppendorf tube. Then the mixture was dialyzed in a dialysis tube (3.5 kDa molecular weight cut-off) against the TEV reaction buffer overnight at 4 °C. To purify the cut protein fraction (without His6-tag) from the uncut fraction, the reaction mixture was run through a Buffer A-equilibrated HisTrap™ affinity column (1 mL or 5 mL, GE Health Care Inc.) and the flow through was collected. The flow through was then analyzed with a SDS-PAGE to confirm that it contains the cut protein (without His6-tag) (Figure A5).

4.2.16 GUV formation and functionalization with iLID

The assisted gel formation method was used to prepare the GUVs.[34] First 50 µL of 5% (w/v in Milli-Q water) of PVA (polyvinyl alcohol, 145000 g/mol, containing 100 mM sucrose) were dried as a thin layer on a 60x24 mm glass slide at 50 ˚C for 30 minutes. Then, 5 µL of a lipid solution (10 mg/mL 1-Palmitoyl-2-oleoylphosphatidylcholine (POPC) + 10 mol% 1-palmitoyl-2-oleoyl-sn-glycero-3-phospho-(1'-rac-glycerol) (POPG) + 0.1 mol% 1,2-dioleoyl-sn-glycero-3-[(N-(5-amino-1-carboxypentyl)iminodiacetic acid) succinyl] Ni^{2+} Salt (DGS-NTA-Ni^{2+}) + 1 mol% 1,1'-Dioctadecyl-3,3,3',3'-Tetramethylindodicarbo-cyanine (DiD) dye in chloroform, all lipids are purchased from Avanti Polar Lipids) were dried on the PVA layer at 30 ˚C or

under vacuum for 1 hour. Using silica grease as a spacer and a second glass slide a chamber was built on top of the slide with PVA and lipid layers. The lipids were then hydrated with 1 mL of Buffer A minimal for 1 hour at room temperature allowing GUV formation. The chamber was then inverted and GUVs were harvested with a syringe. iLID protein was immobilized on the GUVs through the His6-tag-Ni^{2+}-NTA interaction by adding iLID (final concentration of 10 nM) to the 100 µL of harvested GUVs in suspension and incubating them for 30 minutes in the dark to allow the functionalization.

4.2.17 Protein recruitment to GUVs

A self-made chamber (cut Eppendorf tube attached on top of a 60x24 mm glass slide with silica grease) was incubated with 3% bovine serum albumin (BSA w/v in Millli-Q water) for 20 minutes prior to the experiment to prevent unspecific protein adsorption and the GUV bursting. The chamber was then washed 3 times with Buffer A minimal. After that a solution of iLID-functionalized GUVs mixed in a 1:1 ratio with a solution of 50 nM mOrange-Nano was transferred into the chamber.

The samples were imaged either using a Leica SP5 laser scanning confocal microscope (for all the experiments except for the patterning) or a Leica SP8 laser scanning confocal microscope with a FRAP (Fluorescence Recovery after Photobleaching) module (for the patterning experiments). An argon laser (488 nm) was used to illuminate the samples with the blue light continuously in order to activate protein recruitment from the solution. TRITC channel was used to detect the mOrange (excitation max: 557 nm; emission max: 576 nm) signal and visualize the protein recruitment. A HeNe laser was used to excite the DiD dye (Cy5 channel, excitation max: 644 nm; emission max: 665 nm) in the GUVs for easier handling of the samples.

To quantify the protein recruitment to GUV membrane the mean fluorescence intensity of a whole GUV was analysed using ImageJ software. For this a circle was drawn around the GUV close to its borders. Mean grey value was measured for all the time points, where the first time point was always the sample in the dark. The mean intensity at the data time point t=0 was subtracted from all other data points. The data was then normalized by setting the maximum value

to 100 and calculating the percentage of intensity change. The experiments were repeated multiple times and at least 3 GUVs were analysed in each case.

4.2.18 Effect of lipid fluidity on the protein recruitment

GUVs with different composition were prepared to compare the dependence of protein recruitment to GUV on the lipid membrane fluidity. To modulate the fluidity 20 mol% or 40 mol% cholesterol were added to the standard lipid preparation (10 mg/mL POPC + 10 mol% POPG + 0.1 mol % DGS-NTA-Ni^{2+} + 1 mol% DiD). Additionally, a 1,2-dioleoyl-*sn*-glycero-3-phosphocholine (DOPC) (10 mg/mL DOPC + 10 mol% POPG + 0.1 mol% DGS-NTA-Ni^{2+} + 1 mol% DiD) lipid preparation was used for the comparison.

The GUVs were prepared, hydrated with Buffer A minimal, harvested and functionalized with iLID protein as described above. After 30 minutes incubation in the dark 25 nM final concentration of mOrange-Nano was added to the imaging chamber. The GUVs were illuminated with an Argon laser (488 nm, 5%) through the 63x water objective for 15 minutes, while continuously acquiring fluorescent images for mOrange-Nano in TRITC channel and DID in Cy5 channel.

4.2.19 Protein recruitment to ROI

The protein recruitment to region of interest (ROI) was performed following the same protocol as in the protein recruitment to the whole GUV. In this case only a small ROI on the side of a GUV was constantly illuminated with Argon laser (488 nm, 5% power), while acquiring images at a rate of 1 image/second in the TRITC channel for up to 30 minutes.

4.2.20 Protein recruitment to a single GUV

For the protein recruitment to a single GUV experiments the GUVs (10 mg/mL 1-Palmitoyl-2-oleoylphosphatidylcholine (POPC) + 10 mol% 1-palmitoyl-2-oleoyl-sn-glycero-3-phospho-(1'-rac-glycerol) (POPG) + 0.1 mol% 1,2-dioleoyl-sn-glycero-3-[(N-(5-amino-1-carboxypentyl)iminodiacetic acid) succinyl] (DGS-NTA) Ni^{2+} Salt + 1 mol% 1,1'-Dioctadecyl-3,3,3',3'-Tetramethylindodicarbocyanine (DiD) dye in chloroform, from Avanti Polar Lipids) were prepared and

functionalized as described above. The GUVs were allowed to settle down in the 50 nM Nano-mOrange solution and a region with several GUVs close but not touching each other was chosen. One of the GUVs in the field of view was illuminated with a blue light laser (Argon laser, 488 nm, 5%) through 63x water objective for 15 minutes, while the other GUVs in the field of view were not illuminated. Fluorescent images for mOrange-Nano in TRITC channel were acquired for the whole field of view.

4.2.21 Patterning on GUV carpet

For the patterning experiments a layer of GUVs (4 mM total lipid concentration, POPC + 10% POGP + 1% N-succinyldioctadecylamine with three NTA groups (trisNTA-Suc-DODA)) was prepared as described above with following differences. Instead of harvesting GUVs after the hydration, they were directly used in the hydration chamber. For the hydration step a modified buffer was used to prevent the GUVs from bursting (10 mM Tris, 100 mM NaCl, pH 7.4). The GUVs were then functionalized with iLID protein as described above and afterwards 50 nM mOrange-Nano was flushed into the chamber. To create a pattern the FRAP-Module of the Leica SP8 laser scanning confocal microscope was used to define the ROI. The regions of interest were illuminated with a blue laser (496 nm) for up to 1 minute, while continuously acquiring the fluorescent images for mOrange-Nano.

Chapter 5: Bibliography

1. Luisi, P. L., Walde, P. and Oberholzer, T., Lipid vesicles as possible intermediates in origin of life. *Current Opinion in Colloid & Interface Science* **1999,** *4,* 33-39.

2. Szostak, J. W., Bartel, D. P. and Luisi, P.L., Synthesizing life. *Nature* **2001,** *409,* 387-390.

3. Schwille, P.; Spatz, J.; Landfester, K.; Bodenschatz, E.; Herminghaus, S.; Sourjik, V.; Erb, T.; Bastiaens, P.; Lipowsky, R.; Hyman, A.; Dabrock, P.; Baret, J. C.; Vidakovic-Koch, T.; Bieling, P.; Dimova, R.; Mutschler, H.; Robinson, T.; Tang, D.; Wegner, S.; Sundmacher, K., MaxSynBio - Avenues towards creating cells from the bottom up. *Angew Chem Int Ed Engl* **2018** *10.1002/anie.201802288*.

4. Noireaux, V.; Maeda, Y. T.; Libchaber, A., Development of an artificial cell, from self-organization to computation and self-reproduction. *Proc Natl Acad Sci U S A* **2011,** *108,* 3473-3480.

5. Noireaux, V. a. L., A., A vesicle bioreactor as a step toward an artificial cell assembly. *Proc Natl Acad Sci U S A* **2004,** *101,* 17669–17674.

6. Monnard, P. A.; Deamer, D. W., Membrane self-assembly processes: steps toward the first cellular life. *Anat Rec* **2002,** *268,* 196-207.

7. Forster, A. C.; Church, G. M., Towards synthesis of a minimal cell. *Mol Syst Biol* **2006,** *2,* 45.

8. Endy, D., Foundations for engineering biology. *Nature* **2005,** *438,* 449-453.

9. Majumder, S.; Liu, A. P., Bottom-up synthetic biology: modular design for making artificial platelets. *Phys Biol* **2017,** *15,* 013001.

10. Salehi-Reyhani, A.; Ces, O.; Elani, Y., Artificial cell mimics as simplified models for the study of cell biology. *Exp Biol Med (Maywood)* **2017,** *242,* 1309-1317.

11. Gibson, D. G., Glass, J. I., Lartigue, C., Noskov, V. N., Chuang, R. Y., Algire, M. A., Benders, G. A., Montague, M. G., Ma, L., Moodie, M. M.,; Merryman, C., Vashee, S., Krishnakumar, R., Assad-Garcia, N.,; Andrews-Pfannkoch, C., Denisova, E. A., Young, L., Qi, Z. Q.,; Segall-Shapiro, T. H., Calvey, C. H., Parmar, P. P., Hutchison III, C. A.,; Smith, H. O. a. V., J. C., Creation of a Bacterial Cell Controlled by a Chemically Synthesized Genome. *Science* **2010,** *329,* 52-56.

12. Schwille, P., Jump-starting life? Fundamental aspects of synthetic biology. *J Cell Biol* **2015,** *210,* 687-690.

13. Glass, J. I., Assad-Garcia, N., Alperovich, N., Yooseph, S., Lewis,M. R., Maruf, M., Hutchison III,C. A., Smith, H. O. and Venter, J. C., Essential genes of a minimal bacterium. *Proc Natl Acad Sci U S A* **2006,** *103*, 425-430.

14. Roberts, M. A.; Cranenburgh, R. M.; Stevens, M. P.; Oyston, P. C., Synthetic biology: biology by design. *Microbiology* **2013,** *159*, 1219-1220.

15. Schwille, P., Bottom-Up Synthetic Biology: Engineering in a Tinkerer's World. *Science* **2011,** *333*, 1252-1254.

16. Pasotti, L.; Politi, N.; Zucca, S.; Cusella De Angelis, M. G.; Magni, P., Bottom-up engineering of biological systems through standard bricks: a modularity study on basic parts and devices. *PLoS One* **2012,** *7*, e39407.

17. Otrin, L.; Marusic, N.; Bednarz, C.; Vidakovic-Koch, T.; Lieberwirth, I.; Landfester, K.; Sundmacher, K., Toward Artificial Mitochondrion: Mimicking Oxidative Phosphorylation in Polymer and Hybrid Membranes. *Nano Lett* **2017,** *17*, 6816-6821.

18. Terasawa, H.; Nishimura, K.; Suzuki, H.; Matsuura, T.; Yomo, T., Coupling of the fusion and budding of giant phospholipid vesicles containing macromolecules. *Proc Natl Acad Sci U S A* **2012,** *109*, 5942-5947.

19. Suzuki, Y.; Nagai, K. H.; Zinchenko, A.; Hamada, T., Photoinduced Fusion of Lipid Bilayer Membranes. *Langmuir* **2017,** *33*, 2671-2676.

20. Weiss, M.; Frohnmayer, J. P.; Benk, L. T.; Haller, B.; Janiesch, J. W.; Heitkamp, T.; Borsch, M.; Lira, R. B.; Dimova, R.; Lipowsky, R.; Bodenschatz, E.; Baret, J. C.; Vidakovic-Koch, T.; Sundmacher, K.; Platzman, I.; Spatz, J. P., Sequential bottom-up assembly of mechanically stabilized synthetic cells by microfluidics. *Nat. Mater.* **2018,** *17*, 89-96.

21. Shimizu, Y.; Kanamori, T.; Ueda, T., Protein synthesis by pure translation systems. *Methods* **2005,** *36*, 299-304.

22. Fritz, B. R.; Timmerman, L. E.; Daringer, N. M.; Leonard, J. N.; Jewett, M. C., Biology by design: from top to bottom and back. *J Biomed Biotechnol* **2010,** *2010*, 11.

23. Mantri, S.; Sapra, K. T., Evolving protocells to prototissues: rational design of a missing link. *Biochem. Soc. Trans.* **2013,** *41*, 1159-1165.

24. Dzieciol, A. J.; Mann, S., Designs for life: protocell models in the laboratory. *Chem. Soc. Rev.* **2012,** *41*, 79-85.

25. Robinson, P. K., Enzymes: principles and biotechnological applications. *Essays Biochem* **2015,** *59*, 1-41.

26. Alberts B, J. A., Lewis J, Raff, M., Roberts, K. and Walter, P., In *Molecular Biology of the Cell*, 4th ed.; Ny.: Garland Science: 2002; pp 659-669.

27. Grosberg, R. K.; Strathmann, R. R., The Evolution of Multicellularity: A Minor Major Transition? *Annu. Rev. Ecol. Evol. Syst.* **2007,** *38*, 621-654.

28. Li, Q.; Wang, X.; Ma, S.; Zhang, Y.; Han, X., Electroformation of giant unilamellar vesicles in saline solution. *Colloids Surf B Biointerfaces* **2016,** *147*, 368-375.

29. Beales, P. A.; Ciani, B.; Cleasby, A. J., Nature's lessons in design: nanomachines to scaffold, remodel and shape membrane compartments. *Phys Chem Chem Phys* **2015,** *17*, 15489-15507.

30. Huang, X.; Li, M.; Green, D. C.; Williams, D. S.; Patil, A. J.; Mann, S., Interfacial assembly of protein-polymer nano-conjugates into stimulus-responsive biomimetic protocells. *Nat. Commun.* **2013,** *4*, 2239.

31. Qiao, Y.; Li, M.; Booth, R.; Mann, S., Predatory behaviour in synthetic protocell communities. *Nat. Chem.* **2017,** *9*, 110-119.

32. Tang, T. D.; Cecchi, D.; Fracasso, G.; Accardi, D.; Coutable-Pennarun, A.; Mansy, S. S.; Perriman, A. W.; Anderson, J. L. R.; Mann, S., Gene-Mediated Chemical Communication in Synthetic Protocell Communities. *ACS Synth. Biol.* **2018,** *7*, 339-346.

33. Walde, P.; Cosentino, K.; Engel, H.; Stano, P., Giant vesicles: preparations and applications. *Chembiochem* **2010,** *11*, 848-865.

34. Weinberger, A.; Tsai, F. C.; Koenderink, G. H.; Schmidt, T. F.; Itri, R.; Meier, W.; Schmatko, T.; Schroder, A.; Marques, C., Gel-assisted formation of giant unilamellar vesicles. *Biophys J* **2013,** *105*, 154-164.

35. Li, F.; Josephson, D. P.; Stein, A., Colloidal assembly: the road from particles to colloidal molecules and crystals. *Angew. Chem. Int. Ed.* **2011,** *50*, 360-388.

36. Merindol, R.; Walther, A., Materials learning from life: concepts for active, adaptive and autonomous molecular systems. *Chem. Soc. Rev.* **2017,** *46*, 5588-5619.

37. Dewey, D. C.; Strulson, C. A.; Cacace, D. N.; Bevilacqua, P. C.; Keating, C. D., Bioreactor droplets from liposome-stabilized all-aqueous emulsions. *Nat. Commun.* **2014,** *5*, 4670.

38. Villringer, S.; Madl, J.; Sych, T.; Manner, C.; Imberty, A.; Romer, W., Lectin-mediated protocell crosslinking to mimic cell-cell junctions and adhesion. *Sci. Rep.* **2018,** *8*, 1932.

39. Alivisatos, A. P., Johnsson, K. P., Peng, X., Wilson, T. E., Loweth, C. J., Bruchez, M. P. and Schultz, P.G., Organization of 'nanocrystal molecules' using DNA. . *Nature 382*, 609-611.

40. Mirkin, C. A., Letsinger, R. L., Mucic, R. C. and Storhoff, J. J., A DNA-based method for rationally assembling nanoparticles into macroscopic materials. *Nature* **1996,** *382*, 607-609.

41. Watson, J. D. a. C., F., Genetical Implications of the Structure of Deoxyribonucleic Acid. *Nature* **1953,** *171*, 964-967.

42. Watson, J. D. a. C., F., Molecular Structure of Nucleic Acids: A Structure for Deoxyribose Nucleic Acid. *Nature* **1953,** *171*, 737-738.

43. Di Michele, L.; Eiser, E., Developments in understanding and controlling self assembly of DNA-functionalized colloids. *Phys. Chem. Chem. Phys.* **2013,** *15*, 3115-3129.

44. Di Michele, L.; Varrato, F.; Kotar, J.; Nathan, S. H.; Foffi, G.; Eiser, E., Multistep kinetic self-assembly of DNA-coated colloids. *Nat. Commun.* **2013,** *4*, 1-7.

45. Macfarlane, R. J.; Lee, B.; Jones, M. R.; Harris, N.; Schatz, G. C.; Mirkin, C. A., Nanoparticle Superlattice Engineering with DNA. *Science* **2011,** *334*, 204-208.

46. Valignat, M. P.; Theodoly, O.; Crocker, J. C.; Russel, W. B.; Chaikin, P. M., Reversible self-assembly and directed assembly of DNA-linked micrometer-sized colloids. *Proc. Natl. Acad. Sci. U.S.A.* **2005,** *102*, 4225-4229.

47. Van der Meulen, S. A.; Leunissen, M. E., Solid colloids with surface-mobile DNA linkers. *J. Am. Chem. Soc.* **2013,** *135*, 15129-15134.

48. Wang, Y.; Wang, Y.; Zheng, X.; Ducrot, E.; Lee, M. G.; Yi, G. R.; Weck, M.; Pine, D. J., Synthetic Strategies Toward DNA-Coated Colloids that Crystallize. *J. Am. Chem. Soc.* **2015,** *137*, 10760-10766.

49. Wang, Y.; Wang, Y.; Zheng, X.; Ducrot, E.; Yodh, J. S.; Weck, M.; Pine, D. J., Crystallization of DNA-coated colloids. *Nat. Commun.* **2015,** *6*, 7253-7261.

50. Higashi, N.; Ochiai, T.; Kanazawa, C.; Koga, T., Site-specific adsorption of gold nanoparticles coated with thermo-responsive peptides. *Polym. J.* **2012,** *45*, 523-528.

51. Hamner, K. L.; Maye, M. M., Thermal aggregation properties of nanoparticles modified with temperature sensitive copolymers. *Langmuir* **2013,** *29*, 15217-15223.

52. Schoen, A. P.; Hommersom, B.; Heilshorn, S. C.; Leunissen, M. E., Tuning colloidal association with specific peptide interactions. *Soft Matter* **2013,** *9*, 6781-6785.

53. Klajn, R.; Bishop, K. J. M.; Grzybowski, B. A., Light-controlled self-assembly of reversible and irreversible nanoparticle suprastructures. *Proc. Natl. Acad. Sci. U.S.A.* **2007,** *104*, 10305-10309.

54. Manna, D.; Udayabhaskararao, T.; Zhao, H.; Klajn, R., Orthogonal light-induced self-assembly of nanoparticles using differently substituted azobenzenes. *Angew. Chem. Int. Ed.* **2015,** *54*, 12394-12397.

55. Zhang, L.; Dai, L.; Rong, Y.; Liu, Z.; Tong, D.; Huang, Y.; Chen, T., Light-triggered reversible self-assembly of gold nanoparticle oligomers for tunable SERS. *Langmuir* **2015,** *31*, 1164-1171.

56. Zhang, Q.; Dong, R.; Chang, X.; Ren, B.; Tong, Z., Spiropyran-Decorated SiO(2)-Pt Janus Micromotor: Preparation and Light-Induced Dynamic Self-Assembly and Disassembly. *ACS Appl. Mater. Interfaces* **2015,** *7*, 24585-24591.

57. He, H.; Feng, M.; Chen, Q., ; ; Zhang, X.; Zhan, H., Light-Induced Reversible Self-Assembly of Gold Nanoparticles Surface-Immobilized with Coumarin Ligands. *Angew. Chem. Int. Ed.* **2016,** *55*, 936-940.

58. Han, K.; Go, D.; Tigges, T.; Rahimi, K.; Kuehne, A. J. C.; Walther, A., Social Self-Sorting of Colloidal Families in Co-Assembling Microgel Systems. *Angew. Chem. Int. Ed.* **2017,** *56*, 2176-2182.

59. Han, K.; Go, D.; Hoenders, D.; Kuehne, A. J. C.; Walther, A., Switchable Supracolloidal Coassembly of Microgels Mediated by Host/Guest Interactions. *ACS Macro Lett.* **2017,** *6*, 310-314.

60. Zhou, Y.; Wang, D.; Huang, S.; Auernhammer, G.; He, Y.; Butt, H. J.; Wu, S., Reversible Janus particle assembly via responsive host-guest interactions. *Chem. Commun.* **2015,** *51*, 2725-2727.

61. Lan, Y.; Wu, Y.; Karas, A.; Scherman, O. A., Photoresponsive hybrid raspberry-like colloids based on cucurbit[8]uril host-guest interactions. *Angew. Chem. Int. Ed.* **2014,** *53*, 2166-2169.

62. Stoffelen, C.; Voskuhl, J.; Jonkheijm, P.; Huskens, J., Dual stimuli-responsive self-assembled supramolecular nanoparticles. *Angew. Chem. Int. Ed.* **2014,** *53*, 3400-3404.

63. Zhang, Q.; Qu, D. H.; Wang, Q. C.; Tian, H., Dual-Mode Controlled Self-Assembly of TiO2 Nanoparticles Through a Cucurbit[8]uril-Enhanced Radical Cation Dimerization Interaction. *Angew. Chem. Int. Ed.* **2015,** *54*, 15789-15793.

64. Zhang, J.; Grzybowski, B. A.; Granick, S., Janus Particle Synthesis, Assembly, and Application. *Langmuir* **2017,** *33*, 6964-6977.

65. Mukhopadhyay, P.; Wu, A.; Isaacs, L., Social Self-Sorting in Aqueous Solution. *J. Org. Chem.* **2004,** *69*, 6157-6164.

66. Morris, K. L.; Chen, L.; Raeburn, J.; Sellick, O. R.; Cotanda, P.; Paul, A.; Griffiths, P. C.; King, S. M.; O'Reilly, R. K.; Serpell, L. C.; Adams, D. J., Chemically programmed self-sorting of gelator networks. *Nat. Commun.* **2013,** *4,* 1480-1486.

67. Vilanova, N.; Feijter, I.; Teunissen, A. J. P.; Voets, I. K., Light induced assembly and self-sorting of silica microparticles. *Sci. Rep.* **2018,** *8,* 1271.

68. Kretschmer, S.; Schwille, P., Pattern formation on membranes and its role in bacterial cell division. *Curr Opin Cell Biol* **2016,** *38,* 52-59.

69. Kretschmer, S.; Zieske, K.; Schwille, P., Large-scale modulation of reconstituted Min protein patterns and gradients by defined mutations in MinE's membrane targeting sequence. *PLoS One* **2017,** *12,* e0179582.

70. Zieske, K.; Chwastek, G.; Schwille, P., Protein Patterns and Oscillations on Lipid Monolayers and in Microdroplets. *Angew Chem Int Ed Engl* **2016,** *55,* 13455-13459.

71. Murray, S. M.; Sourjik, V., Self-organization and positioning of bacterial protein clusters. *Nature Physics* **2017,** *13,* 1006-1013.

72. Shvartsman, S. Y.; Coppey, M.; Berezhkovskii, A. M., Dynamics of maternal morphogen gradients in Drosophila. *Curr Opin Genet Dev* **2008,** *18,* 342-347.

73. Christian, J. L., Morphogen gradients in development: from form to function. *Wiley Interdiscip Rev Dev Biol* **2012,** *1,* 3-15.

74. Filipponi, L.; Livingston, P.; Kaspar, O.; Tokarova, V.; Nicolau, D. V., Protein patterning by microcontact printing using pyramidal PDMS stamps. *Biomed Microdevices* **2016,** *18,* 9-15.

75. Bernard, A.; Renault, J. P.; Michel, B.; Bosshard, H. R.; Delamarche, E., Microcontact Printing of Proteins. *Advanced Materials* **2000,** *12,* 1067-1070.

76. Hoff, J. D., Cheng, L. J., Meyhoefer, E., Guo, L. J. and Hunt A. J., Nanoscale Protein Patterning by Imprint Lithography. *Nano Lett.* **2004,** *4,* 853-857.

77. Reuther, C.; Tucker, R.; Ionov, L.; Diez, S., Programmable patterning of protein bioactivity by visible light. *Nano Lett* **2014,** *14,* 4050-4057.

78. Chen, Z.; He, S.; Butt, H. J.; Wu, S., Photon upconversion lithography: patterning of biomaterials using near-infrared light. *Adv Mater* **2015,** *27,* 2203-2206.

79. Wegner, S. V.; Senturk, O. I.; Spatz, J. P., Photocleavable linker for the patterning of bioactive molecules. *Sci Rep* **2015,** *5,* 18309.

80. Laboria, N.; Wieneke, R.; Tampe, R., Control of nanomolar interaction and in situ assembly of proteins in four dimensions by light. *Angew Chem Int Ed Engl* **2013,** *52,* 848-853.

81. Terai, T.; Maki, E.; Sugiyama, S.; Takahashi, Y.; Matsumura, H.; Mori, Y.; Nagano, T., Rational development of caged-biotin protein-labeling agents and some applications in live cells. *Chem Biol* **2011,** *18*, 1261-1272.

82. Zhang, J.; Hu, T.; Liu, Y.; Ma, Y.; Dong, J.; Xu, L.; Zheng, Y.; Yang, H.; Wang, G., Photoswitched protein adsorption on electrostatically self-assembled azobenzene films. *Chemphyschem* **2012,** *13*, 2671-2675.

83. Pearson, D.; Abell, A. D., Structural optimization of photoswitch ligands for surface attachment of alpha-chymotrypsin and regulation of its surface binding. *Chemistry* **2010,** *16*, 6983-6992.

84. Beharry, A. A. a. W., G. A., Azobenzene photoswitches for biomolecules. *Chem. Soc. Rev.* **2011,** *40*, 4422-4437.

85. Muller, K.; Weber, W., Optogenetic tools for mammalian systems. *Mol. Biosyst.* **2013,** *9*, 596-608.

86. Muhlhauser, W. W.; Fischer, A.; Weber, W.; Radziwill, G., Optogenetics - Bringing light into the darkness of mammalian signal transduction. *Biochim Biophys Acta* **2017,** *1864*, 280-292.

87. Tischer, D.; Weiner, O. D., Illuminating cell signalling with optogenetic tools. *Nat Rev Mol Cell Biol* **2014,** *15*, 551-558.

88. Scheib, U., Stehfest, K., Gee, C. E., Koerschen, H.G., Fudim, R., Oertner, T. G. and Hegemann, P., The rhodopsin–guanylyl cyclase of the aquatic fungus Blastocladiella emersonii enables fast optical control of cGMP signaling. *Science Signaling* **2015,** *8*.

89. Yu, G.; Onodera, H.; Aono, Y.; Kawano, F.; Ueda, Y.; Furuya, A.; Suzuki, H.; Sato, M., Optical manipulation of the alpha subunits of heterotrimeric G proteins using photoswitchable dimerization systems. *Sci. Rep.* **2016,** *6*, 35777-35786.

90. Yüz, S. G.; Ricken, J.; Wegner, S. V., Independent Control over Multiple Cell Types in Space and Time Using Orthogonal Blue and Red Light Switchable Cell Interactions. *Advanced Science* **2018**, 1800446.

91. Yizhar, O.; Fenno, L. E.; Davidson, T. J.; Mogri, M.; Deisseroth, K., Optogenetics in neural systems. *Neuron* **2011,** *71*, 9-34.

92. Yawo, H.; Asano, T.; Sakai, S.; Ishizuka, T., Optogenetic manipulation of neural and non-neural functions. *Dev Growth Differ* **2013,** *55*, 474-490.

93. Bruegmann, T.; Malan, D.; Hesse, M.; Beiert, T.; Fuegemann, C. J.; Fleischmann, B. K.; Sasse, P., Optogenetic control of heart muscle in vitro and in vivo. *Nat Methods* **2010,** *7*, 897-900.

94. Doroudchi, M. M.; Greenberg, K. P.; Liu, J.; Silka, K. A.; Boyden, E. S.; Lockridge, J. A.; Arman, A. C.; Janani, R.; Boye, S. E.; Boye, S. L.; Gordon, G. M.; Matteo, B. C.; Sampath, A. P.; Hauswirth, W. W.; Horsager, A., Virally delivered channelrhodopsin-2 safely and effectively restores visual function in multiple mouse models of blindness. *Mol Ther* **2011,** *19*, 1220-1229.

95. Borthwick, H. A., Hendricks, S. B., Schneider, M. J., Taylorson, R. B. and Toole V. K. , The high-energy light action controlling plant responses and development. *Proc Natl Acad Sci U S A* **1969,** *64*, 479–486.

96. Shinomura, T., Nagatani, A., Chory, J. and Furuya, M., The Induction of Seed Germination in Arabidopsis thaliana Is Regulated Principally by Phytochrome B and Secondarily by Phytochrome A. *Plant Physiology* **1994,** *104*, 363-371.

97. Jarillo, J. A., Capel, J., Tang,R. H., Yang, H. Q.,; Alonso, J. M., Ecker, J. R. and Cashmore, A. R., An Arabidopsis circadian clock component interacts with both CRY1 and phyB. *Nature* **2001,** *410*, 487-490.

98. Li, J.; Li, G.; Wang, H.; Wang Deng, X., Phytochrome signaling mechanisms. *Arabidopsis Book* **2011,** *9*, e0148.

99. Levskaya, A.; Weiner, O. D.; Lim, W. A.; Voigt, C. A., Spatiotemporal control of cell signalling using a light-switchable protein interaction. *Nature* **2009,** *461*, 997-1001.

100. Levskaya, A.; Chevalier, A. A.; Tabor, J. J.; Simpson, Z. B.; Lavery, L. A.; Levy, M.; Davidson, E. A.; Scouras, A.; Ellington, A. D.; Marcotte, E. M.; Voigt, C. A., Synthetic biology: engineering Escherichia coli to see light. *Nature* **2005,** *438*, 441-442.

101. Jost, A. P.; Weiner, O. D., Probing Yeast Polarity with Acute, Reversible, Optogenetic Inhibition of Protein Function. *ACS Synth Biol* **2015,** *4*, 1077-1085.

102. Yang, X.; Jost, A. P.; Weiner, O. D.; Tang, C., A light-inducible organelle-targeting system for dynamically activating and inactivating signaling in budding yeast. *Mol Biol Cell* **2013,** *24*, 2419-2430.

103. Buckley, C. E.; Moore, R. E.; Reade, A.; Goldberg, A. R.; Weiner, O. D.; Clarke, J. D. W., Reversible Optogenetic Control of Subcellular Protein Localization in a Live Vertebrate Embryo. *Dev Cell* **2016,** *36*, 117-126.

104. Adrian, M.; Nijenhuis, W.; Hoogstraaten, R. I.; Willems, J.; Kapitein, L. C., A Phytochrome-Derived Photoswitch for Intracellular Transport. *ACS Synth Biol* **2017,** *6*, 1248-1256.

105. Gomez, E. J.; Gerhardt, K.; Judd, J.; Tabor, J. J.; Suh, J., Light-Activated Nuclear Translocation of Adeno-Associated Virus Nanoparticles Using Phytochrome B for

Enhanced, Tunable, and Spatially Programmable Gene Delivery. *ACS Nano* **2016,** *10,* 225-237.

106. Beyer, H. M.; Juillot, S.; Herbst, K.; Samodelov, S. L.; Muller, K.; Schamel, W. W.; Romer, W.; Schafer, E.; Nagy, F.; Strahle, U.; Weber, W.; Zurbriggen, M. D., Red Light-Regulated Reversible Nuclear Localization of Proteins in Mammalian Cells and Zebrafish. *ACS Synth Biol* **2015,** *4*, 951-958.

107. Muller, K.; Engesser, R.; Metzger, S.; Schulz, S.; Kampf, M. M.; Busacker, M.; Steinberg, T.; Tomakidi, P.; Ehrbar, M.; Nagy, F.; Timmer, J.; Zubriggen, M. D.; Weber, W., A red/far-red light-responsive bi-stable toggle switch to control gene expression in mammalian cells. *Nucleic Acids Res* **2013,** *41*, e77.

108. Muller, K.; Zurbriggen, M. D.; Weber, W., Control of gene expression using a red- and far-red light-responsive bi-stable toggle switch. *Nat Protoc* **2014,** *9*, 622-632.

109. Muller, K.; Engesser, R.; Schulz, S.; Steinberg, T.; Tomakidi, P.; Weber, C. C.; Ulm, R.; Timmer, J.; Zurbriggen, M. D.; Weber, W., Multi-chromatic control of mammalian gene expression and signaling. *Nucleic Acids Res* **2013,** *41*, e124.

110. Hughes, R. M.; Bolger, S.; Tapadia, H.; Tucker, C. L., Light-mediated control of DNA transcription in yeast. *Methods* **2012,** *58,* 385-391.

111. Hochrein, L.; Machens, F.; Messerschmidt, K.; Mueller-Roeber, B., PhiReX: a programmable and red light-regulated protein expression switch for yeast. *Nucleic Acids Res* **2017,** *45*, 9193-9205.

112. Hochrein, L.; Mitchell, L. A.; Schulz, K.; Messerschmidt, K.; Mueller-Roeber, B., L-SCRaMbLE as a tool for light-controlled Cre-mediated recombination in yeast. *Nat Commun* **2018,** *9,* 1931.

113. Ruess, J.; Parise, F.; Milias-Argeitis, A.; Khammash, M.; Lygeros, J., Iterative experiment design guides the characterization of a light-inducible gene expression circuit. *Proc Natl Acad Sci U S A* **2015,** *112,* 8148-8153.

114. Muller, K.; Siegel, D.; Rodriguez Jahnke, F.; Gerrer, K.; Wend, S.; Decker, E. L.; Reski, R.; Weber, W.; Zurbriggen, M. D., A red light-controlled synthetic gene expression switch for plant systems. *Mol Biosyst* **2014,** *10,* 1679-1688.

115. Toettcher, J. E.; Weiner, O. D.; Lim, W. A., Using optogenetics to interrogate the dynamic control of signal transmission by the Ras/Erk module. *Cell* **2013,** *155,* 1422-1434.

116. Reichhart, E.; Ingles-Prieto, A.; Tichy, A. M.; McKenzie, C.; Janovjak, H., A Phytochrome Sensory Domain Permits Receptor Activation by Red Light. *Angew Chem Int Ed Engl* **2016,** *55*, 6339-6342.

117. Lamparter, T., Esteban, B. and Hughes, J., Phytochrome Cph1 from the cyanobacterium Synechocystis PCC6803: Purification, assembly, and quaternary structure. *Eur. J. Biochem. 268*, 4720-4730.

118. Fernandez-Rodriguez, J.; Moser, F.; Song, M.; Voigt, C. A., Engineering RGB color vision into Escherichia coli. *Nat Chem Biol* **2017,** *13*, 706-708.

119. Schmidl, S. R.; Sheth, R. U.; Wu, A.; Tabor, J. J., Refactoring and optimization of light-switchable Escherichia coli two-component systems. *ACS Synth Biol* **2014,** *3*, 820-831.

120. Ma, S.; Luo, S.; Wu, L.; Liang, Z.; Wu, J.-R., Re-engineering the two-component systems as light-regulated in Escherichia coli. *Journal of Biosciences* **2017,** *42*, 565-573.

121. Schlessinger, J., Cell Signaling by Receptor Tyrosine Kinases. *Cell* **2000,** *103*, 211-225.

122. Pudasaini, A.; El-Arab, K. K.; Zoltowski, B. D., LOV-based optogenetic devices: light-driven modules to impart photoregulated control of cellular signaling. *Front Mol Biosci* **2015,** *2*, 18.

123. Kennis, J. T. M., van Stokkum, I. H. M., Crosson, S., Gauden, M., Moffat, K. and van Grondelle, R., The LOV2 Domain of Phototropin: A Reversible Photochromic Switch. *J Am Chem Soc* **2004,** *126*, 4512-4513.

124. Lungu, O. I.; Hallett, R. A.; Choi, E. J.; Aiken, M. J.; Hahn, K. M.; Kuhlman, B., Designing photoswitchable peptides using the AsLOV2 domain. *Chem. Biol.* **2012,** *19*, 507-517.

125. Kawano, F.; Suzuki, H.; Furuya, A.; Sato, M., Engineered pairs of distinct photoswitches for optogenetic control of cellular proteins. *Nat. Commun.* **2015,** *6*, 6256-6264.

126. Guntas, G.; Hallett, R. A.; Zimmerman, S. P.; Williams, T.; Yumerefendi, H.; Bear, J. E.; Kuhlman, B., Engineering an improved light-induced dimer (iLID) for controlling the localization and activity of signaling proteins. *Proc. Natl. Acad. Sci. U.S.A.* **2015,** *112*, 112-117.

127. Nihongaki, Y.; Suzuki, H.; Kawano, F.; Sato, M., Genetically engineered photoinducible homodimerization system with improved dimer-forming efficiency. *ACS Chem Biol* **2014,** *9*, 617-621.

128. Zoltowski, B. D.; Vaccaro, B.; Crane, B. R., Mechanism-based tuning of a LOV domain photoreceptor. *Nat Chem Biol* **2009,** *5*, 827-834.

129. Zimmerman, S. P.; Hallett, R. A.; Bourke, A. M.; Bear, J. E.; Kennedy, M. J.; Kuhlman, B., Tuning the Binding Affinities and Reversion Kinetics of a Light Inducible Dimer Allows Control of Transmembrane Protein Localization. *Biochemistry* **2016,** *55,* 5264-5271.

130. Zimmerman, S. P.; Asokan, S. B.; Kuhlman, B.; Bear, J. E., Cells lay their own tracks - optogenetic Cdc42 activation stimulates fibronectin deposition supporting directed migration. *J Cell Sci* **2017,** *130,* 2971-2983.

131. Yumerefendi, H.; Lerner, A. M.; Zimmerman, S. P.; Hahn, K.; Bear, J. E.; Strahl, B. D.; Kuhlman, B., Light-induced nuclear export reveals rapid dynamics of epigenetic modifications. *Nat Chem Biol* **2016,** *12,* 399-401.

132. Adikes, R. C.; Hallett, R. A.; Saway, B. F.; Kuhlman, B.; Slep, K. C., Control of microtubule dynamics using an optogenetic microtubule plus end–F-actin cross-linker. *J Cell Biol* **2017,** *217,* 779-793.

133. Johnson, H. E.; Goyal, Y.; Pannucci, N. L.; Schupbach, T.; Shvartsman, S. Y.; Toettcher, J. E., The Spatiotemporal Limits of Developmental Erk Signaling. *Dev Cell* **2017,** *40,* 185-192.

134. Hallett, R. A.; Zimmerman, S. P.; Yumerefendi, H.; Bear, J. E.; Kuhlman, B., Correlating in Vitro and in Vivo Activities of Light-Inducible Dimers: A Cellular Optogenetics Guide. *ACS Synth Biol* **2016,** *5,* 53-64.

135. O'Neill, P. R.; Kalyanaraman, V.; Gautam, N., Subcellular optogenetic activation of Cdc42 controls local and distal signaling to drive immune cell migration. *Mol Biol Cell* **2016,** *27,* 1442-1450.

136. O'Neill, P. R.; Castillo-Badillo, J. A.; Meshik, X.; Kalyanaraman, V.; Melgarejo, K.; Gautam, N., Membrane Flow Drives an Adhesion-Independent Amoeboid Cell Migration Mode. *Dev Cell* **2018,** *46,* 9-22.

137. Yu, Q.; Wang, Y.; Zhao, S.; Ren, Y., Photocontrolled reversible self-assembly of dodecamer nitrilase. *Bioresour Bioprocess* **2017,** *4,* 36.

138. Nakamura, H.; Lee, A. A.; Afshar, A. S.; Watanabe, S.; Rho, E.; Razavi, S.; Suarez, A.; Lin, Y. C.; Tanigawa, M.; Huang, B.; DeRose, R.; Bobb, D.; Hong, W.; Gabelli, S. B.; Goutsias, J.; Inoue, T., Intracellular production of hydrogels and synthetic RNA granules by multivalent molecular interactions. *Nat Mater* **2018,** *17,* 79-89.

139. Smith, W. J., Hamel, B., Yohe, M. E., Sondek, J., Cerione, R. A. and Snyder, J. T., A Cdc42 Mutant Specifically Activated by Intersectin. *Biochemistry* **2005,** *44,* 13282-13290.

140. Muller, K.; Engesser, R.; Timmer, J.; Zurbriggen, M. D.; Weber, W., Orthogonal optogenetic triple-gene control in Mammalian cells. *ACS Synth Biol* **2014,** *3,* 796-801.

141. Wang, W.; Shi, X. Y.; Wei, D. Z., Light-mediated control of gene expression in filamentous fungus Trichoderma reesei. *J Microbiol Methods* **2014,** *103*, 37-39.

142. Wang, X.; Chen, X.; Yang, Y., Spatiotemporal control of gene expression by a light-switchable transgene system. *Nat Methods* **2012,** *9*, 266-269.

143. Zhang, G.; Liu, P.; Wei, W.; Wang, X.; Wei, D.; Wang, W., A light-switchable bidirectional expression system in filamentous fungus Trichoderma reesei. *J Biotechnol* **2016,** *240*, 85-93.

144. Han, T.; Chen, Q.; Liu, H., Engineered Photoactivatable Genetic Switches Based on the Bacterium Phage T7 RNA Polymerase. *ACS Synth Biol* **2017,** *6*, 357-366.

145. Grusch, M.; Schelch, K.; Riedler, R.; Reichhart, E.; Differ, C.; Berger, W.; Ingles-Prieto, A.; Janovjak, H., Spatio-temporally precise activation of engineered receptor tyrosine kinases by light. *EMBO J* **2014,** *33*, 1713-1726.

146. Kim, K. T.; Song, M. R., Light-induced Notch activity controls neurogenic and gliogenic potential of neural progenitors. *Biochem Biophys Res Commun* **2016,** *479*, 820-826.

147. Nihongaki, Y.; Furuhata, Y.; Otabe, T.; Hasegawa, S.; Yoshimoto, K.; Sato, M., CRISPR-Cas9-based photoactivatable transcription systems to induce neuronal differentiation. *Nat Methods* **2017,** *14*, 963-966.

148. Nihongaki, Y.; Kawano, F.; Nakajima, T.; Sato, M., Photoactivatable CRISPR-Cas9 for optogenetic genome editing. *Nat Biotechnol* **2015,** *33*, 755-760.

149. Kawano, F., Okazaki, R., Yazawa, M. and Sato, M., A photoactivatable Cre–loxP recombination system for optogenetic genome engineering. *Nature Chemical Biology* **2016,** *12*, 1059-1064.

150. Chen, F.; Wegner, S. V., Blue Light Switchable Bacterial Adhesion as a Key Step toward the Design of Biofilms. *ACS Synth Biol* **2017,** *6*, 2170-2174.

151. Furuya, A.; Kawano, F.; Nakajima, T.; Ueda, Y.; Sato, M., Assembly Domain-Based Optogenetic System for the Efficient Control of Cellular Signaling. *ACS Synth. Biol.* **2017,** *6*, 1086-1095.

152. Guglielmi, G.; Falk, H. J.; De Renzis, S., Optogenetic Control of Protein Function: From Intracellular Processes to Tissue Morphogenesis. *Trends Cell. Biol.* **2016,** *26*, 864-874.

153. Chavda, A. P.; Prole, D. L.; Taylor, C. W., A bead aggregation assay for detection of low-affinity protein-protein interactions reveals interactions between N-terminal domains of inositol 1,4,5-trisphosphate receptors. *PLoS One* **2013,** *8*, e60609.

154. Hartman, N. C.; Groves, J. T., Signaling clusters in the cell membrane. *Curr Opin Cell Biol* **2011,** *23*, 370-376.

155. Schweizer, J.; Loose, M.; Bonny, M.; Kruse, K.; Monch, I.; Schwille, P., Geometry sensing by self-organized protein patterns. *Proc Natl Acad Sci U S A* **2012,** *109*, 15283-15288.

156. Hao, J.; Zou, B.; Narayanan, K.; George, A., Differential expression patterns of the dentin matrix proteins during mineralized tissue formation. *Bone* **2004,** *34*, 921-932.

157. Qiao, H.; Hu, N.; Bai, J.; Ren, L.; Liu, Q.; Fang, L.; Wang, Z., Encapsulation of Nucleic Acids into Giant Unilamellar Vesicles by Freeze-Thaw: a Way Protocells May Form. *Orig Life Evol Biosph* **2017,** *47*, 499-510.

158. Giustini, M.; Giuliani, A. M.; Gennaro, G., Natural or synthetic nucleic acids encapsulated in a closed cavity of amphiphiles. *RSC Advances* **2013,** *3*, 8618-8632.

159. Kaszas, N.; Bozo, T.; Budai, M.; Grof, P., Ciprofloxacin encapsulation into giant unilamellar vesicles: membrane binding and release. *J Pharm Sci* **2013,** *102*, 694-705.

160. O'Neil, C. P.; Suzuki, T.; Demurtas, D.; Finka, A.; Hubbell, J. A., A novel method for the encapsulation of biomolecules into polymersomes via direct hydration. *Langmuir* **2009,** *25*, 9025-9029.

161. Liu, X.; Zhou, P.; Huang, Y.; Li, M.; Huang, X.; Mann, S., Hierarchical Proteinosomes for Programmed Release of Multiple Components. *Angew Chem Int Ed Engl* **2016,** *55*, 7095-7100.

162. Su, D.; Liu, X.; Wang, L.; Ma, C.; Xie, H.; Zhang, H.; Meng, X.; Huang, Y.; Huang, X., Bio-inspired engineering proteinosomes with a cell-wall-like protective shell by self-assembly of a metal-chelated complex. *Chem Commun (Camb)* **2016,** *52*, 13803-13806.

Chapter 6: Appendix

6.1 Nucleotide and amino acid sequences of optogenetic proteins

6.1.1 iLID

Nucleotide sequence:

ATGAGAGGATCGCATCACCATCACCATCACGGATCCGGGGAGTTTCTGGCAACCAC
ACTGGAACGGATCGAGAAAAATTTCGTGATTACTGATCCGAGACTGCCTGACAACC
CAATCATTTTTGCGAGCGATTCCTTCCTGCAGCTGACAGAATATTCTCGGGAAGAG
ATCCTGGGGCGCAATTGCCGTTTTCTGCAGGGACCCGAGACAGACCGTGCCACTGT
TCGGAAAATCAGAGATGCTATTGACAACCAGACTGAAGTGACCGTTCAGCTGATCA
ATTATACCAAGAGCGGCAAGAAGTTCTGGAACGTGTTCCACCTGCAGCCGATGCGC
GATTATAAGGGCGACGTCCAGTACTTCATTGGCGTGCAGCTGGATGGCACCGAACG
TCTTCATGGCGCCGCTGAGCGTGAGGCGGTCATGCTGATCAAAAAGACAGCCTTTC
AGATTGCTGAGGCAGCGAACGACGAAAATTACTTTTAA

Amino acid sequence:

MRGSHHHHHHGSGEFLATTLERIEKNFVITDPRLPDNPIIFASDSFLQLTEYSREE
ILGRNCRFLQGPETDRATVRKIRDAIDNQTEVTVQLINYTKSGKKFWNVFHLQPMR
DYKGDVQYFIGVQLDGTERLHGAAEREAVMLIKKTAFQIAEAANDENYF-

6.1.2 MBP-SspB-Nano

Nucleotide sequence:

ATGAGAGGATCGCATCACCATCACCATCACGGATCTAAAATCGAAGAAGGTAAACT
GGTAATCTGGATTAACGGCGATAAAGGCTATAACGGTCTCGCTGAAGTCGGTAAGA
AATTCGAGAAAGATACCGGAATTAAAGTCACCGTTGAGCATCCGGATAAACTGGAA
GAGAAATTCCCACAGGTTGCGGCAACTGGCGATGGCCCTGACATTATCTTCTGGGC
ACACGACCGCTTTGGTGGCTACGCTCAATCTGGCCTGTTGGCTGAAATCACCCCGG
ACAAAGCGTTCCAGGACAAGCTGTATCCGTTTACCTGGGATGCCGTACGTTACAAC
GGCAAGCTGATTGCTTACCCGATCGCTGTTGAAGCGTTATCGCTGATTTATAACAA
AGACCTGCTGCCGAACCCGCCAAAAACCTGGGAAGAGATCCCGGCGCTGGATAAAG
AACTGAAAGCGAAAGGTAAGAGCGCGCTGATGTTCAACCTGCAAGAACCGTACTTC
ACCTGGCCGCTGATTGCTGCTGACGGGGGTTATGCGTTCAAGTATGAAAACGGCAA

GTACGACATTAAAGACGTGGGCGTGGATAACGCTGGCGCGAAAGCGGGTCTGACCT
TCCTGGTTGACCTGATTAAAAACAAACACATGAATGCAGACACCGATTACTCCATC
GCAGAAGCTGCCTTTAATAAAGGCGAAACAGCGATGACCATCAACGGCCCGTGGGC
ATGGTCCAACATCGACACCAGCAAAGTGAATTATGGTGTAACGGTACTGCCGACCT
TCAAGGGTCAACCATCCAAACCGTTCGTTGGCGTGCTGAGCGCAGGTATTAACGCC
GCCAGTCCGAACAAAGAGCTGGCAAAAGAGTTCCTCGAAAACTATCTGCTGACTGA
TGAAGGTCTGGAAGCGGTTAATAAAGACAAACCGCTGGGTGCCGTAGCGCTGAAGT
CTTACGAGGAAGAGTTGGCGAAAGATCCACGTATTGCCGCCACTATGGAAAACGCC
CAGAAAGGTGAAATCATGCCGAACATCCCGCAGATGTCCGCTTTCTGGTATGCCGT
GCGTACTGCGGTGATCAACGCCGCCAGCGGTCGTCAGACTGTCGATGAAGCCCTGA
AAGACGCGCAGACTAATTCGAGCTCGAACAACAACAACAATAACAATAACAACAAC
CTCGGGATCGAGGGAACGACCGAAAACCTGTATTTTCAGGGATCCAGCTCCCCGAA
ACGCCCTAAGCTGCTGCGTGAATATTACGATTGGCTGGTTGATAACAGCTTTACCC
CATATCTGGTGGTGGATGCCACATACCTGGGCGTGAACGTGCCCGTGGAGTATGTG
AAAGACGGTCAGATCGTGCTGAATCTGTCTGCAAGTGCGACCGGCAACCTGCAACT
GACAAATGATTTTATCCAGTTCAACGCCCGCTTTAAGGGCGTGTCTCGTGAACTGT
ATATCCCGATGGGTGCCGCTCTGGCCATTTACGCTCGCGAGAACGGCGATGGTGTG
ATGTTCGAACCAGAAGAAATCTATGACGAGCTGAATATTGGTTAA

Amino acid sequence:

MRGSHHHHHHGSKIEEGKLVIWINGDKGYNGLAEVGKKFEKDTGIKVTVEHPDKLE
EKFPQVAATGDGPDIIFWAHDRFGGYAQSGLLAEITPDKAFQDKLYPFTWDAVRYN
GKLIAYPIAVEALSLIYNKDLLPNPPKTWEEIPALDKELKAKGKSALMFNLQEPYF
TWPLIAADGGYAFKYENGKYDIKDVGVDNAGAKAGLTFLVDLIKNKHMNADTDYSI
AEAAFNKGETAMTINGPWAWSNIDTSKVNYGVTVLPTFKGQPSKPFVGVLSAGINA
ASPNKELAKEFLENYLLTDEGLEAVNKDKPLGAVALKSYEEELAKDPRIAATMENA
QKGEIMPNIPQMSAFWYAVRTAVINAASGRQTVDEALKDAQTNSSSNNNNNNNNNN
LGIEGTTENLYFQGSSSPKRPKLREYYDWLVDNSFTPYLVVDATYLGVNVPVEYVK
DGQIVLNLSASATGNLQLTNDFIQFNARFKGVSRELYIPMGAALAIYARENGDGVM
FEPEEIYDELNIG-

6.1.3 MBP-SspB-Micro

Nucleotide sequence:

ATGAGAGGATCGCATCACCATCACCATCACGGATCTAAAATCGAAGAAGGTAAACT
GGTAATCTGGATTAACGGCGATAAAGGCTATAACGGTCTCGCTGAAGTCGGTAAGA
AATTCGAGAAAGATACCGGAATTAAAGTCACCGTTGAGCATCCGGATAAACTGGAA
GAGAAATTCCCACAGGTTGCGGCAACTGGCGATGGCCCTGACATTATCTTCTGGGC
ACACGACCGCTTTGGTGGCTACGCTCAATCTGGCCTGTTGGCTGAAATCACCCCGG
ACAAAGCGTTCCAGGACAAGCTGTATCCGTTTACCTGGGATGCCGTACGTTACAAC
GGCAAGCTGATTGCTTACCCGATCGCTGTTGAAGCGTTATCGCTGATTTATAACAA
AGACCTGCTGCCGAACCCGCCAAAAACCTGGGAAGAGATCCCGGCGCTGGATAAAG
AACTGAAAGCGAAAGGTAAGAGCGCGCTGATGTTCAACCTGCAAGAACCGTACTTC
ACCTGGCCGCTGATTGCTGCTGACGGGGGTTATGCGTTCAAGTATGAAAACGGCAA
GTACGACATTAAAGACGTGGGCGTGGATAACGCTGGCGCGAAAGCGGGTCTGACCT
TCCTGGTTGACCTGATTAAAAACAAACACATGAATGCAGACACCGATTACTCCATC
GCAGAAGCTGCCTTTAATAAAGGCGAAACAGCGATGACCATCAACGGCCCGTGGGC
ATGGTCCAACATCGACACCAGCAAAGTGAATTATGGTGTAACGGTACTGCCGACCT
TCAAGGGTCAACCATCCAAACCGTTCGTTGGCGTGCTGAGCGCAGGTATTAACGCC
GCCAGTCCGAACAAAGAGCTGGCAAAAGAGTTCCTCGAAAACTATCTGCTGACTGA
TGAAGGTCTGGAAGCGGTTAATAAAGACAAACCGCTGGGTGCCGTAGCGCTGAAGT
CTTACGAGGAAGAGTTGGCGAAAGATCCACGTATTGCCGCCACTATGGAAAACGCC
CAGAAAGGTGAAATCATGCCGAACATCCCGCAGATGTCCGCTTTCTGGTATGCCGT
GCGTACTGCGGTGATCAACGCCGCCAGCGGTCGTCAGACTGTCGATGAAGCCCTGA
AAGACGCGCAGACTAATTCGAGCTCGAACAACAACAACAATAACAATAACAACAAC
CTCGGGATCGAGGGAACGACCGAAAACCTGTATTTTCAGGGATCCAGCTCCCCGAA
ACGCCCTAAGCTGCTGCGTGAATATTACGATTGGCTGGTTGATAACAGCTTTACCC
CATATCTGGTGGTGGATGCCACATACCTGGGCGTGAACGTGCCCGTGGAGTATGTG
AAAGACGGTCAGATCGTGCTGAATCTGTCTGCAAGTGCGACCGGCAACCTGCAACT
GACAAATGATTTTATCCAGTTCAACGCCCAGTTTAAGGGCGTGTCTCGTGAACTGT
ATATCCCGATGGGTGCCGCTCTGGCCATTTACGCTCGCGAGAACGGCGATGGTGTG
ATGTTCGAACCAGAAGAAATCTATGACGAGCTGAATATTGGTTAA

Amino acid sequence:

MRGSHHHHHHGSKIEEGKLVIWINGDKGYNGLAEVGKKFEKDTGIKVTVEHPDKLE
EKFPQVAATGDGPDIIFWAHDRFGGYAQSGLLAEITPDKAFQDKLYPFTWDAVRYN

GKLIAYPIAVEALSLIYNKDLLPNPPKTWEEIPALDKELKAKGKSALMFNLQEPYF
TWPLIAADGGYAFKYENGKYDIKDVGVDNAGAKAGLTFLVDLIKNKHMNADTDYSI
AEAAFNKGETAMTINGPWAWSNIDTSKVNYGVTVLPTFKGQPSKPFVGVLSAGINA
ASPNKELAKEFLENYLLTDEGLEAVNKDKPLGAVALKSYEEELAKDPRIAATMENA
QKGEIMPNIPQMSAFWYAVRTAVINAASGRQTVDEALKDAQTNSSSNNNNNNNNNN
LGIEGTTENLYFQGSSSPKRPKLLREYYDWLVDNSFTPYLVVDATYLGVNVPVEYV
KDGQIVLNLSASATGNLQLTNDFIQFNAQFKGVSRELYIPMGAALAIYARENGDGV
MFEPEEIYDELNIG-

6.1.4 mOrange-Nano

Nucleotide sequence:

ATGAGAGGATCGCATCACCATCACCATCACGGATCTAAAATCGAAGAAGGTAAACT
GGTAATCTGGATTAACGGCGATAAAGGCTATAACGGTCTCGCTGAAGTCGGTAAGA
AATTCGAGAAAGATACCGGAATTAAAGTCACCGTTGAGCATCCGGATAAACTGGAA
GAGAAATTCCCACAGGTTGCGGCAACTGGCGATGGCCCTGACATTATCTTCTGGGC
ACACGACCGCTTTGGTGGCTACGCTCAATCTGGCCTGTTGGCTGAAATCACCCCGG
ACAAAGCGTTCCAGGACAAGCTGTATCCGTTTACCTGGGATGCCGTACGTTACAAC
GGCAAGCTGATTGCTTACCCGATCGCTGTTGAAGCGTTATCGCTGATTTATAACAA
AGACCTGCTGCCGAACCCGCCAAAAACCTGGGAAGAGATCCCGGCGCTGGATAAAG
AACTGAAAGCGAAAGGTAAGAGCGCGCTGATGTTCAACCTGCAAGAACCGTACTTC
ACCTGGCCGCTGATTGCTGCTGACGGGGGTTATGCGTTCAAGTATGAAAACGGCAA
GTACGACATTAAAGACGTGGGCGTGGATAACGCTGGCGCGAAAGCGGGTCTGACCT
TCCTGGTTGACCTGATTAAAAACAAACACATGAATGCAGACACCGATTACTCCATC
GCAGAAGCTGCCTTTAATAAAGGCGAAACAGCGATGACCATCAACGGCCCGTGGGC
ATGGTCCAACATCGACACCAGCAAAGTGAATTATGGTGTAACGGTACTGCCGACCT
TCAAGGGTCAACCATCCAAACCGTTCGTTGGCGTGCTGAGCGCAGGTATTAACGCC
GCCAGTCCGAACAAAGAGCTGGCAAAAGAGTTCCTCGAAAACTATCTGCTGACTGA
TGAAGGTCTGGAAGCGGTTAATAAAGACAAACCGCTGGGTGCCGTAGCGCTGAAGT
CTTACGAGGAAGAGTTGGCGAAAGATCCACGTATTGCCGCCACTATGGAAAACGCC
CAGAAAGGTGAAATCATGCCGAACATCCCGCAGATGTCCGCTTTCTGGTATGCCGT
GCGTACTGCGGTGATCAACGCCGCCAGCGGTCGTCAGACTGTCGATGAAGCCCTGA
AAGACGCGCAGACTAATTCGAGCTCGAACAACAACAACAATAACAATAACAACAAC
CTCGGGATCGAGGGAACGACCGAAAACCTGTATTTTCAGGGATCCGTGAGCAAGGG

CGAGGAGAATAACATGGCCATCATCAAGGAGTTCATGCGCTTCAAGGTGCGCATGG
AGGGCTCCGTGAACGGCCACGAGTTCGAGATCGAGGGCGAGGGCGAGGGCCGCCCC
TACGAGGGCTTTCAGACCGCTAAGCTGAAGGTGACCAAGGGTGGCCCCCTGCCCTT
CGCCTGGGACATCCTGTCCCCTCAGTTCACCTACGGCTCCAAGGCCTACGTGAAGC
ACCCCGCCGACATCCCCGACTACTTCAAGCTGTCCTTCCCCGAGGGCTTCAAGTGG
GAGCGCGTGATGAACTTCGAGGACGGCGGCGTGGTGACCGTGACCCAGGACTCCTC
CCTCCAGGACGGCGAGTTCATCTACAAGGTGAAGCTGCGCGGCACCAACTTCCCCT
CCGACGGCCCCGTAATGCAGAAGAAGACCATGGGCTGGGAGGCCTCCTCCGAGCGG
ATGTACCCCGAGGACGGCGCCCTGAAGGGCGAGATCAAGATGAGGCTGAAGCTGAA
GGACGGCGGCCACTACACCTCCGAGGTCAAGACCACCTACAAGGCCAAGAAGCCCG
TGCAGCTGCCCGGCGCCTACATCGTCGGCATCAAGTTGGACATCACCTCCCACAAC
GAGGACTACACCATCGTGGAACAGTACGAACGCGCCGAGGGCCGCCACTCCACCGG
CGGCATGGACGAGCTGTACAAGGGAGGAAGTGGTACCAGCTCCCCGAAACGCCCTA
AGCTGCTGCGTGAATATTACGATTGGCTGGTTGATAACAGCTTTACCCCATATCTG
GTGGTGGATGCCACATACCTGGGCGTGAACGTGCCCGTGGAGTATGTGAAAGACGG
TCAGATCGTGCTGAATCTGTCTGCAAGTGCGACCGGCAACCTGCAACTGACAAATG
ATTTTATCCAGTTCAACGCCCGCTTTAAGGGCGTGTCTCGTGAACTGTATATCCCG
ATGGGTGCCGCTCTGGCCATTTACGCTCGCGAGAACGGCGATGGTGTGATGTTCGA
ACCAGAAGAAATCTATGACGAGCTGAATATTGGTTAA

Amino acid sequence:

MRGSHHHHHHGSKIEEGKLVIWINGDKGYNGLAEVGKKFEKDTGIKVTVEHPDKLE
EKFPQVAATGDGPDIIFWAHDRFGGYAQSGLLAEITPDKAFQDKLYPFTWDAVRYN
GKLIAYPIAVEALSLIYNKDLLPNPPKTWEEIPALDKELKAKGKSALMFNLQEPYF
TWPLIAADGGYAFKYENGKYDIKDVGVDNAGAKAGLTFLVDLIKNKHMNADTDYSI
AEAAFNKGETAMTINGPWAWSNIDTSKVNYGVTVLPTFKGQPSKPFVGVLSAGINA
ASPNKELAKEFLENYLLTDEGLEAVNKDKPLGAVALKSYEEELAKDPRIAATMENA
QKGEIMPNIPQMSAFWYAVRTAVINAASGRQTVDEALKDAQTNSSSNNNNNNNNNN
LGIEGTTENLYFQGSVSKGEENNMAIIKEFMRFKVRMEGSVNGHEFEIEGEGEGRP
YEGFQTAKLKVTKGGPLPFAWDILSPQFTYGSKAYVKHPADIPDYFKLSFPEGFKW
ERVMNFEDGGVVTVTQDSSLQDGEFIYKVKLRGTNFPSDGPVMQKKTMGWEASSER
MYPEDGALKGEIKMRLKLKDGGHYTSEVKTTYKAKKPVQLPGAYIVGIKLDITSHN
EDYTIVEQYERAEGRHSTGGMDELYKGGSGTSSPKRPKLLREYYDWLVDNSFTPYL

VVDATYLGVNVPVEYVKDGQIVLNLSASATGNLQLTNDFIQFNARFKGVSRELYIP
MGAALAIYARENGDGVMFEPEEIYDELNIG-

6.1.5 nMagHigh

Nucleotide sequence:

ATGCACACACTATATGCTCCCGGAGGGTATGATATAATGGGATACCTAGATCAAAT
AGGCAACCGTCCGAACCCGCAAGTGGAGCTGGGCCCGGTGGACACCAGCTGCGCGC
TGATCCTGTGCGACCTGAAGCAGAAAGATACCCCGATTGTGTACGCGAGCGAGGCG
TTCCTGTACATGACCGGTTATAGCAACGCGGAAGTTCTGGGCCGTAACTGCCGTTT
TCTGCAAAGCCCGGATGGTATGGTGAAGCCGAAAAGCACCCGTAAGTATGTTGACA
GCAACACCATCAACACCATTCGTAAAGCGATCGATCGTAACGCGGAAGTGCAGGTT
GAAGTGGTTAACTTCAAGAAAAACGGCCAACGTTTCGTGAACTTTCTGACCATCAT
TCCGGTTCGTGATGAGACCGGCGAATATCGTTATAGCATGGGTTTTCAATGCGAGA
CCGAAGGCGGTAGCCTCGAGCACCACCACCACCACCACTGA

Amino acid sequence:

MHTLYAPGGYDIMGYLDQIGNRPNPQVELGPVDTSCALILCDLKQKDTPIVYASEA
FLYMTGYSNAEVLGRNCRFLQSPDGMVKPKSTRKYVDSNTINTIRKAIDRNAEVQV
EVVNFKKNGQRFVNFLTIIPVRDETGEYRYSMGFQCETEGGSLEHHHHHH-

6.1.6 pMagHigh

Nucleotide sequence:

ATGCACACACTATATGCTCCCGGAGGGTATGATATAATGGGATACCTACGTCAAAT
ACGCAACCGTCCGAACCCGCAAGTGGAGCTGGGCCCGGTGGACACCAGCTGCGCGC
TGATCCTGTGCGACCTGAAGCAGAAAGATACCCCGATTGTGTACGCGAGCGAGGCG
TTCCTGTACATGACCGGTTATAGCAACGCGGAAGTTCTGGGCCGTAACTGCCGTTT
TCTGCAAAGCCCGGATGGTATGGTGAAGCCGAAAAGCACCCGTAAGTATGTTGACA
GCAACACCATCAACACCATTCGTAAAGCGATCGATCGTAACGCGGAAGTGCAGGTT
GAAGTGGTTAACTTCAAGAAAAACGGCCAACGTTTCGTGAACTTTCTGACCATCAT
TCCGGTTCGTGATGAGACCGGCGAATATCGTTATAGCATGGGTTTTCAATGCGAGA
CCGAAGGCGGTAGCCTCGAGCACCACCACCACCACCACTGA

Amino acid sequence:

MHTLYAPGGYDIMGYLRQIRNRPNPQVELGPVDTSCALILCDLKQKDTPIVYASEA
FLYMTGYSNAEVLGRNCRFLQSPDGMVKPKSTRKYVDSNTINTIRKAIDRNAEVQV
EVVNFKKNGQRFVNFLTIIPVRDETGEYRYSMGFQCETEGGSLEHHHHHH-

6.1.7 pMag

Nucleotide sequence:

ATGCACACACTATATGCTCCCGGAGGGTATGATATAATGGGATACCTACGTCAAAT
ACGCAACCGTCCGAACCCGCAAGTGGAGCTGGGCCCGGTGGACACCAGCTGCGCGC
TGATCCTGTGCGACCTGAAGCAGAAAGATACCCCGATTGTGTACGCGAGCGAGGCG
TTCCTGTACATGACCGGTTATAGCAACGCGGAAGTTCTGGGCCGTAACTGCCGTTT
TCTGCAAAGCCCGGATGGTATGGTGAAGCCGAAAAGCACCCGTAAGTATGTTGACA
GCAACACCATCAACACCAGTCGTAAAGCGATCGATCGTAACGCGGAAGTGCAGGTT
GAAGTGGTTAACTTCAAGAAAAACGGCCAACGTTTCGTGAACTTTCTGACCATGAT
TCCGGTTCGTGATGAGACCGGCGAATATCGTTATAGCATGGGTTTTCAATGCGAGA
CCGAAGGCGGTAGCCTCGAGCACCACCACCACCACCACTGA

Amino acid sequence:

MHTLYAPGGYDIMGYLRQIRNRPNPQVELGPVDTSCALILCDLKQKDTPIVYASEA
FLYMTGYSNAEVLGRNCRFLQSPDGMVKPKSTRKYVDSNTINTSRKAIDRNAEVQV
EVVNFKKNGQRFVNFLTMIPVRDETGEYRYSMGFQCETEGGSLEHHHHHH-

6.1.8 VVDHigh

Nucleotide sequence:

ATGCACACACTATATGCTCCCGGAGGGTATGATATAATGGGATACCTAATTCAAAT
AATGAACCGTCCGAACCCGCAAGTGGAGCTGGGCCCGGTGGACACCAGCTGCGCGC
TGATCCTGTGCGACCTGAAGCAGAAAGATACCCCGATTGTGTACGCGAGCGAGGCG
TTCCTGTACATGACCGGTTATAGCAACGCGGAAGTTCTGGGCCGTAACTGCCGTTT
TCTGCAAAGCCCGGATGGTATGGTGAAGCCGAAAAGCACCCGTAAGTATGTTGACA
GCAACACCATCAACACCATTCGTAAAGCGATCGATCGTAACGCGGAAGTGCAGGTT
GAAGTGGTTAACTTCAAGAAAAACGGCCAACGTTTCGTGAACTTTCTGACCATCAT
TCCGGTTCGTGATGAGACCGGCGAATATCGTTATAGCATGGGTTTTCAATGCGAGA
CCGAAGGCGGTAGCCACCACCACCACCACCACTGA

Amino acid sequence:

MHTLYAPGGYDIMGYLIQIMNRPNPQVELGPVDTSCALILCDLKQKDTPIVYASEA
FLYMTGYSNAEVLGRNCRFLQSPDGMVKPKSTRKYVDSNTINTIRKAIDRNAEVQV
EVVNFKKNGQRFVNFLTIIPVRDETGEYRYSMGFQCETEGGSHHHHHH-

6.1.9 Cph1

Nucleotide sequence:

ATGCACCATCACCACCACCACGAGAATCTGTACTTTCAAGGCGGATCCGAATTCGA
GCTCGCAACCACCGTTCAACTGAGCGACCAAAGCCTGCGTCAGCTGGAAACCCTGG
CTATCCACACCGCTCACCTGATTCAGCCGCATGGCCTGGTGGTGGTGCTGCAGGAA
CCGGACCTGACCATCAGCCAGATTAGCGCCAACTGCACCGGCATCCTGGGTCGTAG
CCCGGAGGATCTGCTGGGTCGCACCCTGGGCGAAGTGTTCGACAGCTTTCAGATCG
ATCCAATCCAGAGCCGCCTGACCGCCGGTCAGATCAGCAGCCTGAACCCGAGCAAG
CTGTGGGCTCGTGTGATGGGTGACGATTTCGTGATTTTTGACGGCGTGTTCCACCG
CAACAGCGATGGTCTGCTGGTGTGCGAGCTGGAACCGGCGTACACCAGCGACAACC
TGCCGTTCCTGGGTTTTTATCACATGGCTAATGCCGCGCTGAACCGTCTGCGTCAG
CAGGCGAACCTGCGTGACTTTTACGATGTGATCGTGGAGGAAGTGCGTCGCATGAC
CGGCTTCGACCGTGTGATGCTGTATCGCTTTGATGAGAACAACCACGGTGACGTGA
TTGCGGAGGATAAACGTGACGATATGGAACCGTACCTGGGCCTGCACTATCCGGAA
AGCGACATCCCACAGCCAGCTCGTCGCCTGTTCATTCACAACCCGATCCGCGTGAT
TCCGGACGTGTACGGTGTGGCTGTGCCACTGACCCCGGCTGTGAACCCGAGCACCA
ACCGTGCTGTGGACCTGACCGAGAGCATCCTGCGCAGCGCCTACCACTGCCACCTG
ACCTATCTGAAGAACATGGGCGTGGGTGCTAGCCTGACCATCAGCCTGATCAAGGA
TGGTCACCTGTGGGGCCTGATTGCTTGCCACCACCAGACCCCGAAAGTGATCCCGT
TTGAGCTGCGTAAAGCCTGCGAGTTCTTCGGCCGCGTGGTGTTCAGCAACATCAGC
GCGCAGGAAGACACCGAAACCTTTGATTATCGTGTGCAGCTGGCGGAGCACGAAGC
TGTGCTGCTGGACAAGATGACCACCGCTGCCGATTTCGTGGAGGGTCTGACCAATC
ATCCAGACCGTCTGCTGGGCCTGACCGGTAGCCAGGGCGCGGCTATCTGCTTTGGT
GAAAAGCTGATTCTGGTGGGCGAAACCCCGGATGAAAAAGCCGTGCAGTACCTGCT
GCAGTGGCTGGAGAACCGTGAAGTGCAGGACGTGTTCTTTACCAGCAGCCTGAGCC
AGATCTATCCGGATGCGGTGAACTTCAAAAGCGTGGCTAGCGGCCTGCTGGCTATC
CCAATTGCCCGTCACAACTTCCTGCTGTGGTTTCGCCCGGAAGTGCTGCAGACCGT
GAACTGGGGCGGTGACCCGAACCATGCCTACGAGGCGACCCAGGAAGATGGCAAGA

TTGAGCTGCACCCGCGTCAGAGCTTTGACCTGTGGAAAGAAATCGTGCGCCTGCAG
AGCCTGCCATGGCAGAGCGTGGAGATTCAATCCGCGCTGGCACTGAAAAAGGCTAT
CGTGAACCTGATTCTGCGTCAAGCTGAGTAA

Amino acid sequence:

MHHHHHHENLYFQGGSEFELATTVQLSDQSLRQLETLAIHTAHLIQPHGLVVVLQE
PDLTISQISANCTGILGRSPEDLLGRTLGEVFDSFQIDPIQSRLTAGQISSLNPSK
LWARVMGDDFVIFDGVFHRNSDGLLVCELEPAYTSDNLPFLGFYHMANAALNRLRQ
QANLRDFYDVIVEEVRRMTGFDRVMLYRFDENNHGDVIAEDKRDDMEPYLGLHYPE
SDIPQPARRLFIHNPIRVIPDVYGVAVPLTPAVNPSTNRAVDLTESILRSAYHCHL
TYLKNMGVGASLTISLIKDGHLWGLIACHHQTPKVIPFELRKACEFFGRVVFSNIS
AQEDTETFDYRVQLAEHEAVLLDKMTTAADFVEGLTNHPDRLLGLTGSQGAAICFG
EKLILVGETPDEKAVQYLLQWLENREVQDVFFTSSLSQIYPDAVNFKSVASGLLAI
PIARHNFLLWFRPEVLQTVNWGGDPNHAYEATQEDGKIELHPRQSFDLWKEIVRLQ
SLPWQSVEIQSALALKKAIVNLILRQAE-

6.1.10 PhyB

Nucleotide sequence:

ATGGTTAGCGGTGTTGGTGGTAGCGGTGGTGGTCGTGGTGGCGGTCGCGGAGGTGA
AGAAGAACCGAGCAGCAGCCATACCCCGAATAATCGCCGTGGTGGTGAACAGGCAC
AGAGCAGCGGCACCAAAAGCCTGCGTCCGCGTAGCAATACCGAAAGCATGAGCAAA
GCAATTCAGCAGTATACCGTTGATGCACGTCTGCATGCCGTTTTCGAACAGAGCGG
TGAAAGCGGTAAAAGCTTTGATTATAGCCAGAGCCTGAAAACCACCACCTATGGTA
GCAGCGTGCCGGAACAGCAGATTACCGCATATCTGAGCCGTATTCAGCGTGGTGGC
TACATTCAGCCGTTTGGCTGCATGATCGCAGTTGATGAAAGCAGCTTTCGCATTAT
TGGCTACAGCGAAAATGCACGTGAAATGCTGGGCATTATGCCGCAGAGCGTTCCGA
CCCTGGAAAAACCGGAAATTCTGGCAATGGGCACCGATGTTCGTAGCCTGTTTACC
AGCAGCAGCTCCATTCTGCTGGAACGTGCCTTTGTTGCCCGTGAAATTACCCTGCT
GAATCCGGTTTGGATTCATAGCAAAAACACCGGCAAACCGTTTTATGCAATTCTGC
ATCGTATTGATGTTGGCGTGGTTATTGATCTGGAACCGGCACGTACCGAAGATCCG
GCACTGAGCATTGCCGGTGCAGTTCAGAGCCAGAAACTGGCAGTTCGTGCAATTAG
CCAGCTGCAGGCACTGCCTGGTGGTGATATCAAACTGCTGTGTGATACCGTTGTTG
AAAGCGTTCGTGATCTGACCGGCTACGACCGTGTTATGGTGTATAAATTCCACGAA

GATGAACATGGTGAAGTTGTTGCAGAAAGCAAACGTGATGACCTGGAACCGTATAT
TGGTCTGCATTATCCAGCAACCGATATTCCGCAGGCAAGCCGTTTCCTGTTCAAAC
AGAATCGTGTGCGCATGATTGTTGATTGTAATGCAACACCGGTTCTGGTTGTTCAG
GATGATCGTCTGACCCAGAGCATGTGTCTGGTTGGTAGCACCCTGCGTGCACCGCA
TGGTTGTCATAGCCAGTATATGGCAAATATGGGTAGCATCGCAAGCCTGGCCATGG
CGGTGATCATCAATGGTAATGAAGATGATGGTAGCAATGTTGCAAGCGGTCGTAGC
AGCATGCGTCTGTGGGGTCTGGTTGTGTGTCATCATACCAGCAGTCGCTGCATTCC
GTTTCCGCTGCGTTATGCATGTGAATTTCTGATGCAGGCATTTGGACTGCAGCTGA
ATATGGAACTGCAACTGGCACTGCAGATGAGCGAAAAACGTGTTCTGCGTACCCAG
ACCCTGCTGTGCGATATGCTGCTGCGTGATAGTCCGGCAGGCATTGTTACCCAGAG
CCCGAGCATTATGGATCTGGTGAAATGCGATGGTGCAGCCTTTCTGTATCACGGTA
AATACTATCCGCTGGGTGTTGCACCGAGCGAAGTTCAGATTAAAGATGTTGTTGAG
TGGCTGCTGGCAAATCATGCAGATAGCACCGGTCTGAGCACCGATAGCCTGGGTGA
TGCAGGTTATCCGGGTGCAGCAGCACTGGGAGATGCAGTTTGTGGTATGGCAGTTG
CATACATTACCAAACGCGATTTTCTGTTTTGGTTTCGTAGCCATACCGCCAAAGAA
ATCAAATGGGGTGGTGCAAAACATCACCCGGAAGATAAAGATGACGGTCAGCGTAT
GCATCCGCGTAGTAGCTTTCAGGCATTTCTGGAAGTGGTGAAAAGCCGTAGCCAGC
CGTGGGAAACCGCAGAAATGGATGCAATTCATAGCCTGCAACTGATTCTGCGCGAT
AGCTTCAAAGAAAGCGAAGCAGCAATGAATAGCAAAGTTGTTGATGGTGTTGTTCA
GCCGTGTCGTGATATGGCAGGCGAACAGGGTATTGATGAACTGGGTGCAGGTTCTG
GTAGCGGTCTGAACGACATCTTCGAAGCTCAGAAAATCGAATGGCACGAACATCAT
CACCATCACCATTAA

Amino acid sequence:

MVSGVGGSGGGRGGGRGGEEEPSSSHTPNNRRGGEQAQSSGTKSLRPRSNTESMSK
AIQQYTVDARLHAVFEQSGESGKSFDYSQSLKTTTYGSSVPEQQITAYLSRIQRGG
YIQPFGCMIAVDESSFRIIGYSENAREMLGIMPQSVPTLEKPEILAMGTDVRSLFT
SSSSILLERAFVAREITLLNPVWIHSKNTGKPFYAILHRIDVGVVIDLEPARTEDP
ALSIAGAVQSQKLAVRAISQLQALPGGDIKLLCDTVVESVRDLTGYDRVMVYKFHE
DEHGEVVAESKRDDLEPYIGLHYPATDIPQASRFLFKQNRVRMIVDCNATPVLVVQ
DDRLTQSMCLVGSTLRAPHGCHSQYMANMGSIASLAMAVIINGNEDDGSNVASGRS
SMRLWGLVVCHHTSSRCIPFPLRYACEFLMQAFGLQLNMELQLALQMSEKRVLRTQ
TLLCDMLLRDSPAGIVTQSPSIMDLVKCDGAAFLYHGKYYPLGVAPSEVQIKDVVE

WLLANHADSTGLSTDSLGDAGYPGAAALGDAVCGMAVAYITKRDFLFWFRSHTAKE
IKWGGAKHHPEDKDDGQRMHPRSSFQAFLEVVKSRSQPWETAEMDAIHSLQLILRD
SFKESEAAMNSKVVDGVVQPCRDMAGEQGIDELGAGSGSGLNDIFEAQKIEWHEHH
HHHH-

6.2 Appendix figures

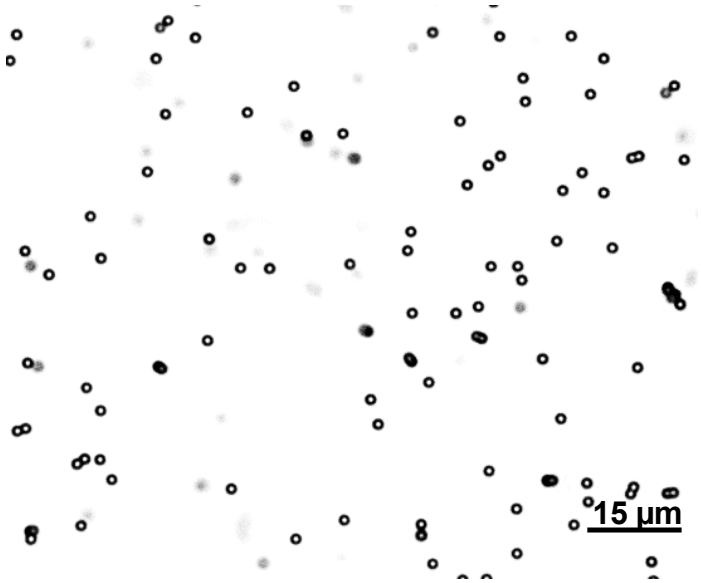

Figure A1. Non-functionalized 2 µm beads. The scale bar is 15 µm.

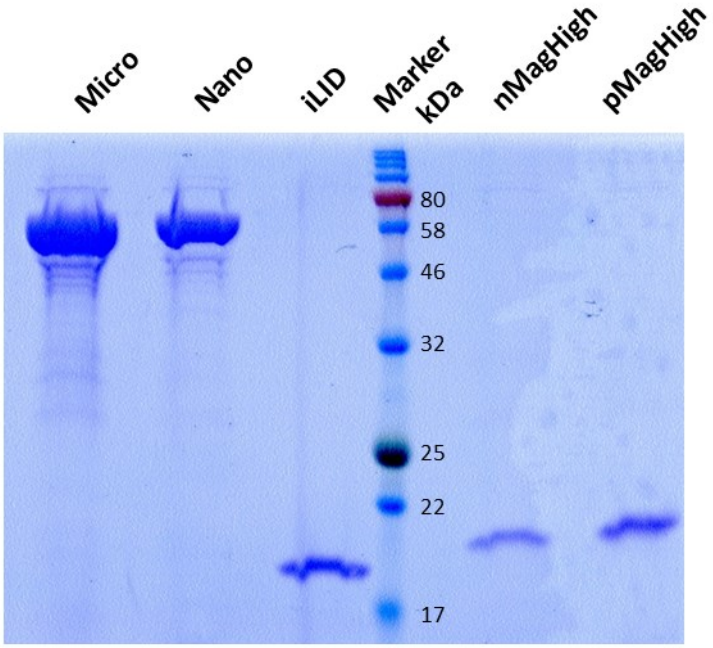

Figure A2. SDS-PAGE of purified proteins: Micro, Nano, iLID, nMagHigh and pMagHigh.

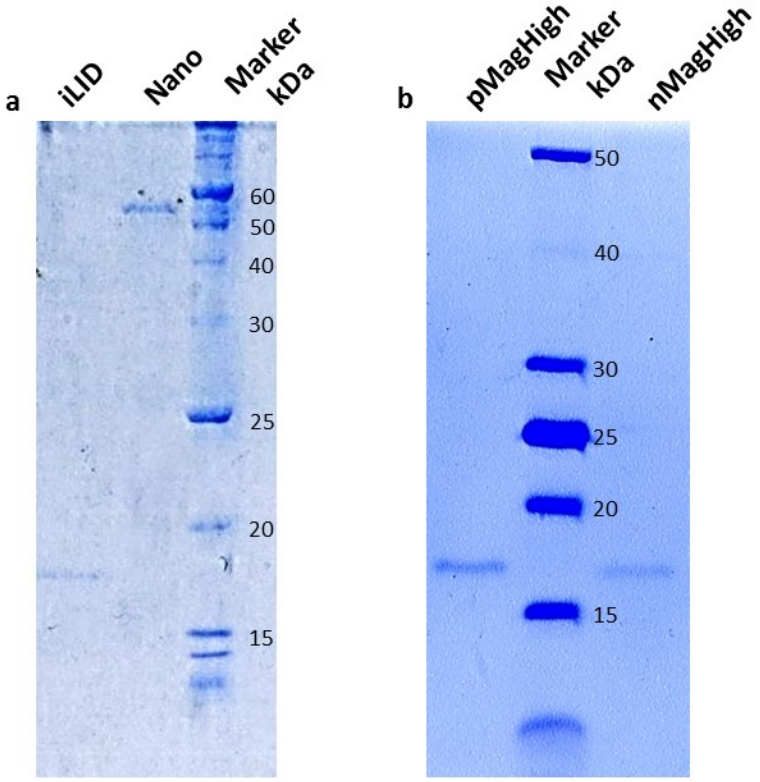

Figure A3. SDS-PAGEs of proteins that were bound to beads: a) iLID/Nano pair; b) nMagHigh/pMagHigh pair.

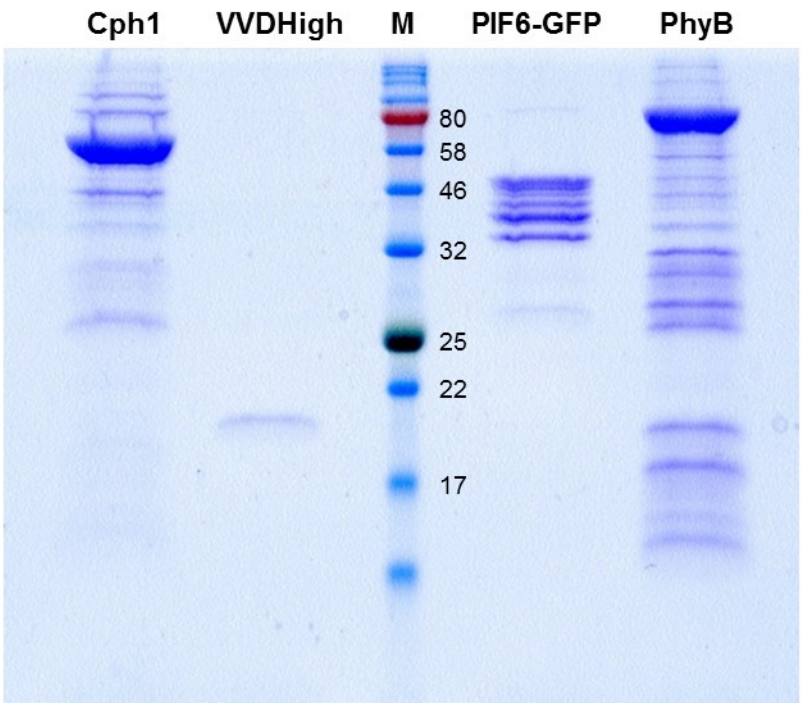

Figure A4. SDS-PAGE of purified proteins: Cph1, VVDHigh, PIF6-GFP and PhyB.

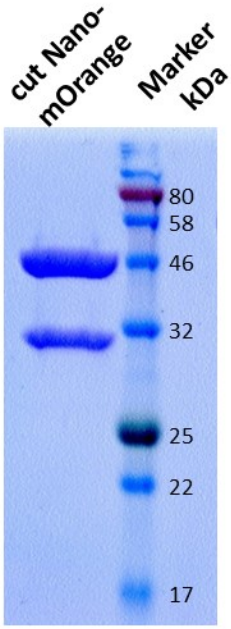

Figure A5. SDS-PAGE of Nano-mOrange protein after cutting its His6-tag using TEV protease.